CNWRA *A center of excellence in earth sciences and engineering*

A Division of Southwest Research Institute™
6220 Culebra Road • San Antonio, Texas, U.S.A. 78228-5166
(210) 522-5160 • Fax (210) 522-5155

June 18, 2003
Contract No. NRC–02–02–012
Account No. 20.06002.01.081

U.S. Nuclear Regulatory Commission
ATTN: Tamara Bloomer
Two White Flint North
11545 Rockville Pike
Mail Stop T7 F3
Washington, DC 20555

Subject: Submittal of Intermediate Milestone—Effect of Fabrication Processes on Material Stability—Characterization and Corrosion, Intermediate Milestone 06002.01.081.320

Dear Ms. Bloomer:

Enclosed is the subject intermediate milestone on the effects of fabrication processes on material stability and corrosion. A description of the fabrication processes for the construction and closure of waste packages proposed by the U.S. Department of Energy (DOE) for the disposal of high-level waste is included in Chapter 2. A review of the DOE results characterizing the effects of fabrication processes on the microstructure and corrosion resistance of Alloy 22 are provided in Chapters 3 and 4.

Reports by the DOE have suggested that microstructural alteration resulting from fabrication processes will not affect long-term waste package corrosion performance. Studies conducted at the Center for Nuclear Waste Regulatory Analyses (CNWRA) however, have concluded fabrication processes such as welding and solution annealing may have a significant effect on the material stability and localized corrosion resistance of Alloy 22. Solution annealing of the Alloy 22 disposal container has been proposed by the DOE as a method to mitigate residual stresses that develop during fabrication operations. Microstructural examinations of solution annealed weld metal conducted by the CNWRA showed the formation and growth of detrimental secondary phases as a result of molybdenum and tungsten segregation in the fusion zone. These observations were supported by phase stability calculations as well as localized corrosion tests of the solution annealed weld metal. The results of this study will directly support prelicensing interactions with the DOE.

If you have any questions regarding this report, please feel free to contact me (210) 522-5439.

Sincerely yours,

Y.-M. Pan for V. Jain

Vijay Jain
Element Manager
Corrosion Science & Process Engineering

VJ:jg

Attachment

cc: M. Leach, D. DeMarco, B. Meehan, E. Whitt, W. Reamer, J. Greeves, K. Stablein, B. Leslie, A. Campbell, L. Campbell, T. McCartin, T. Ahn, A. Csontos, J. Thomas, D. Brooks, J. Schlueter, W. Patrick, B. Sagar, G. Cragnolino, O. Pensado, L. Yang, D. Dunn, Y.-M. Pan, CNWRA EMs & Dirs. (ltr only), D. Daruwalla (Div. 01), P. Maldonado, Record Copy B, IQS

Washington Office • Twinbrook Metro Plaza #210
12300 Twinbrook Parkway • Rockville, Maryland 20852-1606

CNWRA 2003-xxx

EFFECT OF FABRICATION PROCESSES ON MATERIAL STABILITY—CHARACTERIZATION AND CORROSION

Prepared for

U.S. Nuclear Regulatory Commission
Contract NRC–02–02–012

Prepared by

D. Dunn
D. Daruwalla
Y.-M. Pan

Center for Nuclear Waste Regulatory Analyses
San Antonio, Texas

June 2003

PREVIOUS REPORTS IN SERIES

Number	Name	Date Issued
CNWRA 91-004	A Review of Localized Corrosion of High-Level Nuclear Waste Container Materials—I	April 1991
CNWRA 91-008	Hydrogen Embrittlement of Candidate Container Materials	June 1991
CNWRA 92-021	A Review of Stress Corrosion Cracking of High-Level Nuclear Waste Container Materials—I	August 1992
CNWRA 93-003	Long-Term Stability of High-Level Nuclear Waste Container Materials: I—Thermal Stability of Alloy 825	February 1993
CNWRA 93-004	Experimental Investigations of Localized Corrosion of High-Level Nuclear Waste Container Materials	February 1993
CNWRA 93-014	A Review of the Potential for Microbially Influenced Corrosion of High-Level Nuclear Waste Containers	June 1993
CNWRA 94-010	A Review of Degradation Modes of Alternate Container Designs and Materials	April 1994
CNWRA 94-028	Environmental Effects on Stress Corrosion Cracking of Type 316L Stainless Steel and Alloy 825 As High-Level Nuclear Waste Container Materials	October 1994
CNWRA 95-010	Experimental Investigations of Failure Processes of High-Level Radioactive Waste Container Materials	May 1995
CNWRA 95-020	Expert-Panel Review of the Integrated Waste Package Experiments Research Project	September 1995
CNWRA 96-004	Thermal Stability and Mechanical Properties of High-Level Radioactive Waste Container Materials: Assessment of Carbon and Low-Alloy Steels	May 1996
CNWRA 97-010	An Analysis of Galvanic Coupling Effects on the Performance of High-Level Nuclear Waste Container Materials	August 1997
CNWRA 98-004	Effect of Galvanic Coupling Between Overpack Materials of High-Level Nuclear Waste Containers—Experimental and Modeling Results	March 1998
CNWRA 98-008	Effects of Environmental Factors on Container Life	July 1998

PREVIOUS REPORTS IN SERIES (continued)

Number	Name	Date Issued
CNWRA 99-003	Assessment of Performance Issues Related to Alternate Engineered Barrier System Materials and Design Options	September 1999
CNWRA 99-004	Effects of Environmental Factors on the Aqueous Corrosion of High-Level Radioactive Waste Containers—Experimental Results and Models	September 1999
CNWRA 2000-06 Revision 1	Assessment of Methodologies to Confirm Container Performance Model Predictions	January 2001
CNWRA 2001-003	Effect of Environment on the Corrosion of Waste Package and Drip Shield Materials	September 2001
CNWRA 2002-01	Effect of In-Package Chemistry on the Degradation of Vitrified High-Level Radioactive Waste and Spent Nuclear Fuel Cladding	October 2001
CNWRA 2002-02	Evaluation of Analogs for the Performance Assessment of High-level Waste Container Materials	March 2002
CNWRA 2003-01	Passive Dissolution of Container Materials—Modeling and Experiments	October 2002
CNWRA 2003-02	Stress Corrosion Cracking and Hydrogen Embrittlement of Container and Drip Shield Materials	October 2002
CNWRA 2003-05	Assessment of Mechanisms for Early Waste Package Failures	March 2003

ABSTRACT

A long lifetime of the waste packages, which are main components of the engineered barrier subsystem, is identified by the U.S. Department of Energy (DOE) as a key system attribute for the performance of the proposed high-level waste repository at Yucca Mountain, Nevada. Uniform corrosion, localized corrosion, and stress corrosion cracking are considered important degradation processes that may influence the lifetime of the waste packages. Fabrication of the waste packages will require multiple operations that may alter the microstructure and affect the corrosion and stress corrosion cracking resistance of the waste package materials. In support of the U.S. Nuclear Regulatory Commission (NRC) prelicensing activities on issues important to the postclosure performance of the proposed repository, the Center for Nuclear Waste Regulatory Analyses (CNWRA) is conducting an independent technical assessment of the effects of fabrication processes on the performance of the engineered barrier materials. This report presents results of the CNWRA experimental work, as well as a review of the DOE evaluation, on the effects of fabrication processes such as welding and annealing on the microstructure, uniform corrosion rate, localized corrosion susceptibility, and stress corrosion cracking resistance of Alloy 22. The CNWRA investigations indicate that fabrication processes may alter the microstructure of Alloy 22 and lead to the formation of topologically close-packed phases. Uniform corrosion rates and stress corrosion cracking resistance were not significantly affected by welding or thermal aging. Fabrication processes were found to have a significant effect, however, on the localized corrosion susceptibility of Alloy 22. Several deficiencies and limitations of the DOE approach are identified for the evaluation of fabrication processes on corrosion and stress corrosion cracking of the Alloy 22 outer container. The effects of waste package environments, welding and solution annealing, compositional variation, and thermal aging need to be properly considered to evaluate the performance of the waste packages. These concerns have been addressed in the DOE and NRC agreements, and DOE has provided a path forward for resolving all the deficiencies and limitations identified in this report at the time of the license application.

CONTENTS

CONTENTS (continued)

CONTENTS (continued)

FIGURES

FIGURES (continued)

FIGURES (continued)

TABLES

ACKNOWLEDGMENTS

This report was prepared to document work performed by the Center for Nuclear Waste Regulatory Analyses (CNWRA) for the U.S. Nuclear Regulatory Commission (NRC) under Contract No. NRC–02–02–012. The activities reported here were performed on behalf of the NRC Office of Nuclear Material Safety and Safeguards, Division of Waste Management. The views expressed in the report are those of the author and do not necessarily reflect the views or regulatory position of the NRC.

The authors gratefully acknowledge G.A. Cragnolino for technical review, the programmatic review of W. Patrick, and the editorial reviews of C. Cudd and B. Long. Appreciation is due to J. Gonzalez for assistance in preparing this report.

QUALITY OF DATA: Sources of data are referenced in each chapter. CNWRA-generated laboratory data contained in this report meet quality assurance requirements described in the CNWRA Quality Assurance Manual. Data from other sources, however, are freely used. The respective sources of non-CNWRA data should be consulted for determining levels of quality assurance. Experimental data have been recorded in CNWRA scientific notebook numbers 288, 366, 485, 498, 505, 520, 540, and 578.

ANALYSES AND CODES: Thermo-Calc Version N was used for the phase stability and theoretical calculations presented in this report. This code is controlled according to requirements of CNWRA Technical Operating Procedure (TOP)–018. Detailed phase stability calculations can be found in CNWRA scientific notebook number 498.

REFERENCE:

Thermo-Calc Software AB. "Thermo-Calc Classic." Version N. Stockholm, Sweden: Thermo-Calc Software AB. 2001.

EXECUTIVE SUMMARY

Performance of the engineered barriers after waste emplacement is important to protecting the public from any undue long-term risk, as recognized by the U.S. Department of Energy (DOE) in its repository safety strategy for the proposed Yucca Mountain repository. As stated in 10 CFR Part 63, the engineered barrier subsystem must be designed so that, working in combination with natural barriers, radiological exposures to the reasonably maximally exposed individual and release of radionuclides into the accessible environment are limited, as specified in 10 CFR 63.311. For these reasons, the performance of the waste package and the main component of the engineered barrier subsystem is noted by DOE to be among the principal factors for the postclosure safety case. The uniform corrosion rate, localized corrosion susceptibility and stress corrosion cracking resistance, which are important degradation modes affecting the lifetimes of the waste package, can be altered by fabrication processes necessary to construct and close the waste packages. These degradation modes of the waste package are considered in subissues 1 and 2 of the Container Life and Source Term Key Technical Issue. Through the process of prelicensing consultation for issue resolution between DOE and the U.S. Nuclear Regulatory Commission (NRC), these two subissues are considered closed-pending according to the DOE and NRC agreements. DOE agreed to provide additional information pertaining to each agreement for the NRC staff to have all the information needed for regulatory decisionmaking at the time of the license application.

In support of the NRC prelicensing activities on topics important to the postclosure performance of the proposed repository, the Center for Nuclear Waste Regulatory Analyses (CNWRA) is conducting an independent technical assessment of the effects of fabrication processes on the degradation of the engineered barrier materials. This report provides a review of the DOE assessment of the effects of fabrication processes on the degradation of Alloy 22 (Ni-22Cr-13Mo-4Fe-3W) and presents results of more recent experimental work conducted at CNWRA.

Waste packages designed for disposing high-level nuclear waste in the proposed repository at Yucca Mountain include an Alloy 22 outer container to provide corrosion resistance. Fabrication and closure of the waste packages will require forming processes including rolling and machining operations. The rolled cylinders will be welded to construct the Alloy 22 disposal container. The disposal containers will be solution annealed and water quenched to remove residual stresses. After loading, welding will be used to close the waste packages. Several postclosure weld stress mitigation methods have been proposed by DOE including induction annealing, laser peening, and low-plasticity burnishing. The combination of cold work associated with the forming operations, welding, and postweld stress mitigation methods may alter the microstructure and corrosion resistance of the Alloy 22 waste package outer barrier. Characterization of the effects of fabrication processes on the microstructure and corrosion resistance is necessary to assess performance of the waste packages.

DOE evaluated the phase stability of Alloy 22 assuming the precipitation of secondary topologically close-packed phases and carbides and long-range ordering. The kinetics of phase transformations were determined based on aging data measured from samples treated in accelerated, high-temperature conditions and several assumptions involved in predicting phase stability for repository-relevant conditions. Extrapolation of the short-term data showed that both bulk precipitation of topologically close-packed phases and long-range ordering in the Alloy 22 base metal are not predicted in 10,000 years at 300 °C [572 °F]. Formation of 5- and

10-volume percent topologically close-packed phases in Alloy 22 welds is also not predicted for a 10,000-year life at 300 °C [572 °F]. Review of the DOE approach for the phase stability of Alloy 22 indicated the assumptions of the same precipitation kinetics for all secondary phases and the temperature-independent precipitation mechanism need to be evaluated further for Alloy 22. Reliance on the limited aging data also may lead to a large uncertainty in the extrapolation of the short-term, high-temperature results. Furthermore, the possible effects of compositional variation, cold work, and weld thickness on the kinetics of phase transformations in Alloy 22 have not been evaluated. On the other hand, the DOE theoretical modeling of phase transformations was based on simplified alloy systems and phases. Additional evaluations are necessary to assess the databases and validate the model predictions.

CNWRA performed a limited analysis to evaluate the effect of thermal aging on the microstructure of Alloy 22 for mill-annealed and welded conditions and to model the phase stability of Alloy 22 as influenced by compositional variations. Thermal exposure of the mill-annealed Alloy 22 at 870 °C [1,598 °F] for only 5 minutes, which may occur during fabrication of waste packages, resulted in formation of topologically close-packed phases at grain boundaries; however, no significant alloy depletion was detected in the grain-boundary regions. All aging and solution annealing treatments of the welded material conducted in this work promoted precipitation of the secondary phases. Results from both experiments and theoretical calculations indicated that heat-to-heat variations in the base metal and element segregation in the weld may affect significantly the stability of topologically close-packed phases as a consequence of the proposed fabrication and closure processes. This phase stability issue has not been adequately considered by DOE. According to agreements CLST 2.04 and 2.05, DOE agreed to conduct additional evaluations to reduce uncertainty and to provide additional information on the effects of the entire fabrication sequence on phase instability of both mill-annealed and welded Alloy 22 materials.

DOE evaluated the effects of welding and thermal aging on the uniform corrosion rate, localized corrosion, and stress corrosion cracking resistance of Alloy 22. The uniform corrosion rate of welded Alloy 22 was measured using weight loss specimens exposed to simulated groundwaters based on the variations of J–13 Well water. The effects of thermal aging on the corrosion rate of Alloy 22 were characterized using short-term electrochemical tests. The localized corrosion susceptibility of welded Alloy 22 was characterized using electrochemical tests in simulated groundwaters and concentrated chloride solutions. Based on the results of these tests, DOE assessed the effect of fabrication processes will not increase significantly the localized corrosion susceptibility of the Alloy 22 waste package outer barrier. The effects of fabrication processes are modeled by the DOE using an enhancement factor for the uniform corrosion rate that has a value distributed from 1 to 2.5. The effects of welding, postweld thermal aging and postweld solution annealing have been characterized using standardized tests. Corrosion rates measured after immersion of test specimens in boiling acid solutions also suggest that fabrication processes proposed for construction and closure of the waste packages do not degrade significantly the corrosion resistance of the alloy.

Limited tests conducted by DOE suggest the fabrication processes may increase the stress corrosion cracking susceptibility of Alloy 22 based on crack propagation rates for both cold-worked and thermally aged materials. Results of crack initiation tests under constant load conditions were likely compromised by galvanic protection of the test specimens by test fixtures.

CNWRA evaluated the effects of fabrication processes on the uniform corrosion rate and localized corrosion susceptibility using a range of electrochemical tests. Uniform corrosion rates for either thermally aged or welding materials were typically three to five times the corrosion rates for Alloy 22 in the mill-annealed condition. Although welding and thermal aging did not substantially increase the uniform corrosion rate, localized corrosion resistance was reduced significantly by either short-term thermal aging or welding. Crevice corrosion repassivation potential measurements also revealed a lower critical chloride concentration necessary to initiate localized corrosion for both thermally aged and welded Alloy 22. Localized corrosion on thermally aged materials was characterized by severe intergranular corrosion. Intergranular corrosion also was observed in the heat-affected zone of welded material, together with preferential attack in the fusion zone. Solution annealing was found beneficial for reducing the intergranular corrosion in the heat-affected zone but did not improve the localized corrosion resistance of the welded material. For both the mill-annealed and welded Alloy 22, nitrate was found an effective inhibitor of localized corrosion.

The CNWRA evaluation of the effects of fabrication processes on the stress corrosion cracking resistance of Alloy 22, conducted using thermally aged specimens, did not reveal an increased stress corrosion cracking susceptibility. Thermal aging, however, has led to intergranular corrosion, especially in crevices. According to agreements CLST 1.09, 1.10, 1.12, and 1.15, DOE will conduct additional evaluations to reduce uncertainty and provide additional information on the effects of fabrication processes on the uniform corrosion rate, localized corrosion susceptibility, and stress corrosion cracking resistance of Alloy 22.

1 INTRODUCTION

Performance of the engineered barriers after waste emplacement is important to protecting the public from any undue long-term risk, as recognized by the U.S. Department of Energy (DOE) in its repository safety strategy for the proposed Yucca Mountain repository (CRWMS M&O, 2000a). As an independent regulatory agency, the U.S. Nuclear Regulatory Commission (NRC) has published licensing criteria for disposing high-level wastes in the proposed repository. According to 10 CFR Part 63, the engineered barrier subsystem must be designed so that, working in combination with natural barriers, radiological exposures to the reasonably maximally exposed individual and release of radionuclides into the accessible environment are limited, as specified in 10 CFR 63.311. For these reasons, the performance of both the waste package and the drip shield, the two main components of the engineered barrier subsystem, are noted by DOE among the principal factors for the postclosure safety case (CRWMS M&O, 2000a). The reference waste package design in the DOE site recommendation (CRWMS M&O, 2000b) consists of an outer container made of a highly corrosion-resistant nickel-chromium-molybdenum alloy, Alloy 22 (Ni-22Cr-13Mo-4Fe-3W), and an inner container made of Type 316 nuclear grade stainless steel (low C-high N-Fe-18Cr-12Ni-2.5Mo). Additionally, an inverted U-shaped drip shield, fabricated with Titanium Grade 7 (Ti-0.15Pd), will be extended over the length of the emplacement drifts to enclose the top and sides of the waste packages. For undisturbed repository conditions, corrosion is expected to be the primary degradation process limiting the life of the waste package and the drip shield. Loss of containment as a result of corrosion will allow the release of radionuclides to the environment surrounding the waste packages.

The corrosion-related processes considered important in the degradation of the waste package and the drip shield include dry-air oxidation, humid-air and uniform aqueous (general) corrosion, localized (pitting, crevice, and intergranular) corrosion, microbially influenced corrosion, stress corrosion cracking, and hydrogen embrittlement. Fabrication processes such as cold work, welding, and residual stress mitigation methods such as induction annealing, laser peening, and low-plasticity burnishing may alter the microstructure and corrosion resistance of the waste package materials. Localized corrosion and stress corrosion cracking are known to occur in welds and in the weld heat-affected zone for iron-chromium-nickel and nickel-chromium-molybdenum alloys. Fabrication effects are known to contribute to failures of engineered components. This report focuses on the effect of fabrication processes on the material stability and corrosion of waste package materials. Emphasis was placed on the effects of fabrication processes on Alloy 22 because the waste package outer container is designed to be a corrosion resistant barrier, and the performance of the alloy may be affected by microstructural alterations that occur as a result of fabrication processes (CRWMS M&O 2000c,d,e).

1.1 Objective

In support of the NRC prelicensing activities on topics important to the postclosure performance of the proposed repository, the Center for Nuclear Waste Regulatory Analyses (CNWRA) is conducting an independent technical assessment of the effects of fabrication processes on the material stability and corrosion of engineered barrier materials. A summary of the effects of material stability on corrosion and stress corrosion cracking/environmental assisted cracking of nickel- and titanium-based alloys is provided in Cragnolino, et al. (1999). In addition, previous experimental work on the effects of fabrication processes on the thermal stability of Alloy 22 has been reported by Pan, et al. (2003). The effects of thermal aging and welding on the uniform

corrosion rate and localized corrosion resistance has been reported by Dunn, et al. (2003, 2000). This report provides a review of the DOE waste package design, fabrication methods, and material stability studies for Alloy 22, and presents results of more recent experimental work conducted at CNWRA.

1.2 Scope and Organization of the Report

Corrosion processes potentially important in the degradation of the engineered barriers have been reviewed in the Integrated Issue Resolution Status Report (NRC, 2002) and are the subject of Subissues 1 and 6 of the Container Life and Source Term Key Technical Issue (NRC, 2001). Fabrication processes may alter the mechanical properties, the range of passive film stability, and the localized corrosion resistance of the Alloy 22 outer container, which could lead to early through-wall penetration of the waste package. Several limitations and deficiencies in the DOE approach and in the technical bases provided for evaluating the effects of fabrication processes on the performance of the Alloy 22 waste package outer barrier have been identified by NRC (2002).

The DOE approach to evaluate the effects of fabrication processes on the degradation of Alloy 22 considers that the alloy will be susceptible to a marginal enhancement of the passive corrosion rate based on limited electrochemical corrosion tests. Enhanced susceptibility to localized corrosion is not considered based on the results of both immersion tests and short-term electrochemical tests in solutions where the initiation of localized corrosion is prevented by a high concentration of inhibitive species relative to the concentration of aggressive species known to promote localized corrosion and stress corrosion cracking. Additional tests to evaluate the effects of fabrication processes have been performed limited to standardized tests with specimens that do not represent the full range of fabrication processes that will be used to construct disposal containers and close the waste packages. It is not clear how the results of some standardized tests will be used to assess the performance of the waste packages.

Fabrication and closure of the waste packages will involve a range of forming and machining operations, welding, postweld heat treatments, and residual stress mitigation methods. Alloy 22 as well as other similar nickel-chromium-molybdenum alloys are known to exhibit phase instability at elevated temperatures. The formation of secondary phases as a consequence of welding or thermal exposure may promote localized corrosion, intergranular corrosion, and stress corrosion cracking leading to failure of the waste packages. Therefore, the effect of fabrication processes on the performance of the waste packages needs to be assessed.

This report is organized into five chapters including an introduction in Chapter 1. Waste package design and fabrication processes are discussed in Chapter 2. An overview of the fabrication process sequence and a description of the proposed fabrication methods and nondestructive examination methods are provided. Chapter 3 addresses the effect of fabrication processes on the microstructure of Alloy 22. A review of the DOE approach and results are included together with results of the microstructural evaluation performed at CNWRA. Chapter 4 addresses the effects of fabrication processes on passive dissolution, uniform corrosion, and stress corrosion cracking. A summary of conclusions and recommendations for future work to provide technical assistance needed to support the resolution of these closed-pending subissues prior to the license application is included in Chapter 5.

1.3 Relevant DOE and NRC Agreements

As noted, degradation processes of the waste package and the drip shield are considered in Subissues 1 and 6 of the Container Life and Source Term Key Technical Issue (NRC, 2001), and incorporated in the Degradation of Engineering Barriers Integrated Subissue (NRC, 2002). Through the process of prelicensing consultation for issue resolution between DOE and NRC, these two subissues are considered closed-pending according to the DOE and NRC agreements. Agreements pertaining to stress corrosion cracking and environmentally assisted cracking of container and drip shield materials are listed in Table 1-1. According to the agreements for resolving all deficiencies and limitations identified in this report, DOE agreed to provide additional information prior to license application.

Table 1-1. DOE and NRC Agreements Related to This Report

Agreement	Agreement Statement
CLST 1.01*	Provide the documentation for Alloy 22 and titanium for the path forward items listed on slide 8 (establish credible range of brine water chemistry; evaluate effect of introduced materials on water chemistry; determine likely concentrations and chemical form of minor constituents in Yucca Mountain waters; characterize Yucca Mountain waters with respect to the parameters which define the type of brine which would evolve; evaluate periodic water drip evaporation) DOE will provide the documentation in a revision to the Analyses Model Report Environment on the Surfaces of the Drip Shield and Waste Package Outer Barrier by license application.
CLST 1.02*	Provide the documentation for the path forward items listed on slide 12. (Surface elemental analysis of alloy test specimens is necessary for determination of selective dissolution; surface analysis of welded specimens for evidence of dealloying; continue testing including simulated saturated repository environment to confirm enhancement factor). DOE will provide the documentation in a revision to the Analysis Model Report General and Localized Corrosion of Waste Package Outer Barrier by license application.
CLST 1.09*	Provide the data that characterize the passive film stability, including the welded and thermally aged specimens. DOE will provide the documentation in a revision to Analysis and Model Reports (ANL–EBS–MD–000003 and ANL–EBS–MD–000004) prior to license application.

Table 1-1. DOE and NRC Agreements Related to This Report (continued)	
Agreement	**Agreement Statement**
CLST 1.10*	Provide the documentation for Alloy 22 and titanium for the path forward items listed on slides 21 and 22 (measure corrosion potentials in the long-term corrosion testing facility to determine any shift of potential with time toward the critical potentials for localized corrosion; determine critical potentials on welded and welded and aged coupons of Alloy 22 versus those for base metal—particularly important if precipitation or severe segregation of alloying elements occurs in the welds; separate effects of ionic mix of specimens in Yucca Mountain waters on critical potentials—damaging species from potentially beneficial species; determine critical potentials in environments containing heavy metal concentrations) DOE will provide the documentation in a revision to Analysis Model Reports (ANL–EBS–MD–000003 and ANL–EBS–MD–000004) prior to license application.
CLST 1.12*	Provide the documentation for Alloy 22 and titanium for the path forward items listed on slides 34 and 35 (qualify and optimize mitigation processes; generate stress corrosion cracking data for mitigated material over full range of metallurgical conditions; new vessels for long-term corrosion testing facility will house many of the stress corrosion cracking specimens; continue slow strain rate test in same types of environments as above, specimens in the same range of metallurgical conditions; determine repassivation constants needed for film rupture stress corrosion cracking model to obtain value for the model parameter 'n'; continue reversing direct current potential drop crack propagation rate determinations in same types of environments and same metallurgical conditions as for slow strain rate test and long-term corrosion testing facility tests; evaluate stress corrosion cracking resistance of welded and laser peened material versus nonwelded unpeened material; evaluate stress corrosion cracking resistance in induction annealed material; evaluate stress corrosion cracking resistance of full thickness material obtained from the demonstration prototype cylinder of Alloy 22) DOE will provide the documentation in a revision to Analysis Model Reports (ANL–EBS–MD–000005 and ANL–EBS–MD–000006) prior to license application.
CLST 1.13*	Provide the data that characterizes the distribution of stresses due to laser peening and induction annealing of Alloy 22. DOE will provide the documentation in a revision to Analysis Model Report (ANL–EBS–MD–000005) prior to license application.

Table 1-1. DOE and NRC Agreements Related to This Report (continued)	
Agreement	**Agreement Statement**
CLST.1 15*	Provide the documentation for Alloy 22 and titanium for the path forward items listed on slide 39 (install specimens cut from welds of site recommendation design mockup in long-term corrosion test facility and in other stress corrosion cracking test environments—determine which specimen geometry is most feasible to complement stress corrosion cracking evaluation; evaluate scaling and weld process factors between thin coupons and dimensions in actual welded waste package containers—including thermal/metallurgical structural effects of multipass weld processes; provide representative weld test specimens for microbially influenced corrosion work, thermal aging and localized corrosion evaluations) DOE will provide documentation for Alloy 22 and titanium path forward items on slide 39 in a revision to the stress corrosion cracking and general and localized corrosion Analysis Model Reports (ANL–EBS–MD–000003, ANL–EBS–MD–000004, ANL–EBS–MD–000005) by license application.
CLST 1.16*	Provide the documentation on the measured thermal profile of the waste package material due to induction annealing. DOE stated that the thermal profiles will be measured during induction annealing, and the results will be reported in the next stress corrosion cracking Analysis Model Report (ANL–EBS–MD–000005) prior to license application.
CLST 2.04*	Provide information on the effect of the entire fabrication sequence on phase instability of Alloy 22, including the effect of welding thick sections using multiple weld passes and the proposed induction annealing process. DOE stated that the aging studies will be expanded to include solution annealed and induction annealed Alloy 22 weld and base metal samples from the mock-ups as well as laser peened thick, multi-pass welds. This information will be included in revisions of the Analysis Model Report Aging and Phase Stability of the Waste Package Outer Barrier, ANL–EBS–MD–000002, before license application.

Table 1-1. DOE and NRC Agreements Related to This Report (continued)	
Agreement	**Agreement Statement**
CLST 2.05*	Provide the Aging and Phase Stability of Waste Package Outer Barrier, Analysis Model Report, including the documentation of the path forward items listed in the Subissue 2: Effects of Phase Instability of Materials and Initial Defects on the Mechanical Failure and Lifetime of the Containers presentation, slides 5 and 6 (data input to current models is being further evaluated and quantified to reduce uncertainty; aging of Alloy 22 samples for microstructural characterization, tensile property test, and Charpy impact test is ongoing; theoretical modeling will be employed to enhance confidence in extrapolating aging kinetic data to repository thermal conditions and time scale—modeling will utilize thermodynamic principles of the processes; Alloy 22 samples for stress corrosion cracking compact tension test are being added to aging studies; test program will be expanded to include welded and cold worked materials; effects of stress mitigation techniques such as laser peening and induction annealing on phase instability will be investigated; aging test facility will be expanded to include aging at lower temperatures) DOE stated that the Aging and Phase Stability of the Waste Package Outer Barrier Analysis Model Report, ANL–EBS–MD–000002, Revision 00 was issued March 20, 2000. This analysis model report will be revised to include the results of the path forward items before license application.
CLST 2.07*	Provide documentation for the fabrication process, controls, and implementation of the phases which affect the total system performance assessment model assumptions for the waste package (e.g., filler metal, composition range). DOE stated that updates of the documentation on the fabrication processes and controls (TDR–EBS–ND–000003, Waste Package Operations Closure Weld Tech. Guidelines Fabrication Process Report and TDP–EBS–ND–000005, Waste Package Operations Fiscal Year 2000 Closure Weld Technical Guidelines Document) will be available to the NRC in January 2001.

Table 1-1. DOE and NRC Agreements Related to This Report (continued)	
Agreement	**Agreement Statement**
CLST 2.08*	Provide documentation of the path forward items in the Subissue 2: Effects of Phase Instability of Materials and Initial Defects on the Mechanical Failure and Lifetime of the Containers presentation, slide 16 [future rockfall evaluations will address (i) effects of potential embrittlement of waste package closure material after stress annealing due to aging, (ii) effects of drip shield wall thinning due to corrosion; (iii) effects of hydrogen embrittlement on titanium drip shield; and (iv) effects of multiple rock blocks falling on waste package and drip shield; future seismic evaluations will address the effects of static loads from fallen rock on drip shield during seismic events]. DOE stated that the rockfall calculations addressing potential embrittlement of the waste package closure weld and rock falls of multiple rock blocks will be included in the next revision of the Analysis Model Report ANL–UDC–MD–000001, Design Analysis for UCF Waste Packages, to be completed prior to license application. Rockfall calculations addressing drip shield wall thinning due to corrosion, hydrogen embrittlement of titanium, and rock falls of multiple rock blocks will be included in the next revision of the AMR ANL–XCS–ME–000001, Design Analysis for the Ex-Container Components, to be completed prior to license application. Seismic calculations addressing the load of fallen rock on the drip shield will be included in the next revision of the AMR ANL–XCS–ME–000001, Design Analysis for the Ex-Container Components, to be completed prior to license application.

*Schlueter, J.R. "U.S. Nuclear Regulatory Commission/U.S. Department of Energy Technical Exchange and Management on Container Life and Source Term (September 12–13, 2000)." Letter (October 4) to S. Brocoum, DOE. Washington, DC: NRC. 2000.

2 DESIGN OF THE WASTE PACKAGE

Once the disposal container is filled with radioactive waste, sealed, and inspected, it is referred to as the waste package. The waste package will be designed to accommodate the various expected waste forms. It will also be designed to protect worker and public health and safety during operations and before final closure of the repository, as defined in 10 CFR Part 63 Subpart K. Specifically, the U.S. Department of Energy (DOE) must ensure that no member of the public in the general environment receives more than an annual dose of 0.15 mSv [15 mrem].

Finally, the waste package design will support attaining long-term repository objectives as defined in 10 CFR Part 63 Subpart L, which includes individual protection, human intrusion, and groundwater protection standards. Using performance assessment, DOE must demonstrate there is a reasonable expectation that for 10,000 years following disposal, the reasonably maximally exposed individual receives no more than an annual dose of 0.15 mSv [15 mrem] from releases from the undisturbed Yucca Mountain disposal site.

2.1 Physical Description of Waste Package

There are several broad classes of waste forms expected for disposal in the repository. These include commercial spent nuclear fuel, plutonium disposition waste, high-level waste, and DOE spent nuclear fuel, as schematically depicted in Figure 2-1.

To accommodate these classes of waste forms, a suite of 10 waste packages has been proposed in the license application. A brief description of these is given in Table 2-1. Four representative waste packages from this set will be more fully developed at the point of license application for construction authorization (Anderson, et al., 2003). These four are indicated with a dagger in Table 2-1.

The 21 PWR (pressurized water reactor) commercial spent nuclear fuel assembly using a neutron absorber plate is the predominant waste package design. This design will contain approximately 38 percent of the repository's capacity of 70,000 metric tons [77,140 tons] of heavy metal (CRWMS M&O, 2002). A schematic of this waste package design is shown in Figure 2-2.

All waste package designs will consist of two concentric cylinders (Figure 2-2). The inner cylinder will be designed for structural support and will be constructed of Type 316 nuclear grade stainless steel. The outer cylinder will be designed for long-term corrosion resistance in the repository environment and will be constructed of Alloy 22. Each waste package design will have a bottom and a top outer lid made of Alloy 22 and two corresponding inner lids made of Type 316 nuclear grade stainless steel. In addition, a second Alloy 22 top closure lid will be used to provide further protection against stress corrosion cracking in the closure weld area (CRWMS M&O, 2002). Upon closure, the inner cylinder will be backfilled with inert, thermally conductive helium gas.

Although they share the features described previously, the internal components of waste packages will vary to accommodate different waste forms. For example, the waste package for uncanistered commercial fuel will have an internal basket designed to support fuel assemblies.

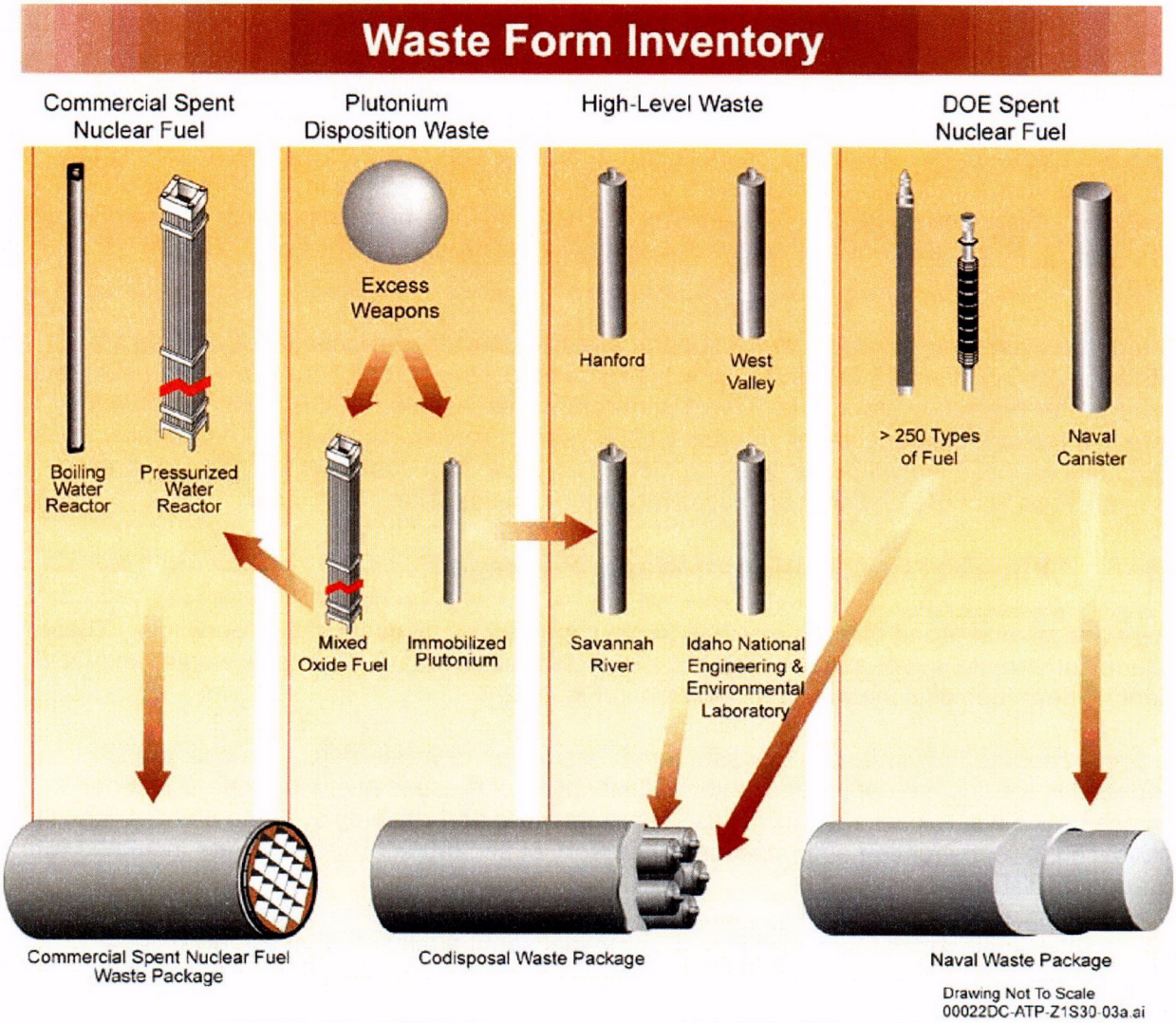

Figure 2-1. Waste Form Inventory (CRWMS M&O, 2002)

In other waste packages, the internal basket will have a different design, or the basket will be contained inside a canister.

The internal components of the commercial spent nuclear fuel waste package illustrated in Figure 2-2 include internal baskets that are composed of interlocking plates, fuel tubes, thermal shunts, and structural guides. The interlocking plates are designed to prevent criticality. They also help with heat transfer and provide structural support for the fuel tubes. The baskets are long, square containers that line the insides of the cavities formed by the interlocking plates. The fuel tubes, in turn, provide support for the fuel assemblies. Thermal shunts are added to facilitate heat transfer from the waste form to the walls of the waste package. Structural guides are used to hold the basket structure in place inside the waste package. Control rods are used in waste packages that need additional long-term criticality control.

C01

Table 2-1. Waste Package Design*	
Waste Package Design	**Description**
21 PWR† absorber plate‡	Capacity: 21 commercial pressurized water reactor assemblies and absorber plates for preventing criticality
21 PWR control rod	Capacity: 21 commercial pressurized water reactor assemblies with higher reactivity, requiring additional criticality control provided by placement of control rods in all assemblies
12 PWR long	Capacity: 12 commercial pressurized water reactor assemblies and absorber plates for preventing criticality; longer than fuel assemblies placed in 21 pressurized water reactor packages; because of its smaller capacity, it also may be used for fuel with higher reactivity or thermal output
44 BWR§‡	Capacity: 44 commercial boiling water reactor assemblies and absorber plates for preventing criticality
24 BWR	Capacity: 24 commercial boiling water reactor assemblies and absorber plates for preventing criticality
5 defense high-level waste/DOE spent nuclear fuel short‡	Capacity: 5 short high-level waste canisters and 1 short DOE spent nuclear fuel canister. When high-level waste includes immobilized plutonium cans, no DOE spent nuclear fuel is placed in the center.‖
5 defense high-level waste/DOE spent nuclear fuel long	Capacity: 5 long high-level radioactive waste canisters and one long spent nuclear fuel canister‖
2 multicanister overpacks/ 2 defense high-level waste long	Capacity: 2 DOE multicanister overpacks and 2 long high-level waste canisters
Naval spent nuclear fuel short	Capacity: 1 short Naval spent nuclear fuel canister
Naval spent nuclear fuel long‡	Capacity: 1 long Naval spent nuclear fuel canister

*CRWMS M&O. "Yucca Mountain Science and Engineering Report—Technical Information Supporting Site Recommendation Consideration." DOE/RW–0539–1. Rev. 1. Las Vegas, Nevada: DOE, Office of Civilian Radioactive Waste Management. 2002.
†PWR—pressurized water reactor.
‡These designs will be developed further at license application for construction authorization.
§BWR—boiling water reactor.
‖DOE non-Naval spent nuclear fuel.

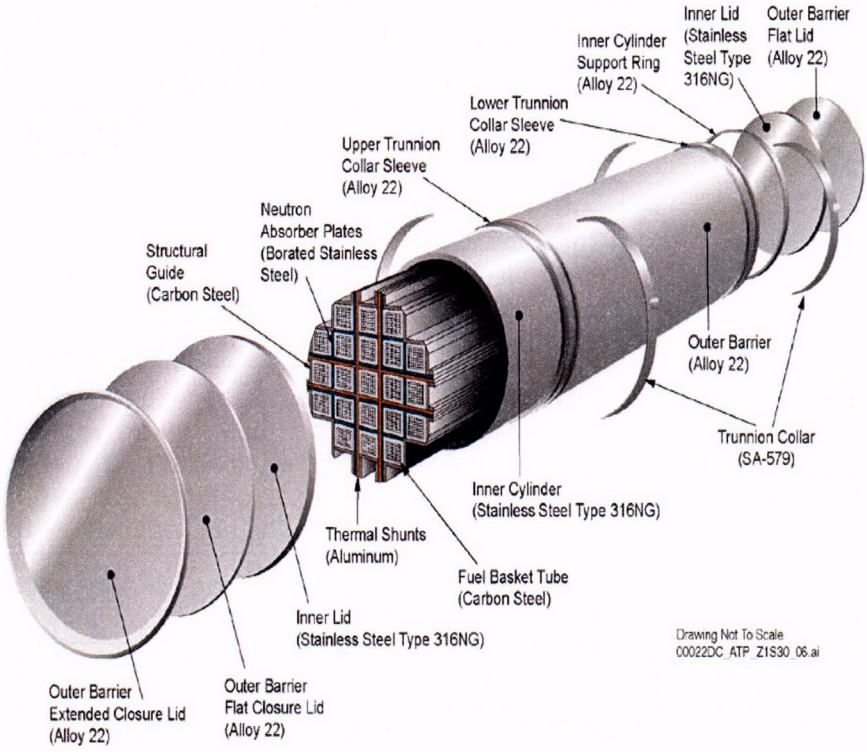

Figure 2-2. 21 Pressurized Water Reactor Absorber Plate Waste Package Design (CRWMS M&O, 2002)

2.1.1 Rationale for Selection of Material of Construction for the Outer Disposal Container

Corrosion resistance is the most important criterion to assure a long waste package lifetime. Predicting the rate of corrosion for the 10,000-year regulatory period requires a good understanding of the temperature, humidity, and environmental conditions that would exist at various times for a range of thermal operating modes in the emplacement drifts. Essential performance qualities of the selected material would have to include resistance to general and localized corrosion, stress corrosion cracking, and hydrogen embrittlement. The effects of long-term thermal aging are also important (CRWMS M&O, 2002). Uniform corrosion rate, localized corrosion susceptibility, and the stress corrosion cracking resistance of the material used may be affected also by the thermal and mechanical processes necessary to fabricate and close the outer disposal container.

A review of waste package designs and candidate materials has been reported by McCright (1988). Recent waste package designs have been proposed with a combination of A516 carbon steel and Alloy 825 (42Ni-30Fe-22Cr-3Mo-2Cu), Alloy 625 (60Ni-22Cr-9Mo-4Nb-4Fe), and Alloy 22 (58Ni-22Cr-13Mo-4Fe-3W). The Total System Performance Assessment–Site Recommendation waste package is designed with an Alloy 22 outer container and a Type 316 nuclear grade stainless steel inner container. Table 2-2 provides the chemical composition of Alloy 22.

C02

Table 2-2. Chemical Composition of Alloy 22*	
Element	**Composition (Weight Percent)**
Carbon (C)	0.015 (max)
Manganese (Mn)	0.50 (max)
Silicon (Si)	0.08 (max)
Chromium (Cr)	20.0 to 22.5
Molybdenum (Mo)	12.5 to 14.5
Cobalt (Co)	2.50 (max)
Tungsten (W)	2.5 to 3.5
Vanadium (V)	0.35 (max)
Iron (Fe)	2.0 to 6.0
Phosphorus (P)	0.02 (max)
Sulfur (S)	0.02 (max)
Nickel (Ni)	Balance

Source: ASTM International B 575-97, Standard Specification for Low-Carbon Nickel-Molybdenum-Chromium, Low-Carbon Nickel-Chromium-Molybdenum, Low-Carbon Nickel-Chromium-Molybdenum-Copper, and Low-Carbon Nickel-Chromium-Molybdenum-Tungsten Alloy Plate, Sheet, and Strip.

*CRWMS M&O. "Yucca Mountain Science and Engineering Report—Technical Information Supporting Site Recommendation Consideration." DOE/RW-0539-1. Rev. 1. Las Vegas, Nevada: DOE, Office of Civilian Radioactive Waste Management. 2002.

2.1.2 Rationale for Selection of Material of Construction for the Inner Disposal Container

The main function of the inner cylinder of the disposal container is to provide structural strength. Type 316 nuclear grade stainless steel is the chosen material of construction for this cylinder. This material has a better compatibility with Alloy 22 than carbon steel and provides the required strength in a cost effective manner (CRWMS M&O, 2002).

Although resistance to corrosion is not a primary consideration in selecting the material of construction for the inner cylinder of the disposal container, it may be useful to consider the corrosion behavior of Type 316 nuclear grade stainless steel for the chemical and thermal conditions of the repository environment. Performance issues such as (i) the susceptibility of Type 316 nuclear grade stainless steel to localized corrosion, in particular, crevice corrosion; (ii) the reduction of the fracture toughness of the weld material because of the presence of ferrite at repository temperatures; and (iii) interactions of the internal components of the waste package with the inner cylinder for chemical and environmental conditions inside the waste

package need to be evaluated. These issues are explored in Cragnolino, et al. (1999). The composition of Type 316 nuclear grade stainless steel is detailed in Table 2-3.

2.1.3 Rationale for Selection of Materials for the Internal Components of the Waste Package for Uncanistered Commercial Fuel Assemblies

The internal components of the waste package include structural guides, interlocking plates, fuel basket tubes, and thermal shunts. The key factors to be considered in selecting these components include mechanical and thermal performances, and compatibility with other materials in the waste package. Mechanical performance is important because components must be capable of sustaining the mechanical loads created by handling, emplacement, and retrieval (if required) of the waste package. Thermal performance is also important as the components are relied on to efficiently conduct heat from the waste form to the walls of the waste package. Chemical compatibility of the fuel tubes with the waste form and the plates is needed to prevent excessive release rates from degradation of the waste form and the loss of criticality control from degradation of the plates (CRWMS M&O, 2002).

After considering two grades of carbon steel (SA 516 Grades 55 and 70), Grade 70 was chosen as the material of construction for the structural guides and fuel basket tubes (Figure 2-2) (CRWMS M&O, 2002).

Performance issues with regard to carbon steel include mechanical embrittlement {from long-term exposure to temperatures in the 200–300 °C [392–572 °F] range}, corrosion, and environmentally-assisted cracking (stress corrosion cracking and hydrogen effects). Despite the extensive investigation of carbon steel for use in a variety of applications, it is important to evaluate the performance for repository conditions. This evaluation is discussed in Sridhar, et al. (1994).

Neutron absorbers are used to reduce the potential for criticality. These materials are typically an additive to a carrier material (e.g., stainless steel alloyed with a boron compound). For the reasons cited in the preceding paragraphs, mechanical and thermal performances, corrosion resistance, and chemical compatibility are all key factors to be considered when selecting materials of construction for these plates.

After careful assessment, Neutronit A978 (having a composition similar to SA 240 stainless steel Type 316, but with 1.6-percent boron added) was selected as the material of construction for the interlocking neutron absorber plates (Figure 2-2) (CRWMS M&O, 2002). Fuel rods are included in another design of the 21 pressurized water reactors.

Control rods are used in waste packages that need additional long-term criticality control. These rods are made of boron carbide and have Zircaloy cladding. Because most fuel rod cladding is also made of Zircaloy, the corrosion properties and longevity of the control rods will be similar to that of fuel rods (CRWMS M&O, 2002).

The main function of thermal shunts is to provide an additional path for conducting heat from the waste form (i.e., commercial spent nuclear fuel) to the walls of the waste package. Therefore, thermal conductivity and chemical compatibility with the materials of the waste form are important factors in selecting the material of construction for this component. Because thermal shunts are only needed during the early period of repository performance when the decay heat

Table 2-3. Chemical Composition of Type 316 Nuclear Grade Stainless Steel*	
Element	**Composition (Weight Percent)**
Carbon (C)	0.020 (max)
Phosphorus (P)	0.030 (max)
Silicon (Si)	0.75 (max)
Copper (Cu)	0.50 (max)
Titanium (Ti)	0.05 (max)
Tantalum (Ta) and Niobium (Nb)	0.05 (max)
Manganese (Mn)	2.00 (max)
Sulfur (S)	0.005 (max)
Nitrogen (N)	0.060 to 0.10
Cobalt (Co)	0.10 (max)
Boron (B)	0.002 (max)
Bismuth (Bi) + Tin (Sn) + Arsenic (As) + Lead (Pb) + Antimony (Sb) + Selenium (Se)	0.02 (max)
Chromium (Cr)	16.00 to 18.00
Molybdenum (Mo)	2.00 to 3.00
Nickel (Ni)	11.00 to 14.00
Vanadium (V)	0.1 (max)
Aluminum (Al)	0.04 (max)
Iron (Fe)	Balance

Sources: For all elements except carbon and nitrogen, values presented are within the ranges and maximum limits provided by ASTM International A 276-91a, Standard Specification for Stainless and Heat-Resisting Steel Bars and Shapes. Values for carbon and nitrogen are given by Danko, J.C. "Corrosion in the Nuclear Power Industry." *Corrosion Metals Handbook.* 9th Edition. Vol. 13. Metals Park, Ohio: ASM International. pp. 928–934c. 1987.

*CRWMS M&O. "Yucca Mountain Science and Engineering Report—Technical Information Supporting Site Recommendation Consideration." DOE/RW–0539–1. Rev. 1. Las Vegas, Nevada: DOE, Office of Civilian Radioactive Waste Management. 2002.

is relatively high, corrosion resistance is not of primary importance. However, the material must be able to withstand the service loads during handling, emplacement, and retrieval operations, and mechanical performance is a consideration. Aluminum Alloys 6061 and 6063 were selected rather than copper because copper can react with chloride ions from a breached waste package and lead to the accelerated degradation of the Zircaloy fuel cladding culminating in the release of radionuclides from the waste (Figure 2-2) (CRWMS M&O, 2002). Table 2-4 provides the composition of aluminum Alloys 6061 and 6063.

Table 2-4. Aluminum Alloys—Composition, Percent*

UNS	Common Name	Chromium	Copper	Magnesium	Manganese	Silicon	Zinc
A96061	Al 6061	0.04–0.35	0.15–0.40	0.8–1.2	0.15 max	0.40–0.8	0.25 max
A96063	Al 6063	0.10 max	0.10 max	0.45–0.9	0.10 max	0.20–0.6	0.10 max

*NACE International. *NACE Corrosion Engineer's Reference Book.* 2nd Edition. R.S. Treseder, R. Baboian, and C.G. Munger, eds. Houston, Texas: NACE International. 1991.

Helium has been selected as the fill gas for the inner cylinder of the waste package. It is an inert gas, routinely used as the fill gas for fuel rods. Therefore, it is not expected to degrade the spent nuclear fuel or waste package. Helium also has good thermal conductivity, which is important for the efficient conduction of heat from the waste form to the internal basket in the waste package. For these reasons it was chosen rather than other gases such as nitrogen, argon, and krypton (CRWMS M&O, 2002).

2.1.4 Internal Components of Other Waste Package Designs

In addition to commercial spent nuclear fuel, the proposed repository will also be used for emplacement of high-level waste, plutonium disposition waste, and DOE spent nuclear fuel (see Figure 2-1). Liquid high-level waste will be vitrified to form a leach-resistant borosilicate glass that will be poured into Type 304L SS canisters, allowed to solidify, and the canisters sealed. In addition, surplus plutonium, which has been immobilized into ceramic discs, will be placed in empty Type 304L SS canisters before these are filled with the high-level borosilicate glass waste. The high-level waste canisters will be packaged with other DOE spent nuclear fuel in codisposal waste packages. Sealed canisters of spent Naval nuclear fuel will be placed directly into waste packages at the repository. Being larger in size, these canisters will not be placed in codisposal packages. Canister guides made of carbon steel (SA 516 Grade 70) will be used to hold the canisters in place inside the waste package (CRWMS M&O, 2002).

2.1.5 Physical Description and Functions of the Waste Package Pallet

The waste package pallet is designed to hold the waste package and maintain it in its normal emplacement position during the preclosure period of up to 300 years. The pallet will also maintain the waste package in its nominal horizontal position for 10,000 years after closure (CRWMS M&O, 2002). The pallet assembly will be fabricated from Alloy 22 plates welded together to form two V-shaped top surfaces, one at each end of the pallet. These will be interconnected by four horizontal square tubes made of Type 316L SS (Figure 2-3). All surfaces in contact with the waste package will, therefore, be made of Alloy 22. Because the

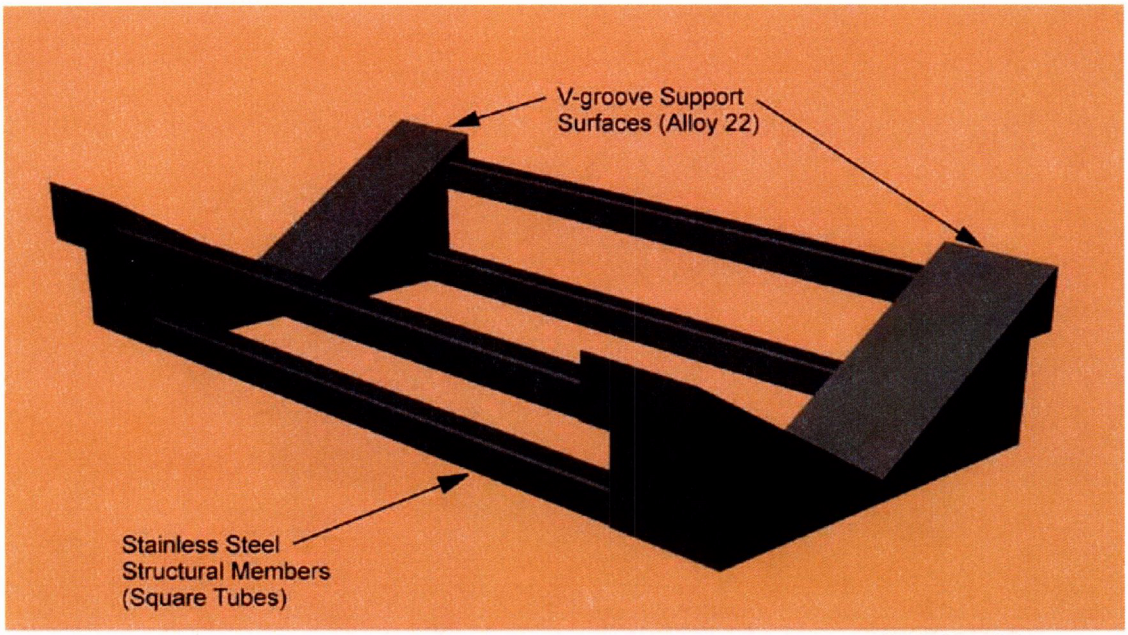

Figure 2-3. Emplacement Pallet Isometric View (CRWMS M&O, 2002)

waste package will cause compressive loads on the end assemblies, it is assured the pallet will not be susceptible to stress corrosion cracking, and corrosion is expected to be negligible during the 300-year preclosure period (CRWMS M&O, 2002). Pallets will be fabricated in two sizes to accommodate all types of waste packages. The V-shaped design of the top surfaces makes it possible for the pallets to accept all waste package diameters. The pallets will be shorter than the waste packages to allow end-to-end close packing of the packages within 10 cm [4 in] of each other in the repository drifts. The packages will rest on the V-groove top surface of the pallets and will be supported between the trunnion collars by the package (Figure 2-4) (CRWMS M&O, 2002).

2.2 Fabrication Methods for the Waste Package

All disposal containers will be fabricated in nearly identical fashion. Because not all disposal container designs have been fully developed, the uncanistered fuel disposal container, which is one of the waste package baseline designs, will be presented in this section. All disposal containers will be constructed of a Type 316 nuclear grade stainless steel inner cylinder to provide structural integrity or sufficient strength and an Alloy 22 outer corrosion barrier (CRWMS M&O, 2001a). This combination of materials is selected for the long-term protection of the inner container material and the contained waste form.

2.2.1 Fabrication and Testing Conditions

Although the disposal container will be fabricated in accordance with requirements of ASME International (1995a) to the maximum extent possible, the disposal container is not a pressure vessel and will not be nuclear or N-stamped (CRWMS M&O, 2001a). ASME

C03

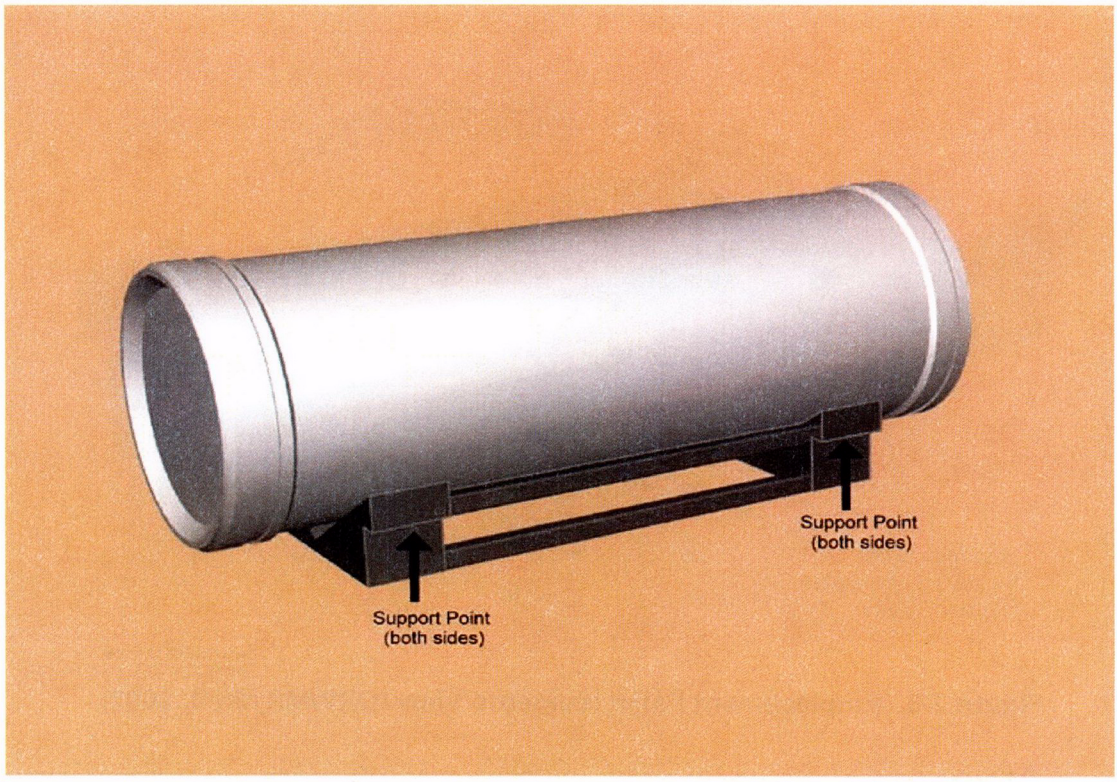

Figure 2-4. Emplacement Pallet Loaded with Waste Package (CRWMS M&O, 2002)

International (1995a) provides a standard for the fabrication of the disposal containers and requirements for inspection.

All materials will be examined per the ASME International Code (1995b) before use in fabrication. Materials used in fabrication of the disposal containers will meet the requirements in ASME International (1995a, Article NB–2000). Expendable materials such as cleaning solvents, materials used for nondestructive examination penetrant tests, and other materials that contact the disposal container surfaces will be low chloride/halogen (less than 100 parts per million) and will not contain more than 200 parts per million total of metal and metal salts such as zinc, lead, copper, cadmium, mercury, or other low-melting metals (CRWMS M&O, 2001a).

Weld filler materials will conform to ASME International requirements (1995c). Filler material for the Type 316 nuclear grade stainless steel inner container will be controlled so that the delta ferrite content in the as-deposited weld filler metal has a ferrite number between 5 and 15, determined by Magna-gage measurements (CRWMS M&O, 2001a). The weld filler material for the Alloy 22 outer container will be ERNiCrMo-10 or a filler material used for welding alloys with the unified numbering system number N06022 designation (CRWMS M&O, 2001a).

The requirements of ASME International (1995d) will be followed for weld preparation and for the procedures used for welding the disposal containers. Welding will not be performed if the

C04

base metal temperature is less than 0 °C [32 °F]. The maximum interpass temperature for both inner and outer container materials will be 175 °C [350 °F]. Each weld pass will be visually free of slag, inclusions, cracks, unacceptable porosity, and lack of fusion. Permissible welding processes used for disposal container fabrication will be limited to shielded metal arc, gas tungsten arc, submerged arc, and gas metal arc. The processes, procedures, or both, will be qualified for the material to be welded (CRWMS M&O, 2001a).

Performance of weld repairs to correct defects in the disposal container will be allowed provided the defects and repairs are appropriately documented, and repairs are made in accordance with ASME International requirements (1995a, Article NB–4000). Only three repair cycles will be permissible without special approval (CRWMS M&O, 2001a).

2.2.2 Inspection of Welds—Methods Used and Acceptance Criteria

Visual examination of finished surfaces of welds of the disposal container will be in accordance with ASME International requirements (1995b, Article 9). Requirements from the ASME International Code (1995a) will be used to verify the external components are assembled per engineering drawings and are free of nicks, gouges, or other damage. The acceptance criteria for visually examined welds will be in accordance with the ASME International Code (1995a, NF–5360; CRWMS M&O, 2001a).

Liquid penetrant examination of welds will be in accordance with the ASME International Code (1995b, Article 6). The acceptance criteria for penetrant examination examined welds will be in accordance with the ASME International Code (1995a, Article NB–5350; CRWMS M&O, 2001a).

Ultrasonic examination of welds will be in accordance with the ASME International Code (1995b, Article 5). The acceptance criteria for ultrasonic examined welds will be in accordance with the ASME International Code (1995a, Article NB–5330; CRWMS M&O, 2001a). Radiographic examination of welds will be in accordance with the ASME International Code (1995b, Article 2). The acceptance criteria for radiographic examined welds will be in accordance with the ASME International Code (1995a, Article NB–5320; CRWMS M&O, 2001a).

2.2.3 Outer Alloy 22 Disposal Container Fabrication

The outer Alloy 22 cylinder will be fabricated from flat metal plates. The plates will be rolled and welded to form the cylinder. Top and bottom lids will be cut and prepared from flat metal plates before being welded to the cylinder. Trunnion collar sleeves will be similarly cut and fabricated from plate material and fitted to the cylinder.

2.2.3.1 Fabrication of the Alloy 22 Outer Cylinder

Size limitations of most, if not all, available rolling equipment will make it necessary to use at least two plates for the fabrication of this cylinder. It is estimated that two rectangular Alloy 22 plates, of the required minimum dimensions but having extra thickness, will be available for fabrication of the cylinder. These plates will be rolled and welded to form two half-length cylinders, which then will be circumferentially welded end to end to form the outer cylindrical

wall of the disposal container. The extra thickness is needed to permit machining of the cylinders to acceptable dimensions after welding (CRWMS M&O, 2001a).

The sequence of operations for fabrication of the outer cylindrical wall of the disposal container will be as follows. The Alloy 22 plate, procured in accordance with specifications, will be receipt inspected, laid out to establish the developed length, and cut to the layout. The plate then will be rolled to size. The cylinder will be adjusted to meet the requirements for diameter and inner circumference. The long seam will be machined and prepared for welding and welded using one of the four approved welding methods. The cylinder may need to be strutted or collapsible mandrels may be used to minimize weld distortion. The struts or mandrels then will be removed and the weld seam prepared for nondestructive examination. The nondestructive examination will include penetrant, radiographic, and ultrasonic examinations. Finally, one end of the cylinder will be prepared for circumferential seam welding. This may require strutting of the cylinder. In parallel, a second identical cylinder will be fabricated using the second Alloy 22 plate. The two cylinders will be joined end to end and circumferentially seam welded using one of the four approved methods. The seam will be prepared for nondestructive examination after removal of the struts, and nondestructive examination will be performed on the weld using penetrant, radiographic, and ultrasonic examination testing. The cylinder will be inspected to verify dimensions including a minimum allowable plate thickness. The inside will be machined to allow for a loose fit {0–4 mm [0–157 in] radial gap} with the stainless steel reinforcement cylinder (CRWMS M&O, 2001a).

2.2.3.2 Fabrication and Assembly of the Alloy 22 Support Ring

The support ring is needed to hold the inner container after it is placed in the outer container. To fabricate the ring, a rectangular piece will be cut from an Alloy 22 plate and rolled into a circular shape. Weld preparations will be made on both circumferential faces, and the ring will be fitted at the bottom end of the cylinder before being welded on both sides. Both welds then will be machined flush to enable the bottom lid to be set on the bottom of the ring and the inner container to be set on the top of the ring. Penetrant examination will be performed on the machined surfaces (CRWMS M&O, 2001a).

2.2.3.3 Fabrication and Assembly of the Alloy 22 Bottom and Top Lids

The outer container will have one bottom lid and two top lids, each made of Alloy 22. The bottom lid will be fabricated from a rectangular plate. The plate will be cut to the correct diameter and the edges cleaned to remove slag and scale before being machined to establish weld preparation (CRWMS M&O, 2001a).

To assemble the bottom lid, the Alloy 22 cylinder will be set in the horizontal position and the lid welded to the cylinder in this position using the gas metal-arc or gas tungsten-arc method. The lid seam then will be prepared for nondestructive examination and inspected using penetrant, radiographic, and ultrasonic examinations (CRWMS M&O, 2001a).

Significant changes to the design of the Alloy 22 top outer lid have been proposed and are still being reviewed by DOE. In the proposed design for license application, this lid design has been modified to eliminate the outer lid extension (Anderson, et al., 2003). Detailed information is not available at present on the modified closure lid design and fabrication methods. The equipment

and operational sequences described in this section reflect the design described in CRWMS M&O (2001a).

The outer top lid will be fabricated from a flat plate. A rectangular plate will be cut to the correct diameter and the edges cleaned to remove slag and scale before being machined to establish weld preparation. A center lifting fixture will be fabricated from a plate. The plate will be laid out, cut to size, deburred, and machined to correct dimension. The attachment then will be welded to the center of the lid (CRWMS M&O, 2001a).

The outer shell middle lid will be fabricated from an Alloy 22 flat plate. The plate will be laid out, flame cut, and deburred around the cut area. A center lifting fixture will be fabricated from a second plate and welded to the center of the lid (CRWMS M&O, 2001a).

2.2.3.4 Trunnion Collar Fabrication

The disposal container will have two trunnion collar sleeves made out of Alloy 22—one for each end of the outer cylinder of the disposal container. The sleeves will be of slightly different dimensions, fabricated as follows: two sleeves of the required length and width will be cut from an Alloy 22 plate and will be rolled into two cylinders. One or two longitudinal welds will be used to join each cylinder. Each cylinder then will be rounded and machined such that the inside diameter of the trunnion sleeve fits around the outside diameter of the Alloy 22 disposal container. The trunnion sleeves will be fitted onto the disposal container by heating each sleeve to approximately 371 °C [700 °F], positioning it over the disposal container and allowing it to cool (CRWMS M&O, 2001a).

Because of lessons learned from fiscal year 2000 closure weld mockup, the assembly sequence of the inner ring, bottom lid, and lower trunnion ring may be altered (CRWMS M&O, 2000f). Higher than expected distortion during the inner ring and bottom lid welding may necessitate the assembly and partial welding of the lower trunnion ring prior to welding the inner ring and bottom lid. The trunnion ring would provide reinforcement for the other welds and reduce distortion (CRMWS M&O, 2000f).

2.2.3.5 Solution Annealing

After assembly of the support ring, bottom lid, and trunnion collars, the Alloy 22 outer cylinder assembly will be solution annealed at approximately 1,125 °C [2,057 °F] to eliminate residual stresses created during the fabrication processes. The outer cylinder will be placed on a furnace car inside a furnace heated to 1,150 °C [2,102 °F]. The soak time at 1,150 °C [2,102 °F] was not specified. The furnace car and cylinder assembly then will be removed from the furnace, and the outer cylinder will be quenched using water spray on the inside and outside surfaces of the cylinder to quickly reduce the temperature from 1,100 °C [2,012 °F] to below 800 °C [1,472 °F] in approximately 4 minutes. The cooling rate then will be decreased to allow for the formation of compressive stresses on the outside (CRWMS M&O, 2001a).

2.2.4 Inner Type 316 Nuclear Grade Stainless Steel Disposal Container Fabrication

The main function of the inner cylinder of the disposal container is to provide structural strength. This cylinder will be constructed of Type 316 nuclear grade stainless steel and will be of thick

wall construction for strength. Like the outer cylinder, this cylinder will be fabricated from flat metal plates (CRWMS M&O, 2001a).

2.2.4.1 Fabrication of the Type 316 Nuclear Grade Stainless Steel Inner Cylinder

The Type 316 nuclear grade stainless steel inner cylinder will be rolled from two rectangular plates. These will be roll-formed and welded to make two half-length cylinders, which then will be welded end to end to form the inner cylinder (CRWMS M&O, 2001a).

The fabrication sequence will be similar to that employed for the Alloy 22 outer cylinder and will include the following main steps. Type 316 nuclear grade stainless steel plates, procured in accordance with specifications, will be cut, machined for size, or both, and prepared for longitudinal welding. Each plate will be roll-formed to make a cylinder of the required diameter but half the length. The rolled plate will be welded longitudinally using one of the four acceptable methods, and the weld subsequently will be examined using penetrant examination. The two half-length cylinders will be prepared for circumferential welding, and welded end to end using one of the four approved methods. Penetrant examination inspection will be performed on the circumferential weld, and the cylinder will be machined to allow a loose fit inside the Alloy 22 outer cylinder of the disposal container. Loose fit is defined as 0–4-mm [0–0.157-in] radial gap between the cylinders (tolerance has not been specified by DOE at present). The minimum finished thickness and inner diameter of the cylinder must be maintained at the design value (CRWMS M&O, 2001a).

2.2.4.2 Fabrication and Assembly of the Bottom and Top Lids for the Type 316 Nuclear Grade Stainless Steel Inner Cylinder

Significant changes to the design of the top and bottom lids have been proposed and are still being reviewed by DOE. In the proposed design for license application, the design of the top lid has been modified. The full penetration lid weld has been replaced with a spread ring and seal weld, and the plate thickness appears to have been decreased (Anderson, et al., 2003).

The top and bottom lids for the inner cylinder will be fabricated from Type 316 nuclear grade stainless steel. The plates will be laid out and cut to produce circles of the correct diameter. The edges will be cleaned to remove slag and scale, and the circles will be machined.

To assemble the bottom lid, the inner cylinder will be set in the horizontal position, and the lid welded to the cylinder in this position using the submerged arc, gas metal-arc, or gas tungsten-arc method. The lid seam then will be prepared for nondestructive examination and inspected using penetrant, radiographic, and ultrasonic examinations (CRWMS M&O, 2001a). No postweld heat treatment is specified for the Type 316 nuclear grade stainless steel container.

2.2.4.3 Assembly of the Inner and Outer Cylinders

The surfaces of the inner and outer cylinders will be machined as described in the preceding sections to provide a radial gap 0–4 mm [0–0.157 in] between cylinders on assembly. The cylinders will be assembled by heating the outer cylinder to approximately 371 °C [700 °F] before inserting the inner cylinder into it and allowing the assembly to cool (CRWMS M&O, 2001a).

2.3 Waste Package Closure

Once the disposal container is filled with radioactive waste, sealed, and inspected, it is referred to as the waste package. The waste package has three closure lids—one for the inner Type 316 nuclear grade stainless steel disposal container and two for the Alloy 22 outer disposal container (Figure 2-2).

2.3.1 Status of Design

Several major changes have been made to the design of the waste package closure lids. These modifications reflect the proposed design for license application and have been briefly mentioned in a presentation.[1] The major changes include the following:

- The design of the inner Type 316 nuclear grade stainless steel closure lid has been modified to replace the full penetration lid weld with a spread ring and seal weld.
- The weld configuration of the Alloy 22 middle closure lid has been changed from a full penetration weld to a fillet weld.
- Laser peening of the Alloy 22 middle closure lid has been eliminated.
- The design of the Alloy 22 outer closure lid has been modified to eliminate the lid extension.
- The stress relief method for the Alloy 22 outer closure lid has been changed from induction annealing to laser peening or low-plasticity burnishing.

Because detailed information on many of the previously listed changes is not available at present, the information presented in this section mostly reflects the design described in CRWMS M&O, 2001b.

2.3.2 The Closure Cell Facility and Its Operations

Disposal container closure operations will be performed in the closure cell facility. The closure operations include the remote placement of nuclear fuel and other waste forms, welding, inspection, and postweld stress relief of the closure lids of the disposal container. A detailed process sequence of the remote operations to be conducted in the closure cell facility is given in the flowchart (Figure 2-5) and in CRWMS M&O (2001b).

The closure cell facility will include two gas metal-arc welding inner lid weld stations, six gas tungsten-arc welding weld stations for welding the two Alloy 22 outer shell closure lids and two postweld heat treatment stations (Figures 2-6 and 2-7) (CRWMS M&O, 2001b). Every station will be equipped with a closure gantry manipulator that delivers lids and end effectors from the maintenance bay via an air lock to the filled disposal container. There will be a clean control

[1]Cogar, J.A. "Overview of the Design." *Presentation at the 5th Nickel Development Institute Workshop on the Fabrication, Welding, and Corrosion of Nickel Alloys and Other Materials for Radioactive Waste Containers, October 16–17, 2002.* Las Vegas, Nevada. 2002.

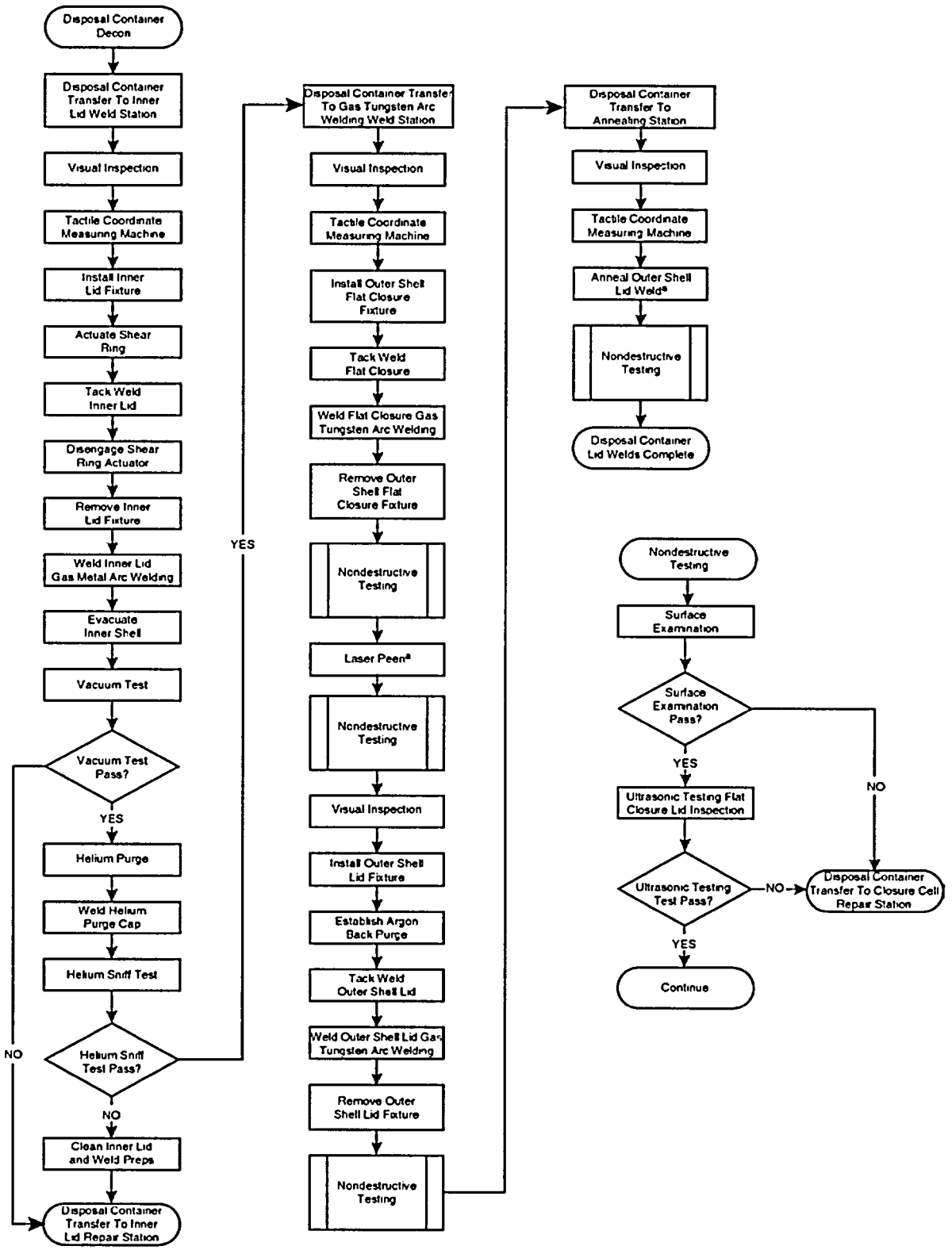

Figure 2-5. Process Sequence Flowchart (CRWMS M&O, 2001b)
[a]This Requirement Has Been Changed. See Text in Section 2.3.1.

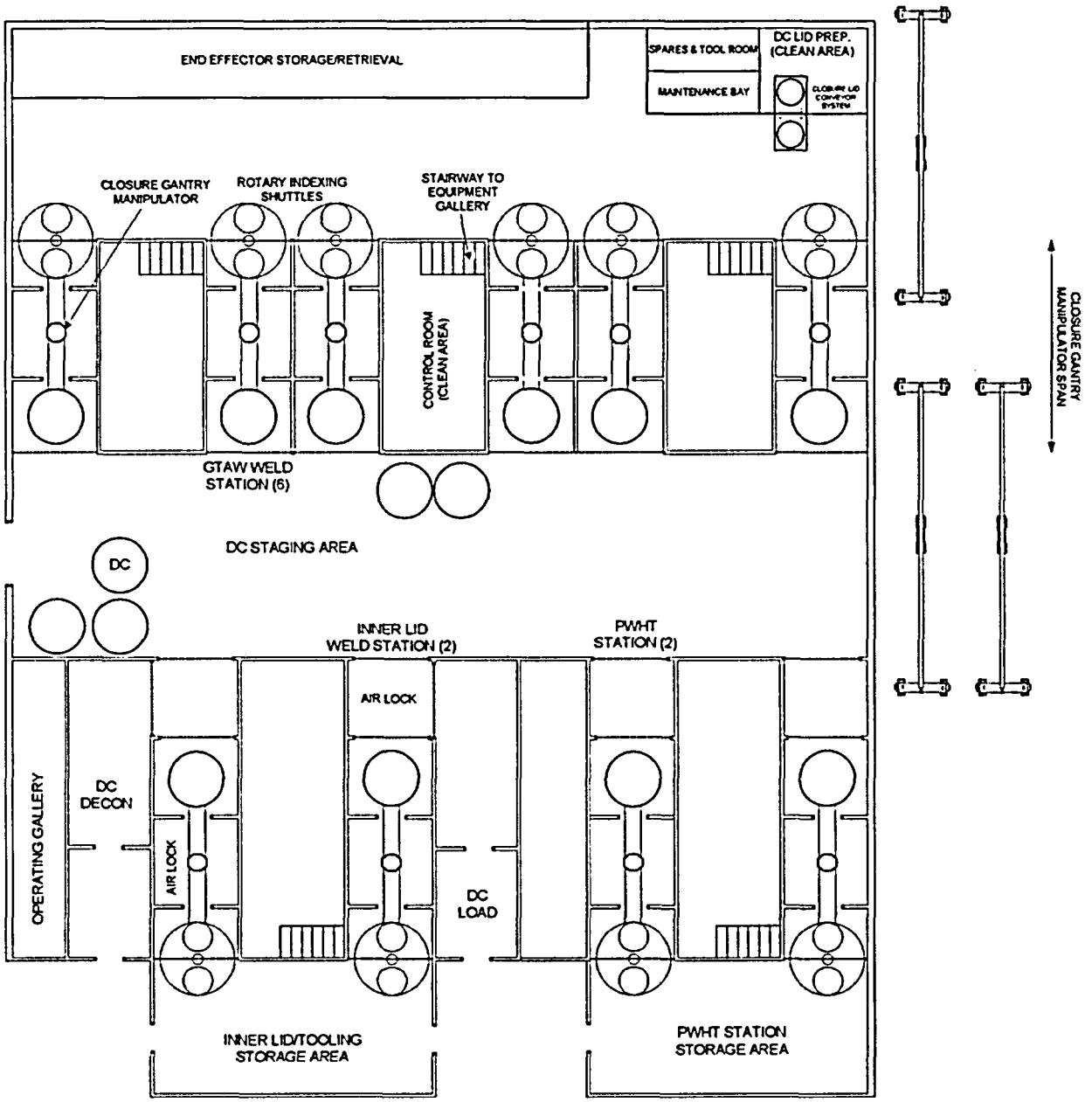

Figure 2-6. Closure Cell Plan View (CRWMS M&O, 2001b)
NOTE: DC—Disposal Container; GTAW—Gas Tungsten-Arc Welding; PWHT—Postweld Heat Treatment

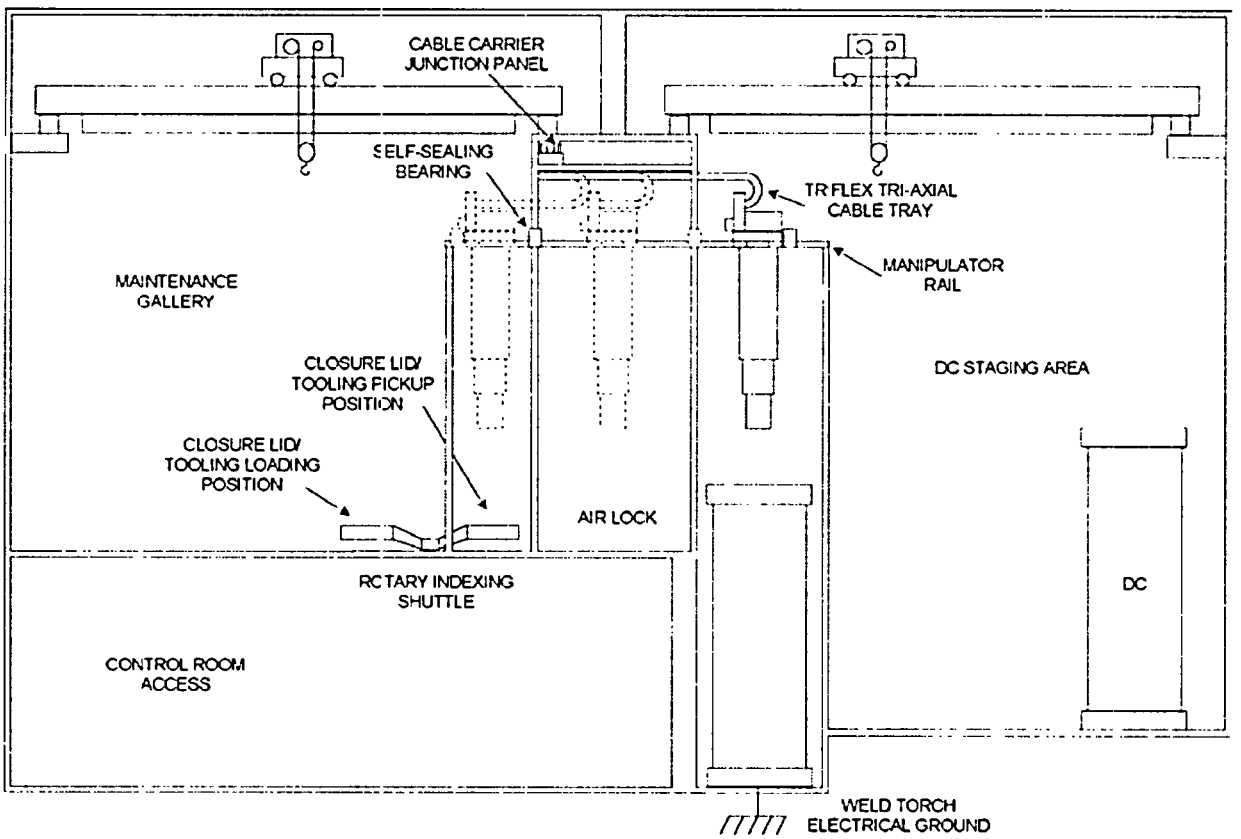

Figure 2-7. Closure Cell Elevation View (CRWMS M&O, 2001b)
NOTE: DC—Disposal Container

room area for operators to oversee, track, and control remote disposal container closure operations.

Control of the remote operations in each closure cell in the facility will be handled by the closure cell control system. This system will control the closure gantry manipulator and end effectors while also controlling the data-acquisition subsystem, machine vision/image processing system, welding power supply, and various valves and regulators. The closure cell control system will also communicate with the human machine interface to provide real-time status and operating conditions, alerts, and a data entry/control means to the operator.

Finally, there will be a central disposal container tracking system to provide central coordination and control for all the cells and storage of data pertaining to each disposal container.

2.3.2.1 Inner Type 316 Nuclear Grade Stainless Steel Closure Lid

The design of the inner Type 316 nuclear grade stainless steel closure lid has been modified in CRWMS M&O (2001b). The full penetration lid weld has been replaced with a spread ring and seal weld. These modifications reflect the proposed design for license application.

Disposal container closure operations will be performed in one of two gas metal arc welding inner lid weld stations located in the closure cell facility. The main steps in the sequence of remote operations will include the following:

- Visual inspection of the weld preps for the inner Type 316 nuclear grade stainless steel closure lid and the two Alloy 22 outer closure lids and of the top of the spent nuclear fuel/high-level waste using a remote pan and tilt high-radiation camera with lights (Figure 2-8) (CRWMS M&O, 2001b). Digital image processing and machine vision techniques will be used. Process parameter anomalies will generate a flag in the data stream and will alert the operator.

- The visual inspection will be followed by a confirmatory check of the weld preps using a tactile coordinate measuring machine (Figure 2-9) (CRWMS M&O, 2001b). This machine uses a linear voltage displacement transducer probe mounted on a rotational axis. The machine will also be used to determine cylindricity of the disposal container by locating the disposal container center relative to the closure gantry manipulator coordinate system.

- The inner lid fixture (Figure 2-10) (CRWMS M&O, 2001b) will be used next to simultaneously deliver the inner lid and the four shear ring segments to the disposal container. Once the lid has been positioned on the disposal container, the four segments will be inserted with the help of pneumatic linear slides, and the shear ring segments will be tack welded. A six-axis gas metal-arc welding robotic arm welder will be used (Figures 2-11 and 2-12) (CRWMS M&O, 2001b).

- The inner lid fixture then will be removed and the inner ring will be seal welded using the gas metal-arc welding robotic arm welder. The gas metal-arc welding robotic arm used for this operation will have a rotational range greater than 360 degrees and the ability to perform a full circumferential weld.

- Digital image processing and machine vision techniques will be used to perform real-time weld inspections. All critical welding parameters such as filler metal usage, weld current, voltage, wire speed, gas flow, and robotic arm coordinates will be recorded in process. The closure cell control system will notify the operator immediately of parameter anomalies, and a flag will be placed in the data stream. If possible, weld repair will be performed in the inner lid weld station. If extensive machining of the weld is necessary, the disposal container will be moved to the inner lid repair station, also located in the closure cell facility.

Once welding is complete, a vacuum check will be performed to verify the integrity of the inner lid shear ring seal weld. The inner shell then will be filled with helium to a pressure of approximately one atmosphere. The purge port will be welded shut using the gas metal-arc welding robotic arm welder, and a final seal integrity test will be conducted.[2] No postweld heat treatment is specified for the Type 316 nuclear grade stainless steel container closure lid seal welds.

[2]Note: There will be no volumetric nondestructive examination performed on the inner Type 316 nuclear grade stainless steel closure lid welds.

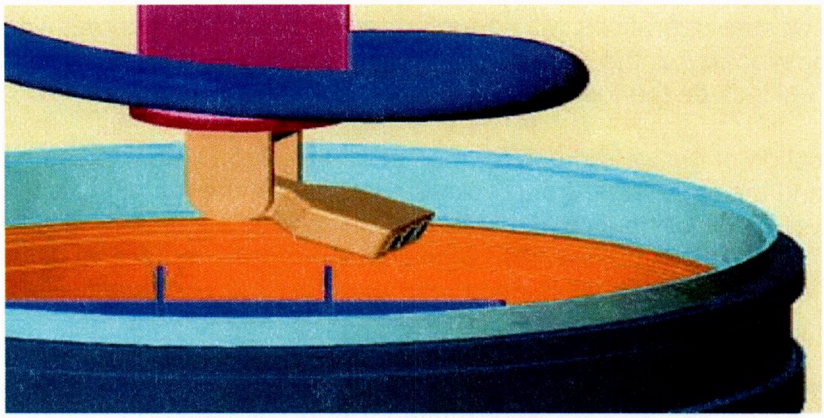

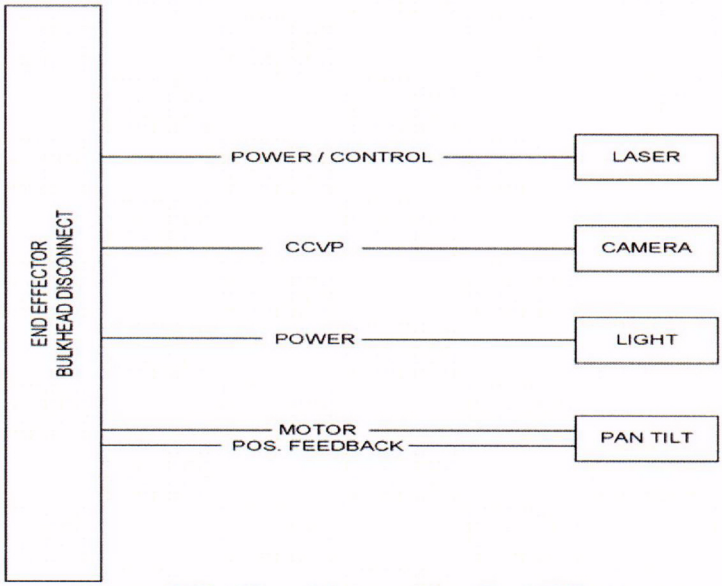

Figure 2-8. Visual Inspection End Effector (CRWMS M&O, 2001b)
NOTE: CCVP—Camera Control Video and Power

Finally, the weld preps for the two Alloy 22 outer cylinder closure lids will be cleaned, and the sealed Type 316 nuclear grade stainless steel inner disposal container will be ready for transport out of the inner weld station. A detailed process sequence of the remote operations conducted in the closure cell facility is given in CRWMS M&O (2001b).

2.3.2.2 Outer Alloy 22 Closure Lids

The Alloy 22 outer cylinder of the disposal container will have two flat closure lids. There will be a middle lid and a thicker outer lid, both constructed of Alloy 22. The welding of the lids will be performed in one of the six gas tungsten-arc welding weld stations in the closure cell facility (Figure 2-6).

C05

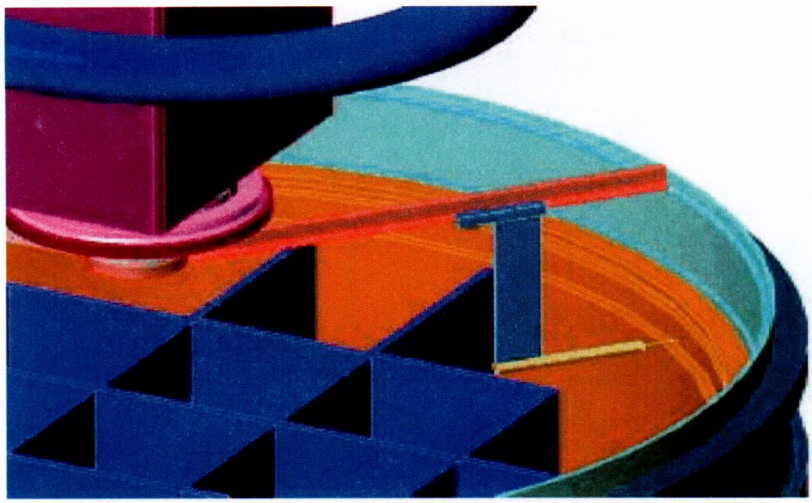

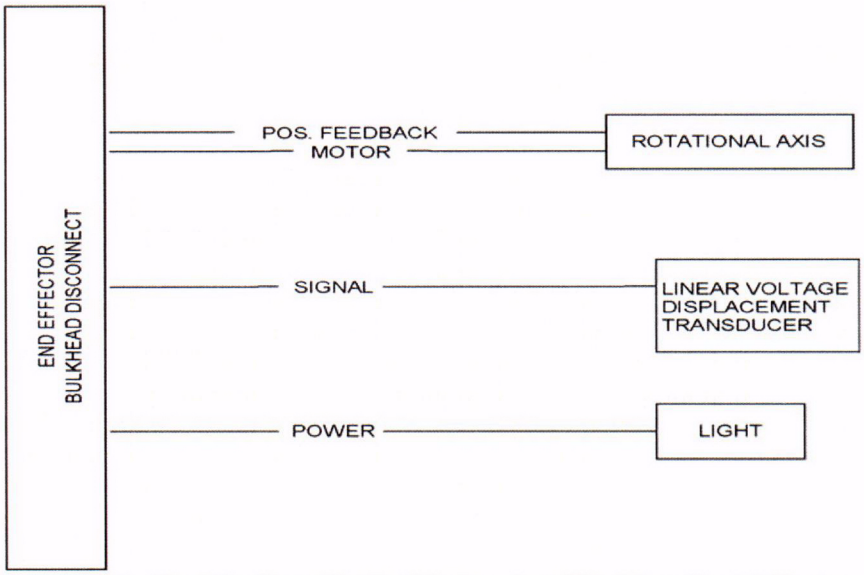

Figure 2-9. Tactile Coordinate Measuring Machine End Effector (CRWMS M&O, 2001b)

2.3.2.3 Middle Closure Lid

The weld configuration of the middle closure lid has been changed from a full penetration weld to a fillet weld, and laser peening of this lid has been eliminated.[3] It is not known what impact if any, the change in design will have on the equipment and operational sequence for the disposal container closure welds. The equipment and operational sequences described in this section reflect the design described in CRWMS M&O (2001b).

---

[3]Cogar, J.A. "Overview of the Design." *Presentation at the 5th Nickel Development Institute Workshop on the Fabrication, Welding, and Corrosion of Nickel Alloys and Other Materials for Radioactive Waste Containers, October 16–17, 2002.* Las Vegas, Nevada. 2002.

C06

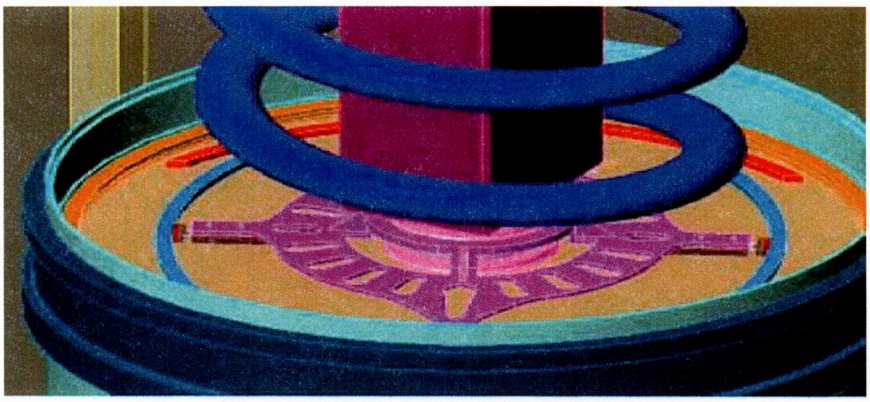

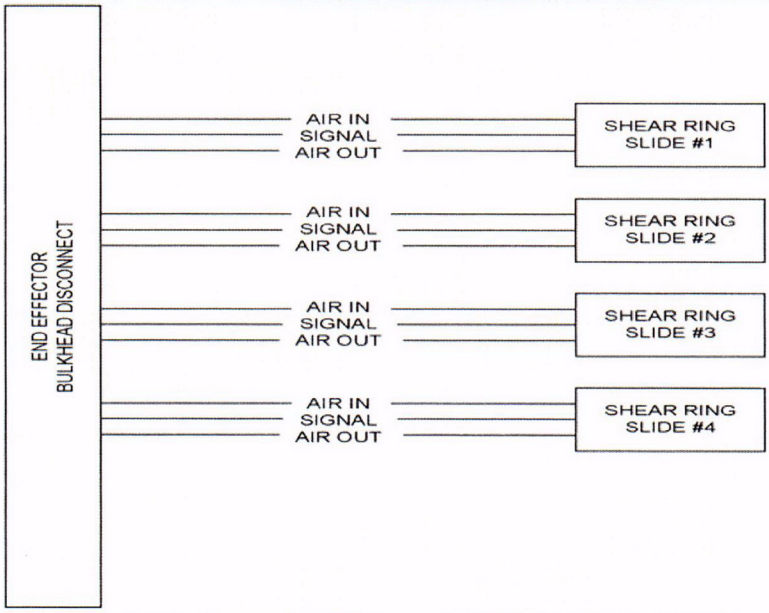

Figure 2-10. Inner Lid Fixture (CRWMS M&O, 2001b)

The sealed disposal container will be transported from the inner lid weld station to the gas tungsten arc welding weld station via the disposal container staging area. The disposal container tracking system will transmit disposal container identification and other pertinent information to the closure cell control system of the gas tungsten-arc welding weld station in which the disposal container has been relocated. The sequence of remote operations performed and equipment used will be similar to that used for the inner lid. Visual inspection of the middle and outer lids weld preparations will be performed using the same visual inspection and end effector systems described previously. The scan will be followed by a determination of the cylindricity and location of the disposal container center relative to the closure gantry manipulator coordinate system using the tactile coordinate measuring machine.

The middle closure lid fixture used will contain the middle closure lid and a gas tungsten-arc welding orbital welder equipped with a cross seam axis, automatic arc voltage control axis, and dual-axis wire manipulator. The fixture will have one rotational axis with a gas tungsten-arc welding torch mounted at a 45-degree angle to an adjustable indexed arm (Figure 2-13)

C07

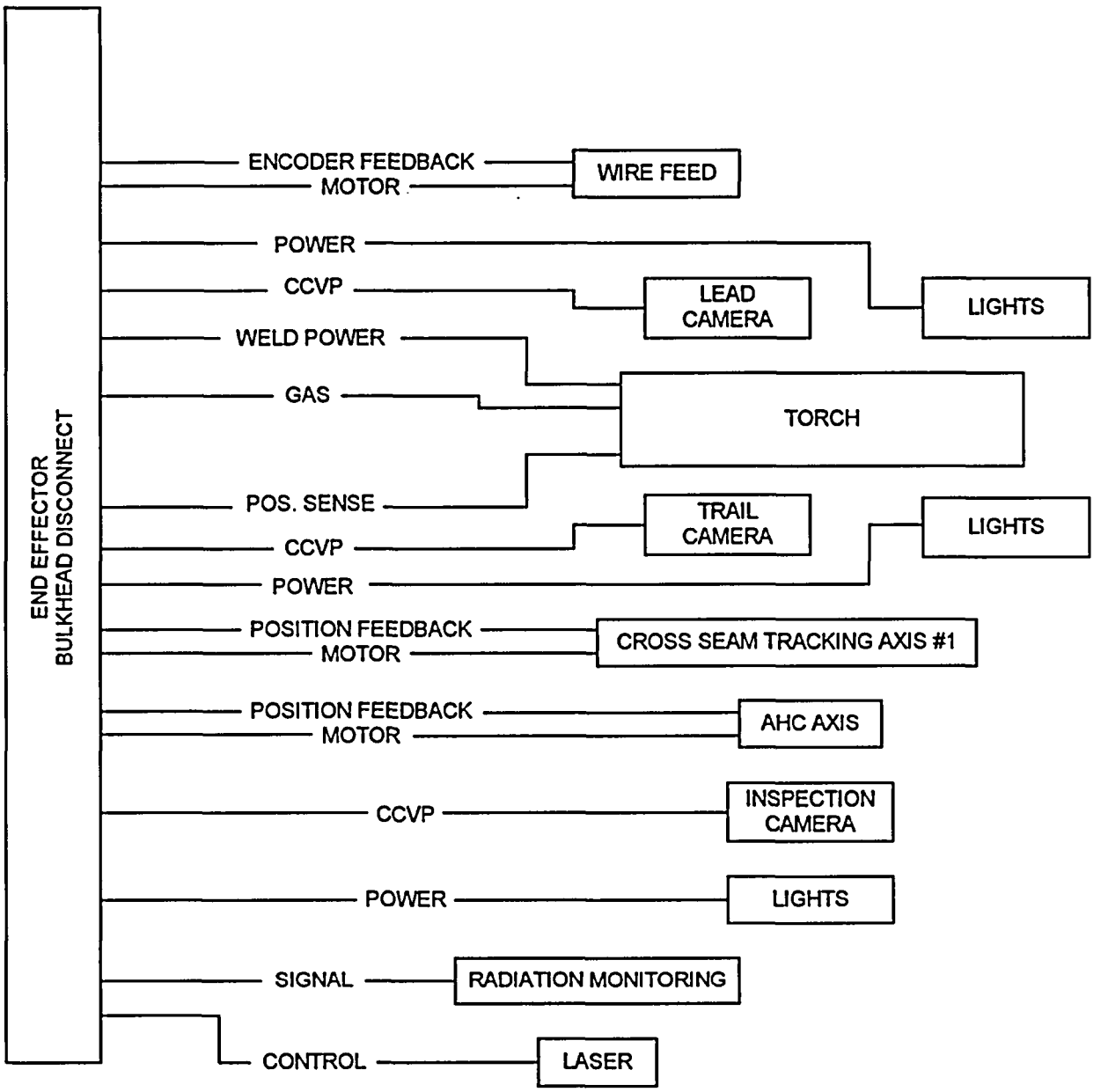

Figure 2-11. Gas Metal-Arc Welding Robotic Arm Welder (CRWMS M&O, 2001b)
NOTE: CCVP—Camera Control Video and Power

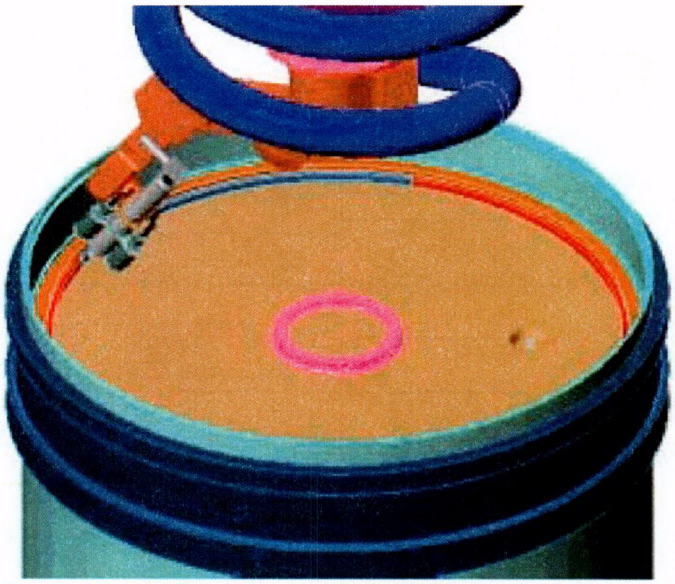

Figure 2-12. Inner Lid Weld (CRWMS M&O, 2001b)

(CRWMS M&O, 2001b). Unlike the gas metal-arc welding robotic arm, the end effector will require water cooling of the welding torch.

All critical welding parameters such as filler metal usage, weld current, voltage, wire speed, gas flow, and robotic arm coordinates will be recorded in process. The closure cell control system will notify the operator immediately of parameter anomalies, and a flag will be placed in the data stream.

It is assumed that nondestructive examination will be performed on the fillet weld[4] of the middle lid. The method and procedure are still being developed.

2.3.2.4 Outer Closure Lid

The design of the Alloy 22 outer lid has been changed to eliminate the outer lid extension. In addition, the stress mitigation method for this lid has been changed from induction annealing to laser peening or low-plasticity burnishing, and studies are presently ongoing on both alternate processes (Anderson, et al., 2003). Detailed information is not available at present on the modified closure lid design and operational methods. The equipment and operational sequences described in this section reflect the design described in CRWMS M&O (2001b).

Once the middle closure lid has been installed and inspected, the disposal container will be fitted with the outer closure lid at the same gas tungsten-arc welding weld station. Visual inspection and scan of the outer lid weld prep will be performed using the same equipment described in the preceding sections. The outer closure lid fixture used will contain the outer closure lid and a nuclear grade-gas tungsten-arc welding orbital welder equipped with the same components as the middle lid orbital welder. The fixture will have one rotational axis with a gas tungsten-arc welding torch mounted at a 90-degree angle to an adjustable indexed arm. The

---

[4]Ibid.

COB

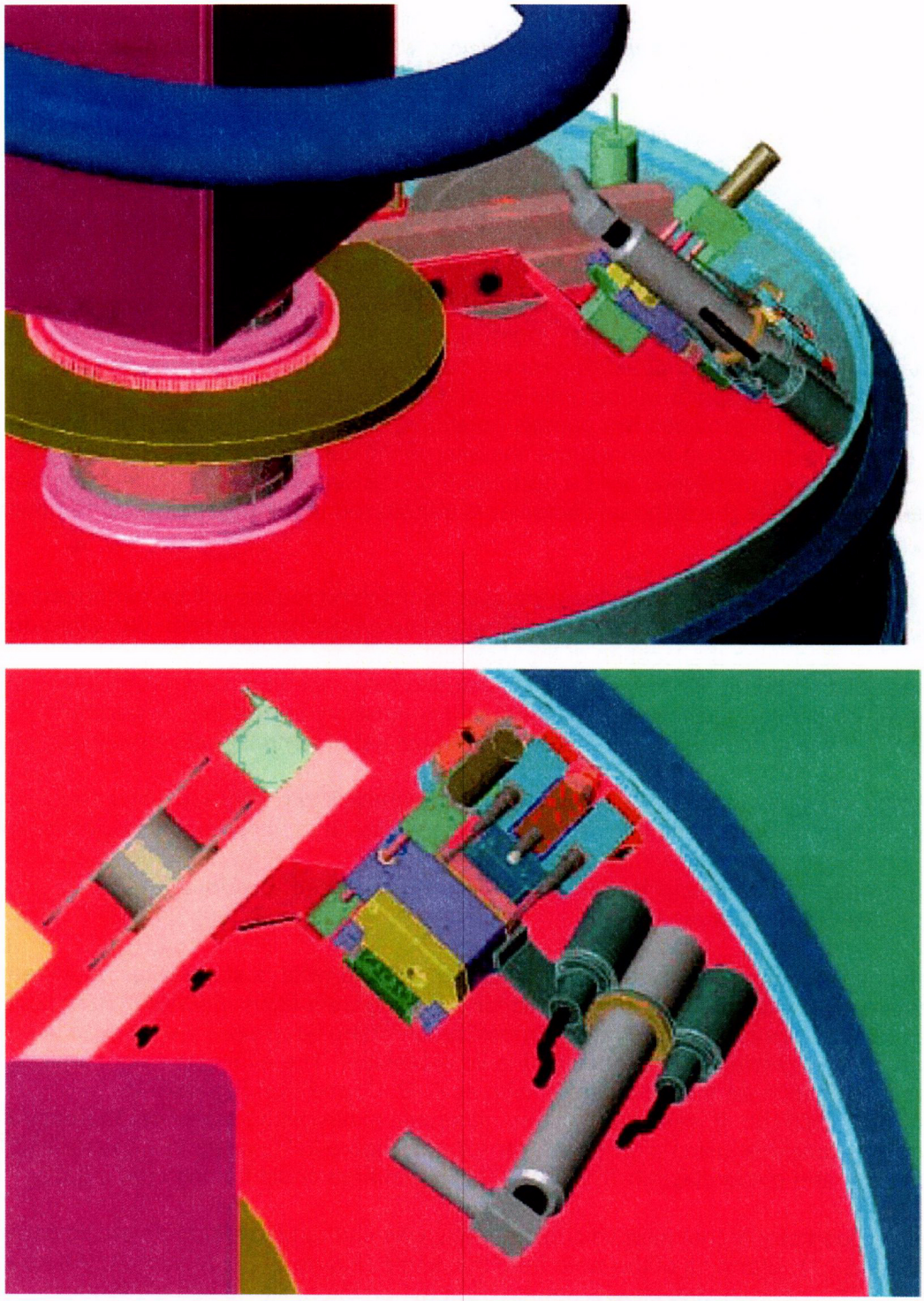

Figure 2-13. Flat Closure Lid Fixture (CRWMS M&O, 2001b)

C09

end effector will require water cooling of the welding torch. Once the outer lid has been positioned on the disposal container, an argon purge will be performed to displace air within the disposal container with argon.

The orbital welder will be used first to tack weld and then weld the lid onto the disposal container. All critical welding parameters such as filler metal usage, weld current, voltage, wire speed, gas flow, and robotic arm coordinates will be recorded in process. The closure cell control system will notify the operator immediately of parameter anomalies, and a flag will be placed in the data stream.

A special end effector capable of performing both surface examination and volumetric inspection (Figure 2-14) (CRWMS M&O, 2001b) will be used to nondestructively examine the lid weld. Alternating current field measurement will be used for surface examination while ultrasonic testing with couplant will be used for volumetric inspection. The present design (CRWMS M&O, 2001b) provides two passes (rotations) to perform the inspection. On the first pass (rotation), the inspection scan will use the alternating current field measurement probe. An ultrasonic examination inspection will be performed on the second scan. Any repairs needed will be performed before the disposal container is transferred to the postweld heat treatment station for annealing.

A visual inspection and tactile, coordinate-measuring machine routine will be performed at the postweld heat-treatment station to verify the disposal container has not been damaged during transfer and to determine the location of the disposal container center relative to the closure gantry manipulator coordinate system. As indicated in the preceding paragraphs, the disposal container will be annealed using laser peening or low-plasticity burnishing. A general description of these processes is provided next. A final set of nondestructive examinations will

be performed using the two methods described in the preceding paragraph. The nondestructive examination will include surface and volumetric inspections of the postannealed closure weld.

2.3.2.5 Impact of Outer Lid Redesign on Weld Flaw Detection Using Ultrasonic Examination

To identify the minimum detectable flaw size for the outer lid weld, a study was conducted to evaluate ultrasonic examination as a method for detecting weld flaws (CRWMS M&O, 2001b). Because the study was conducted prior to modification of the lid design, the mockup used reflected the old lid geometry and included the lid extension. The available scan surfaces for ultrasonic examination for this study are shown as A, B, C, and D in Figure 2-15 (CRWMS M&O, 2001b). It was found that an ultrasonic examination scan from the outer edge of the disposal container using a 0-degree transducer (Figure 2-15, position A) generated the optimal results, and planar flaws 0.161 cm^2 [0.025 in^2] in area could be detected reliably.

Because the geometry of the outer lid subsequently was changed to eliminate the lid extension (see Section 2.3.1), scanning of the weld from this angle (Figure 2-15, position A) will no longer be possible. This change may have a negative impact on the ability to use ultrasonic examination to detect planar flaws of small dimensions.

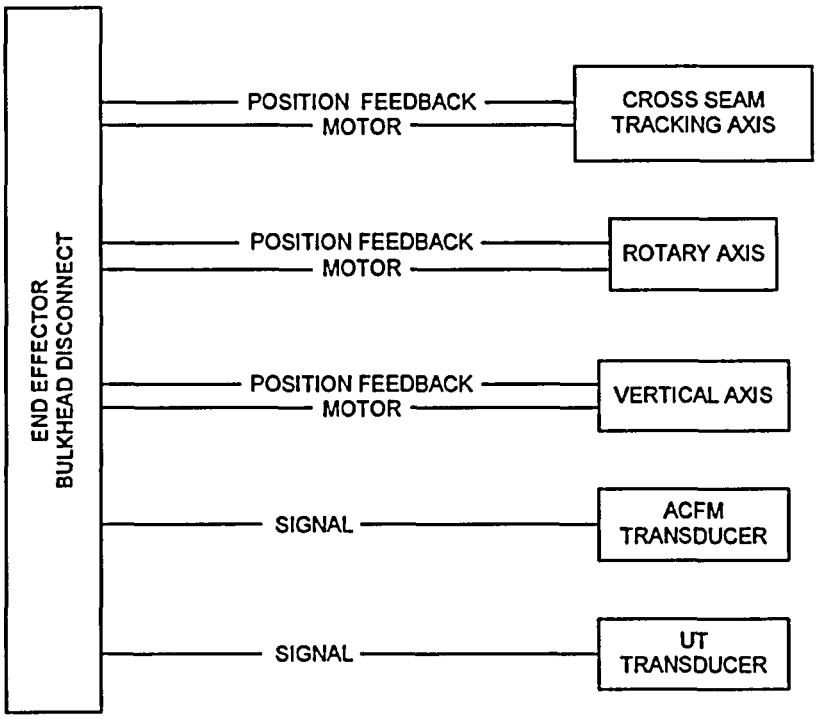

Figure 2-14. SE/VI End Effector (CRWMS M&O, 2001b)
NOTE: ACFM—Alternating Current Field Measurement; UT—Ultrasonic Testing

2.3.2.6 Laser Peening

Laser peening of the closure weld of the Alloy 22 middle lid has been described in CRWMS M&O (2001b). It is assumed that a similar method will be employed in the case of the Alloy 22 outer lid closure weld. A laser peening end effector consisting of a laser mounted on an adjustable indexed arm is likely to be used. A cross seam and vertical axis may be employed to adjust the laser position as it rotates over the weld. The process is likely to require constant water spraying to help direct and propagate the heat-sustained shock wave into the metal interior. The end effector will, therefore, need to incorporate a recirculation system to minimize water usage in the cell. Because the power requirements of such a system are expected to be high (~20 MW), a mirror transmission technique is likely to become necessary. DOE is planning to investigate a fiber optic system developed by Toshiba for *in-situ* laser peening of welds in core shrouds of nuclear power plants (CRWMS M&O, 2001b).

2.3.2.7 Low-Plasticity Burnishing

Low-plasticity burnishing has been proposed as an alternate method to impart compressive residual stresses to the Alloy 22 outer container closure welds. Details of the parameters for low-plasticity burnishing of the Alloy 22 outer container closure welds have not been reported. Low-plasticity burnishing has been used with titanium, nickel, aluminum, and magnesium alloys as well as with high-strength steels. The main advantages of low-plasticity burnishing are the resulting stress profile and a wide range of applications compared to either shot peening or laser peening. Compressive stresses to depths of 1.2–1.5 mm [0.047–0.059 in] with less than

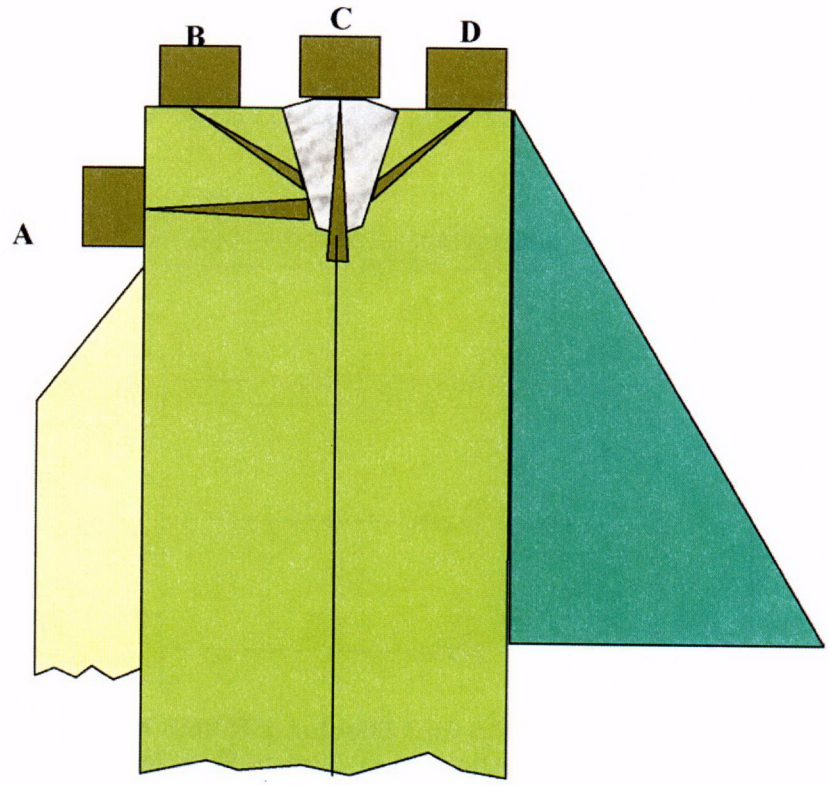

A) Outside Diameter of Outer WP
B) Top of Outer WP
C) Weld
D) Top of Outer Lid

Figure 2-15. Available Scan Surfaces for Ultrasonic Examination (CRWMS M&O, 2001b) NOTE: WP—Waste Package

10-percent cold work throughout the depth of the near-surface region has been reported for Alloy 718 (Migala and Jacobs, 2002; Prevey, et al., 2000). Gordon[5] reported compressive stresses to depths of 8 mm [0.31 in] for 100 mm [1.25 in], with a maximum residual stress of 1,350 MPa [195 ksi] at a depth of 0.2 mm [0.008 in] using high-pressure, low-plasticity burnishing with an applied load of 5,443 kg [12,000 lbs]. For depths of 1 to 8 mm [0.039 to 0.315 in], the compressive residual stress was 480 to 170 MPa [70 to 25 ksi]. The amount of cold work or changes to the microstructure were not reported.

[5]Gordon, G. "Stress Corrosion Cracking and Stress Mitigation." *Presentation at the 5th Nickel Development Institute Workshop on the Fabrication and Welding of Nickel Alloys and Other Materials for Radioactive Waste Containers, October 16–17, 2002.* Las Vegas, Nevada. 2002.

C10

2.4 Summary of Waste Package Design

Fabrication and closure of the disposal containers will use multiple processes such as cold rolling, machining, welding, and postweld heat treatments. The body of the disposal containers will be formed from plate that is rolled into cylinders, machined, and welded. Multiple cylinders may be welded together to provide the necessary length of the disposal container. Lower lids also will be machined from plate and welded to the cylindrical body of the disposal containers. Additional internal structures will be necessary for the Type 316 nuclear grade stainless steel inner container and will be specific to the type of waste that will be contained. The Alloy 22 outer container will have external components such as trunnions to allow lifting the disposal container and emplacing waste packages that will be welded in place. Both the Type 316 nuclear grade stainless steel and the Alloy 22 disposal containers will be solution annealed to remove residual stresses as a consequence of the fabrication processes.

After loading, the Type 316 nuclear grade stainless steel disposal container lid will be installed and held in place using shear rings. A seal weld will be used to hold the closure lid and shear rings in place. The seal weld on the Type 316 nuclear grade stainless steel closure welds will be performed in a hot cell using remote operational control. Remote welding will be used for the final closure welds of the Alloy 22 disposal container lids. It is anticipated that one or more closure weld stress mitigation methods will be used to relieve tensile stresses in the region of the Alloy 22 closure welds.

The structural integrity of the disposal containers will be assessed using a variety of nondestructive examination methods. Although the integrity of the waste packages will be verified by nondestructive examination methods, the fabrication and closure of the disposal containers may affect performance of the waste packages after emplacement. Specifically, fabrication processes such as cold working, welding, and postweld heat treatments will alter the microstructure of the Alloy 22 and may affect the localized corrosion susceptibility, stress corrosion cracking resistance, and uniform corrosion rate of the outer container. Assessment of the effects of fabrication processes on the postclosure waste package performance is necessary to determine the overall performance of the proposed high-level waste repository.

3 EFFECTS OF FABRICATION PROCESSES ON MICROSTRUCTURE

Changes in material microstructure and microchemistry resulting from fabrication processes have been considered possible degradation mechanisms that may impair corrosion resistance and mechanical properties of the outer waste package material (Payer, et al., 2002; NRC, 2002, 2001; Cragnolino, et al., 1999). In this chapter, the effects of fabrication processes on the microstructure of Alloy 22 are discussed. A review of the U.S. Department of Energy (DOE) investigation on phase stability of Alloy 22 and an assessment of the DOE approach are provided. A limited analysis conducted at the Center for Nuclear Waste Regulatory Analyses (CNWRA) to evaluate the effects of thermal aging and solution annealing treatments, as well as compositional variations, are also reported.

3.1 The DOE Investigations

DOE conducted experiments to investigate phase stability issues in Alloy 22, including intermetallic and carbide precipitation, and long-range ordering in both the mill-annealed and the welded materials (CRWMS M&O, 2000e). The kinetics of phase transformations were determined for accelerated, high-temperature conditions and then extrapolated to the anticipated low temperatures in the proposed repository. A review of the DOE investigations to evaluate the effects of thermal processes on phase stability of mill-annealed and welded Alloy 22 and the assessment of the DOE approach are provided in this section.

3.1.1 Mill-Annealed Material

The phase stability of mill-annealed Alloy 22 has been studied by aging samples in the temperature range 260–800 °C [500–1,472 °F] for time periods up to 40,000 hours (CRWMS M&O, 2000e). Metallurgical and microstructural analyses were conducted on these samples using optical microscopy, scanning electron microscopy, and transmission electron microscopy. Metallurgical samples were prepared using standard polishing techniques, followed by electrochemical etching in an oxalic acid solution. The stages of intermetallic precipitation in Alloy 22 base metal as a function of aging temperature and time were determined in a scanning electron microscope, and volume fraction measurements of the intermetallic precipitates were made from optical micrographs using imaging analysis software. Thin foils used for phase identification in a transmission electron microscope were mechanically thinned and then jet polished in a 5-percent, perchloric-acetic acid solution. Because preferential etching of precipitates was observed in the jet polished foils, additional samples were also prepared by the dimpling and ion-milling techniques.

In the mill-annealed condition, Alloy 22 is a single phase face-centered cubic solid solution. Several phases are observed to form in Alloy 22 after thermal aging, including topologically close-packed phases (i.e., σ, P, and μ), carbides, and $Ni_2(Cr,Mo)$ long-range ordering. The DOE observations of phase formation in the thermally aged Alloy 22 are summarized in a time-temperature-transformation diagram in Figure 3-1. The effect of aging temperature and time on the formation of secondary phases is clearly shown in Figure 3-1. Alloy 22, when subjected to thermal aging, undergoes two types of phase transformation depending on the temperature range: precipitation of topologically close-packed phases at temperatures greater than approximately 600 °C [1,112 °F]; long-range ordering at temperatures less than about 600 °C [1,112 °F]. It was observed that the precipitation of topologically close-packed phases in

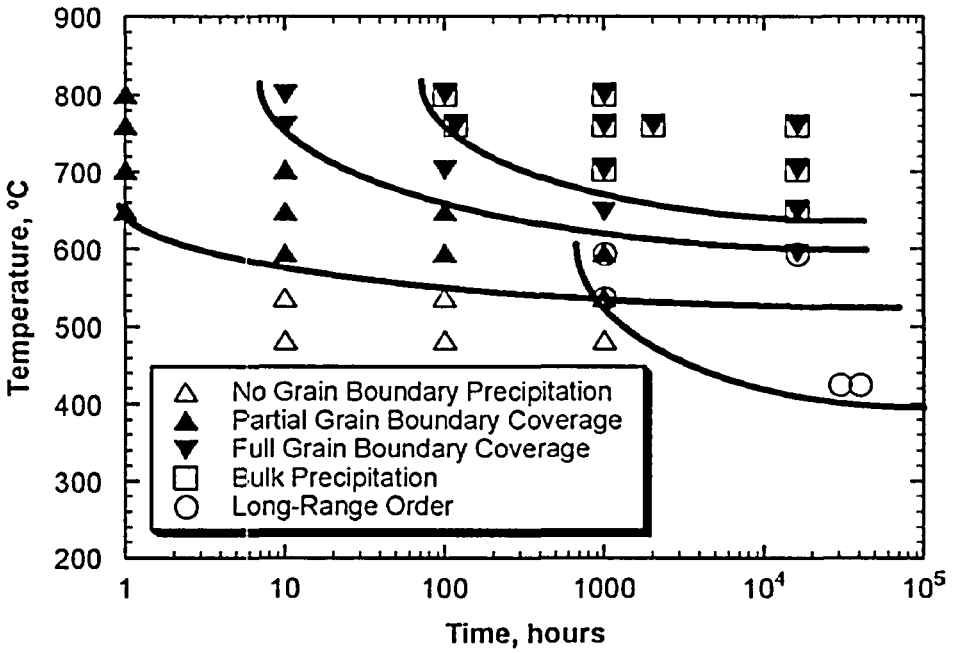

Figure 3-1. Time-Temperature-Transformation Diagram for Alloy 22 Base Metal (CRWMS M&O, 2000e)
NOTE: Temperature Provided in °C; for Conversion to °F use °F = 9/5 °C + 32.

Alloy 22 first starts preferentially at grain boundaries and later within the grains. Three stages of precipitation were determined through scanning electron microscopy examination, including partial grain-boundary coverage, full grain-boundary coverage, and bulk precipitation. It is noted that a limited identification of various topologically close-packed and carbide phases was conducted. In addition, no quantitative data on the relative amounts of each phase were reported. Figure 3-1 also shows that long-range ordering was observed to start after 1,000 hours aging at temperatures of 538 and 593 °C [1,000 and 1,099 °F]. Transmission electron microscopy observations indicate that long-range ordering phases less than 10 nm [3.9×10^{-7} in] were observed in the sample aged at 538 °C [1,000 °F] for 1,000 hours. Long-range ordering was also observed in the samples aged at 427 °C [800 °F] for 30,000 and 40,000 hours.

The phase transformation theory of nucleation and growth was employed in an attempt to derive precipitation kinetics for extrapolation of the short-term, high-temperature data to repository-relevant temperatures. The volume fraction of the topologically close-packed phases, *f*, is a function of time, *t*, at the specific aging temperature as shown in Eq. (3-1)

$$f = 1 - \exp(-kt^n) \tag{3-1}$$

where *k* and *n* are constants. *k* is a function of temperature and can be expressed as

$$k = C_1 \exp(-C_2 / T) \tag{3-2}$$

where C_1 and C_2 are constants, and T is the temperature. Because the various precipitation stages of topologically close-packed phases occur at some fixed volume fractions, the time to yield a given volume fraction, t_f, can be expressed as Eq. (3-3) by combining Eqs. (3-1) and (3-2).

$$\ln(t_f) = \frac{C_2}{n} \cdot \frac{1}{T} + C_f \qquad (3\text{-}3)$$

where C_f is a constant.

Figure 3-2 shows the log(time) versus reciprocal temperature plots for the various precipitation stages of topologically close-packed phases in thermally aged Alloy 22 base metal. Note that the time errors are because of the uncertainty associated with the widely spaced aging time periods. From Eqs. (3-2) and (3-3), and the slopes of the lines in Figure 3-2, an average activation energy for the precipitation of topologically close-packed phases can be determined to be near 280 kJ/mol [66.9 kcal/mol]. Using this activation energy value, the lines associated with grain-boundary coverage and bulk precipitation in Figure 3-2 can be extrapolated to 10,000 years in Figure 3-3. The start of grain-boundary precipitation is not included because of the limited amount of available data. Based on the results of specimens analyzed thus far, both grain-boundary coverage and bulk precipitation of topologically close-packed phases are predicted that will not occur in 10,000 years at 300 °C [572 °F]. Also plotted in Figure 3-3 are lines with the minimum allowed slope from the time-error bars. In these conservative cases, bulk precipitation of topologically close-packed phases is not predicted, but grain-boundary precipitation may occur.

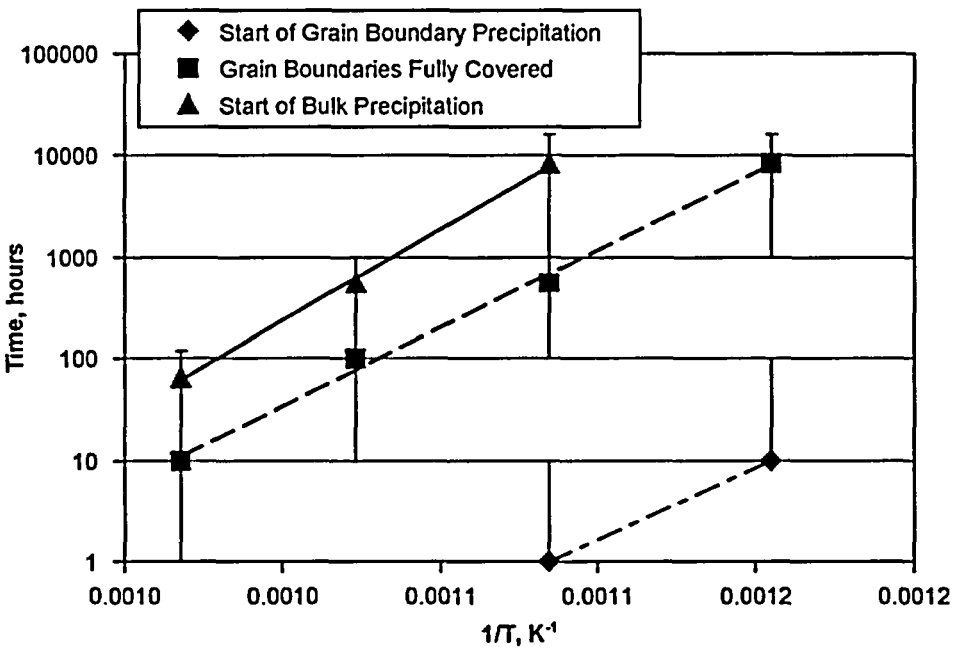

Figure 3-2. Log(Time) Versus Reciprocal Temperature Plots for Various Precipitation Stages of Topologically Close-Packed Phases in Alloy 22 Base Metal (CRWMS M&O, 2000e)

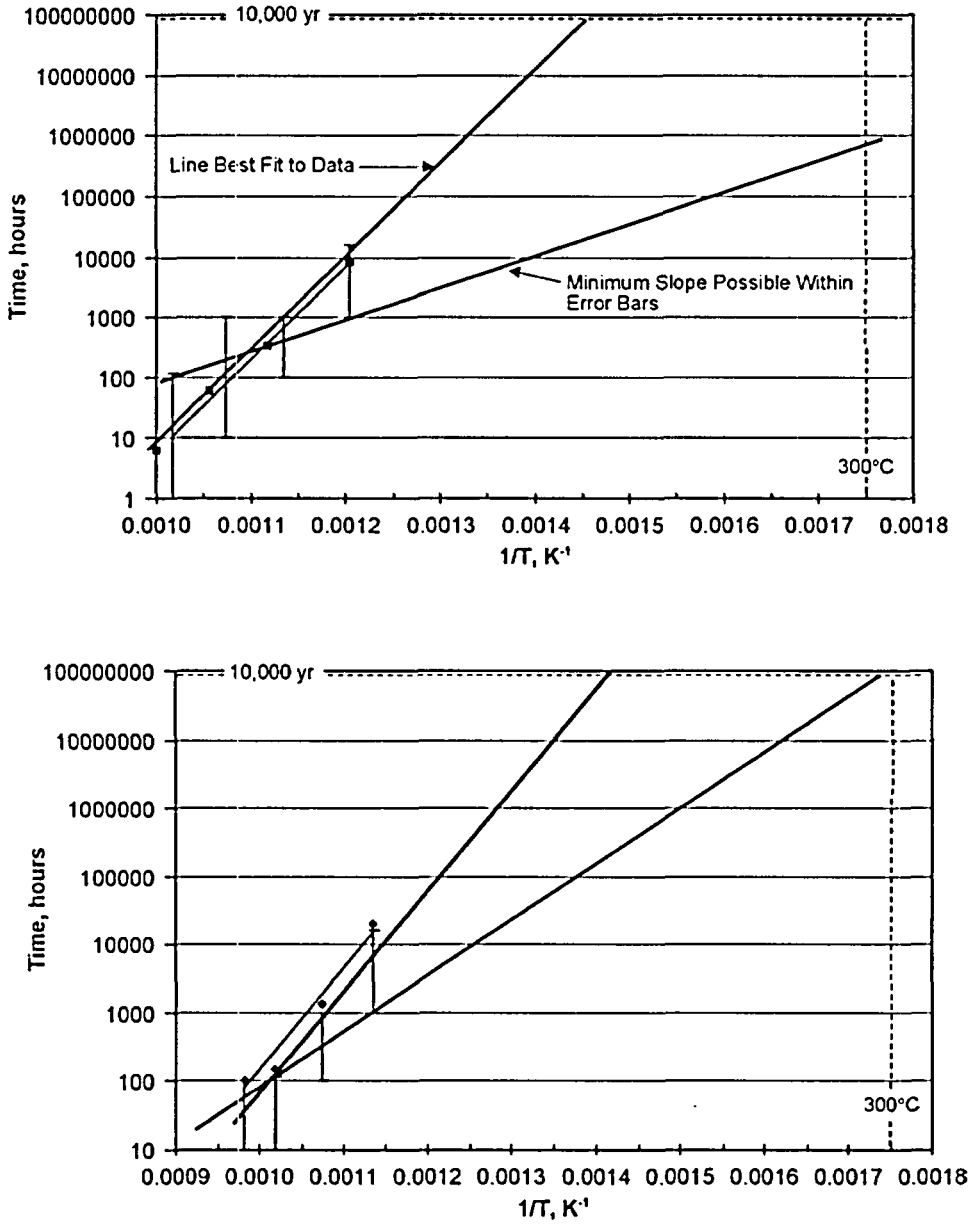

Figure 3-3. Predicted Grain-Boundary Coverage (Top) and Bulk Precipitation (Bottom) of Topologically Close-Packed Phases in Alloy 22 Base Metal to Repository-Relevant Temperatures (CRWMS M&O, 2000e)

A similar extrapolation of the short-term data for long-range ordering in Alloy 22 base metal was reported. The kinetics of long-range ordering in Alloy 22 base metal was estimated using the shortest times at which long-range ordering was observed. From the limited experimental data, two points corresponding to aging at 538 °C [1,000 °F] for 1,000 hours and 427 °C [800 °F] for 30,000 hours were plotted in Figure 3-4. A curve fit to these data yields Eq. (3-4)

$$t = 5 \cdot 10^{-7} \exp (17395 / T) \quad (3\text{-}4)$$

where *T* is temperature in Kelvin, and *t* is time in hours. Extrapolation of this curve fit in Figure 3-4 indicated that, at 300 °C [572 °F], long-range ordering may occur in Alloy 22 base metal in 872 years.

In the Supplemental Science and Performance Analyses Report (CRWMS M&O, 2001c), two new data points corresponding to aging at 538 °C [1,000 °F] for 100 hours and 427 °C [800 °F] for 20,000 hours were considered for assessing the long-range ordering of Alloy 22 base metal using the log(time) versus reciprocal temperature plot. A revised curve fit can be expressed as Eq. (3-5)

$$t = 3 \cdot 10^{-13} \exp (27098 / T) \quad (3\text{-}5)$$

Extrapolation of the revised curve fit in Figure 3-4 showed that the occurrence of long-range ordering in Alloy 22 base metal is not predicted in 10,000 years at 300 °C [572 °F]. It should be noted that from Eqs. (3-4) and (3-5), the activation energy for the formation of long-range ordering can be calculated, and the calculated activation energy varies from 144 kJ/mol [34.4 kcal/mol] to 225 kJ/mol [53.8 kcal/mol] in the DOE assessment.

Theoretical modeling of precipitation of topologically close-packed phases and long-range ordering in Alloy 22 was conducted using the Thermo-Calc and DICTRA software packages. The equilibrium phases predicted in Alloy 22 as a function of temperature from the Thermo-Calc calculations are given in Figure 3-5. The calculations assume an alloy composition of 21.2Cr-13.5Mo-4Fe-3W-2Co-0.5Mn-0.3V-0.08Si-0.01C-balance nickel in weight percent. These results predicted that three phases, OP6 (the ordered phase), P, and the face-centered-cubic solid solution phase are stable at lower temperatures, whereas only the σ-phase is stable from 800 to 950 °C [1,472 to 1,742 °F], in addition to the predominant face-centered-cubic phase. The DICTRA application linked with Thermo-Calc was used to simulate the diffusion-controlled phase transformations for both the ordered Ni_2Cr phase and the topologically close-packed P-phase. The predicted time-temperature-transformation diagrams for bulk precipitation are shown in Figure 3-6, together with experimental results indicated by the data points. In the case of the ordered Ni_2Cr phase, 10-percent transformation of the ordered phase in a binary nickel-chromium matrix was calculated for constant temperature conditions. The predictions are consistent with the results extracted from the work of Karmazin (1982). For the isothermal transformation of P-phase, a ternary nickel-chromium-molybdenum alloy with a composition of 55.7Ni-21.1Cr-13.5Mo in weight percent with the transformation rate ranging from 1 to 20 percent was considered. The time-temperature-transformation diagrams in Figure 3-6 are predicted for precipitation of P-phase controlled by bulk diffusion, however, and the calculated times are longer than the experimental results in the case in which only grain-boundary precipitation was observed.

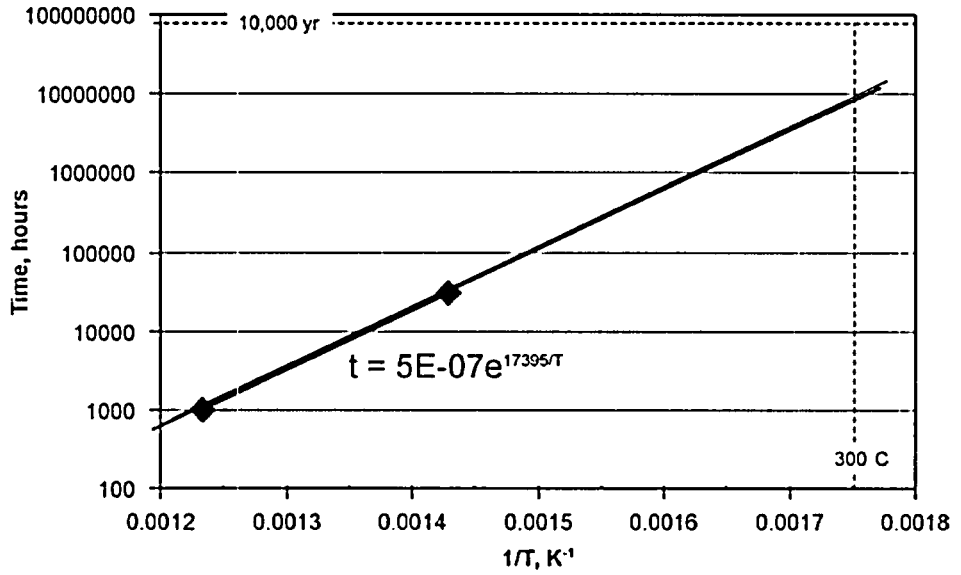

(a)

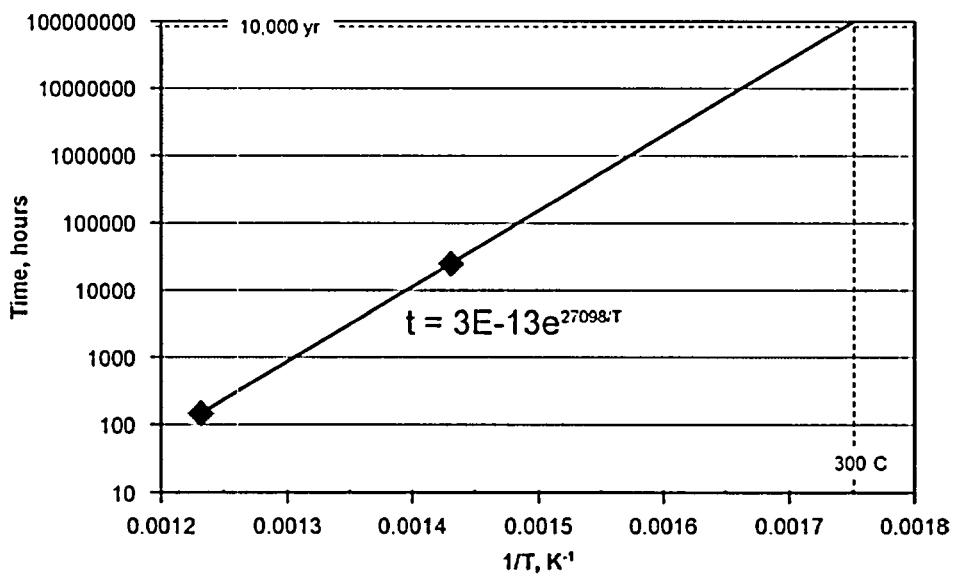

(b)

Figure 3-4. Log(Time) Versus Reciprocal Temperature Plots for Long-Range Ordering in Alloy 22 Base Metal and Extrapolation to Repository-Relevant Conditions (a) in CRWMS M&O (2000e) and (b) in CRWMS M&O (2001c)

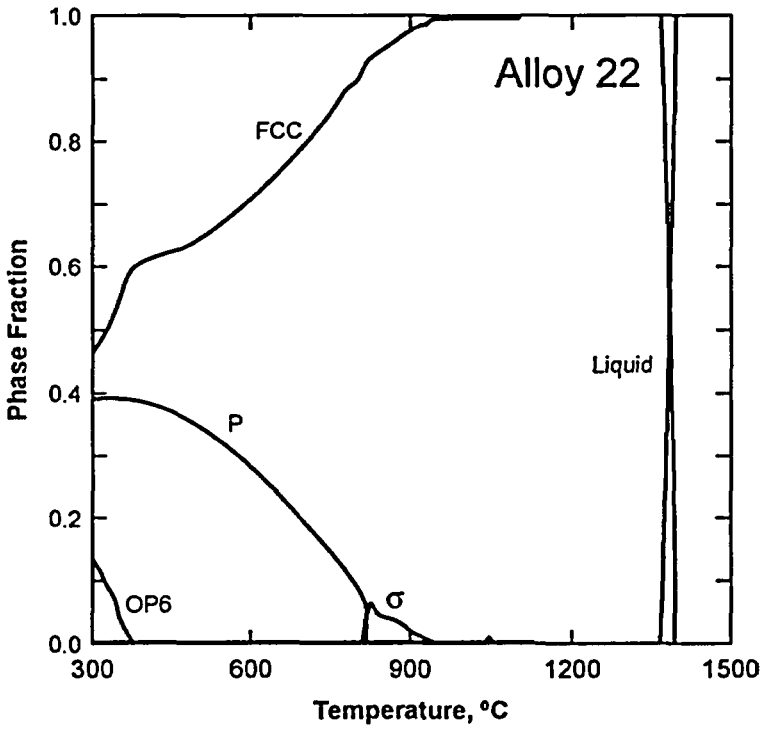

Figure 3-5. Predicted Phase Fraction Versus Temperature Diagram for Alloy 22 (CRWMS M&O, 2001c)
NOTES: Temperature Provided in °C; for Conversion to °F use °F = 9/5 °C + 32; FCC—Face-Centered Cubic

3.1.2 Welded Material

In the Supplemental Science and Performance Analyses Report (CRWMS M&O, 2001c), the phase stability of Alloy 22 gas tungsten-arc welds has been reported, emphasizing formation of topologically close-packed phases. The welded materials were produced from 12.5-mm [0.5-in] thick plates. These welds were much thinner than those described in the waste package design for site recommendation (CRWMS M&O, 2000b). The amount and size of precipitates in the welds were noted to vary with position in the welds. Because of the inhomogeneous distribution of the precipitates, the amount of precipitates in the as-welded condition was measured to be 2.9 and 2.5 volume percent from multiple measurements for several positions at 200 and 400 magnification, respectively. Microstructural characterization of the welds in the as-welded condition showed the formation of a dendritic structure and the presence of topologically close-packed phases in the interdendritic regions (CRWMS M&O, 2000e). In a presentation to the DOE Waste Package Materials Performance Peer Review Panel, Summers[1] reported chemical analysis results of the precipitates in the welds. Energy-dispersive x-ray spectra indicated the precipitates in the interdendritic regions are molybdenum rich, whereas few particles in the dendrite cores appear to be carbides. Additionally, microprobe concentration

[1]Summers, T. "Potential Degradation Modes—Metallurgical Issues." *Presentation to the DOE Waste Package Materials Performance Peer Review Panel, September 25, 2001.* Las Vegas, Nevada. 2001.

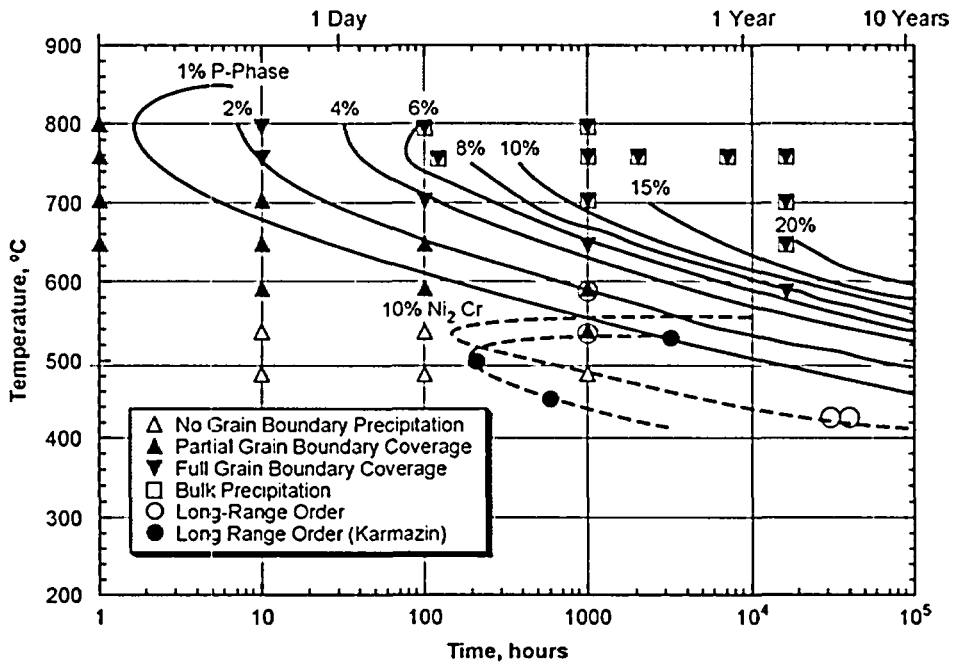

Figure 3-6. Predicted Time-Temperature-Transformation Diagrams for Ni_2Cr and P-Phase (CRWMS M&O, 2001c)
NOTE: Temperature Provided in °C; for Conversion to °F use °F = 9/5 °C + 32.

profiles showed segregation of molybdenum and chromium to a lesser extent in the interdendritic regions.

Summers, et al. (2002) reported precipitate volume fraction measurements in Alloy 22 welds. Aging of the welded materials was conducted at temperatures between 593 and 760 °C [1,099 and 1,400 °F] for time periods up to 1,000 hours. Metallurgical samples were prepared using standard polishing techniques, followed by electrochemical etching in a solution of oxalic acid. The volume fraction measurements of the precipitates were made from optical micrographs using imaging analysis software. The volume fraction of topologically close-packed phases in the welded samples as a function of aging time and temperature is shown in Figure 3-7. From the volume fraction data of topologically close-packed phases in the Alloy 22 welds, a linear plot in ln(ln(1/(1-f))) versus ln(t), a derivative of Eq. (3-1) on the basis of the phase transformation theory, can be constructed for each aging temperature. The times to form 5- and 10-volume percent topologically close-packed phases can then be calculated from the curve fits for various aging temperatures. These times are plotted in Figure 3-8 as a function of reciprocal temperature. The activation energy calculated from the slopes of these plots is approximately 210 kJ/mol [50.2 kcal/mol]. Using this activation energy value, extrapolation to 10,000 years indicated that both predicted temperatures are above 300 °C [572 °F]. However, different extrapolated cutoff temperatures to give a 10,000-year life for both 5- and 10-volume percent topologically close-packed phases precipitation were reported in CRWMS M&O (2001c), as also shown in Figure 3-8. In these cases, further nucleation and growth of the topologically close-packed phases in the welds is possible in 10,000 years at temperatures between 200 and 300 °C [392 and 572 °F] and higher. It should be noted that the original data for precipitation of 5- and 10-volume percent topologically close-packed phases plotted in Figure 3-8 have been slightly shifted.

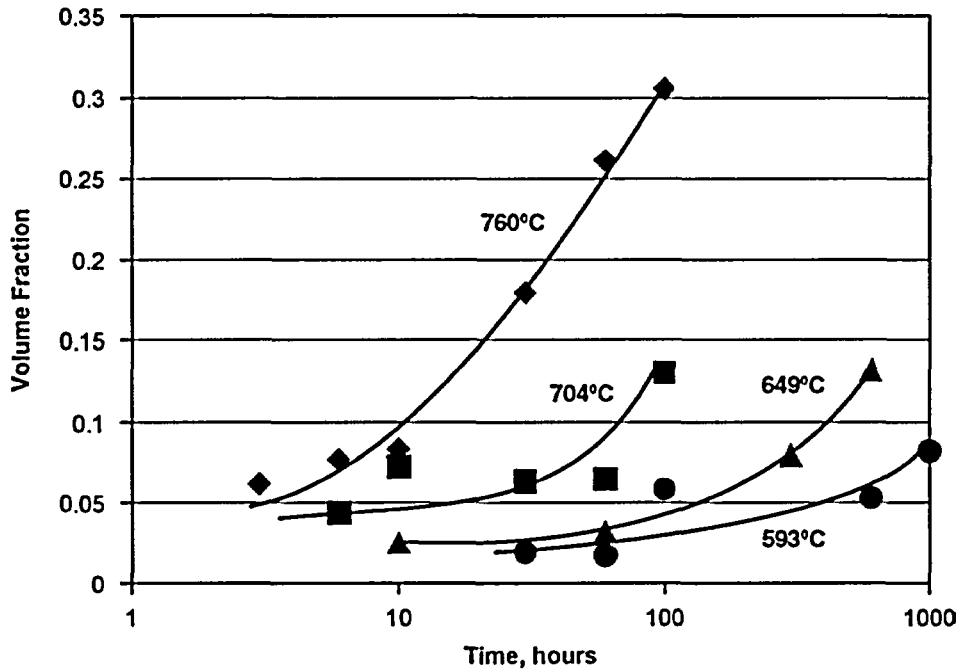

Figure 3-7. Volume Fraction of Precipitates in Alloy 22 Welds As a Function of Time for Various Temperatures (Summers, et al., 2002)
NOTE: Temperature Provided in °C; for Conversion to °F use °F = 9/5 °C + 32.

3.1.3 Assessment of the DOE Approach

Mill-Annealed Material

The DOE evaluation of phase stability of the Alloy 22 waste package outer container assumes the same precipitation kinetics for all topologically close-packed and carbide phases. The effect of compositional variability for time-temperature-transformation diagrams of nickel-base alloys, in particular for Alloy 625 (Ni-21.5Cr-9.0Mo-5.0Fe-3.6Nb-0.10C in weight percent), has been discussed in Floreen (2002). It was reported that the time-temperature-transformation diagram of Alloy 625 can be shifted significantly by changes in niobium content. In addition, precipitation of various carbides (i.e., MC, M_6C, and $M_{23}C_6$) is about one order of magnitude faster than the intermetallic phases in Alloy 625 as a result of the favorable kinetics of carbides precipitation controlled by carbon diffusion because of the fast diffusion of carbon. Because of their similarity in alloy composition, the phase transformation behavior observed in Alloy 625 can be applied to Alloy 22. Zhao, et al. (2000) also observed different precipitation kinetics for formation of M_6C, $M_{23}C_6$, σ- and μ-phases in Hastelloy X (Ni-22Cr-18.5Fe-9Mo-1.5Co-0.15C in weight percent). On the basis of these observations, it is apparent that heat-to-heat variations in alloy composition may have a significant effect on the phase stability in Alloy 22 and thus its mechanical properties. Therefore, the effects of compositional variations need to be evaluated further. DOE agreed to provide additional information on the effect of the entire fabrication sequence on phase instability of Alloy 22 in agreement CLST 2.04.

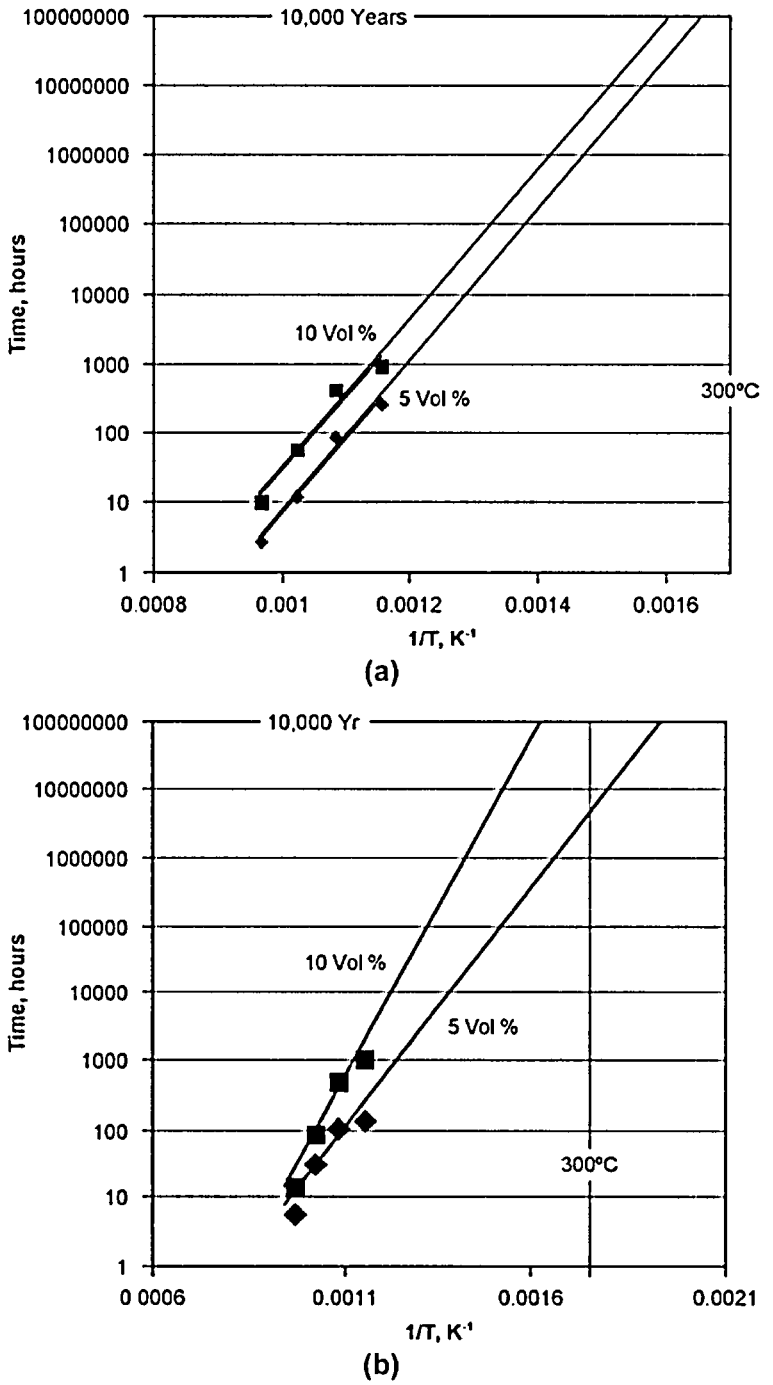

Figure 3-8. Log(Time) Versus Reciprocal Temperature Plots for Topologically Close-Packed Phases in Alloy 22 Welds and Extrapolation to Repository-Relevant Conditions (a) in Summers, et al. (2002) and (b) in CRWMS M&O (2001c)

The effect of cold work before thermal treatment on ordering transformation or intermetallic precipitation in Alloy 22 was not considered in the DOE evaluation. Sridhar, et al. (1980) observed that cold work before aging can increase markedly the kinetics of the long-range ordering transformation for Alloy 276. Surface and near-surface areas of the Alloy 22 waste package outer containers could be affected by cold work arising from sudden mechanical loads, impingement by wall-rock shear offsets, and other interactions leading to localized plastic deformation. Cold work in the form of residual stresses can also result from fabrication during cylinder rolling operations and postweld laser peening treatments, as well as handling accidents. As a result, additional evaluation on the effect of cold work is needed. DOE agreed to expand its aging test program to include cold worked Alloy 22 materials in agreement CLST 2.05.

Modeling of topologically close-packed phases and long-range ordering using Arrhenius relationships is acceptable if sufficient data are available. For precipitation of topologically close-packed phases, an average activation energy value was obtained based on the aging data for four temperatures and widely spaced time periods, whereas, only two data points were implemented in the estimation for long-range ordering. As a result, a large uncertainty is associated with the extrapolation of short-term, high-temperature data to repository-relevant temperatures and times. Therefore, additional data are needed to attain a better estimate of the activation energy values and the preexponential coefficients. In the DOE assessment, the extrapolation of short-term, high-temperature data to repository-relevant temperatures is modeled assuming the precipitation mechanisms are the same at repository temperatures as at the higher testing temperatures. A fundamental understanding of the precipitation mechanism and temperature relationship was not provided. Furthermore, the DOE results from the theoretical modeling of phase transformation in Alloy 22 based on simplified alloy systems and phases are preliminary, and extensive validation of the thermodynamic and mobility databases, as well as validation of the model predictions, has not been performed. Additional evaluations are necessary to support the model predictions. DOE agreed to provide more data and evaluations to reduce the uncertainty in a revised Aging and Phase Stability of Waste Package Outer Barrier document in agreement CLST 2.05.

Welded Material

The DOE evaluation of phase stability in Alloy 22 welds was based on the analysis of specimens from 12.5-mm [0.5-in] thick welded plates. Thin, welded specimens used in the DOE evaluation do not represent the dimensions of the final closure weld for the waste package (CRWMS M&O, 2000b). It is anticipated the thin specimens used have substantially different thermal cycling and lower heat input compared with the actual waste packages. In addition, there are many welding process operations and parameters that may affect the quality of the weld and the resultant weld microstructure. DOE agreed to provide additional information on the effect of the entire fabrication sequence on phase instability of Alloy 22, including the effect of welding thick sections, in agreement CLST 2.04.

The DOE modeling of topologically close-packed phases precipitation in Alloy 22 welds was based on the precipitate volume fraction data from short-term aging experiments. It was assumed that the precipitation kinetics for all phases are the same, and the precipitation mechanism is independent of temperature. Different extrapolated cutoff temperatures to give a 10,000-year life were obtained based on the calculated times for formation of 5- and 10-volume percent topologically close-packed phases. The observed discrepancies of the extrapolated

cutoff temperatures are the result of small changes in the slopes of the lines in Figure 3-8 due to uncertainties in the validity of the extrapolation on the basis of limited data during a short-time span. These model predictions need to be verified for lack of a fundamental understanding of the precipitation behavior in the welded materials. The effect of welding on the precipitation kinetics of secondary phases has been discussed by Floreen (2002). In comparison with the time-temperature-transformation diagram for δ-phase in Alloy 625 base metal, the diagram for the weld was shifted to the right by more than one order of magnitude in time. Precipitation in the welded Alloy 22 material is also expected to be faster than in the base metal because of the presence of existing precipitates that formed during solidification of the welded material. DOE agreed to provide more data and evaluations of welded materials in agreements CLST 2.04 and 2.05.

3.2 The CNWRA Investigations

Whereas the DOE analysis of thermal stability of Alloy 22 focused on long-term thermal aging of the alloy in both the mill-annealed and welded conditions, short-term exposures to elevated temperatures that may occur during welding and induction annealing processes have not been considered. Hence, their effects on phase stability and corrosion of Alloy 22 have not been evaluated adequately. CNWRA conducted a limited analysis to evaluate the effect of thermal aging on the microstructure of both mill-annealed and welded Alloy 22 (Pan, et al., 2003). This analysis is discussed in the following sections.

3.2.1 Mill-Annealed Material

The chemical composition of the mill-annealed Alloy 22 (Heat 2277-8-3175) used in this study is provided in Table 3-1. The mill-annealed Alloy 22 was thermally aged at 870 °C [1,598 °F] for times ranging from 5 to 30 minutes. This heat-treatment temperature is close to the nose of the time-temperature-transformation diagram of Alloy 22 (Heubner, et al., 1989). The aging times indicate the total time during which the specimens were inside the furnace. After placement in the furnace, it took approximately 2 minutes for the specimens to reach 870 °C [1,598 °F] . Transmission electron microscopy thin foils were prepared using dimpling and ion-milling techniques. At least two specimens for each aging condition, including the mill-annealed specimens, were examined. The analytical electron microscopy analyses were conducted using a Phillips CM200 scanning transmission electron microscope operated at 200 kV. The quantitative x-ray microanalyses, both spot analysis and line scan, were conducted with a probe size estimated at 1 to 2 nm [3.9 to 7.8 × 10^{-7} in]. The x-ray intensities were converted to concentration of elements using the Cliff-Lorimer procedure (Goldstein, et al., 1986). In this procedure, the ratio of concentration of elements is assumed proportional to the ratio of the x-ray intensities by a constant *k* factor, hence, the x-ray fluorescence and absorption can be

Table 3-1. Bulk Composition of Alloy 22 Heat 2277-8-3175 (Weight Percent)*

Ni	Cr	Mo	W	Fe	Co	Si	Mn	V	P	S	C
57.8	21.40	13.60	3.00	3.08	0.09	0.030	0.12	0.15	0.008	0.002	0.004

*NOTES: Ni — nickel; Cr — chromium; Mo — molybdenum; W — tungsten; Fe — iron; Co — cobalt; Si — silicon; Mn — manganese; V — vanadium; P — phosphorus; S — sulfur; C — carbon

neglected because of the small thickness of the sample. The *k* factors were calculated by conducting the analysis at a location remote from the grain boundary and using the known bulk chemical composition of the alloy as reference. Nickel, the main alloying element in Alloy 22, was used as the basis for calculating the concentration of other alloying elements.

The microstructures of the grain-boundary regions of the thermally aged Alloy 22 at 870 °C [1,598 °F] for 5 and 30 minutes are shown in Figures 3-9 through 3-11. The effect of aging time on grain-boundary precipitation is clearly shown in these figures. Although an aging time of 5 minutes produced thin-film type grain-boundary precipitates having a thickness of approximately 10 nm [3.9×10^{-7} in], the size of the precipitates increased substantially after aging for 30 minutes. No grain-boundary precipitate was observed in the mill-annealed specimen. Optical microscopic examination of the polished Alloy 22 specimens revealed that while the grain boundaries of the mill-annealed and the 5-minute-aged specimens appeared clean, partial grain-boundary precipitation coverage was observed in the 30-minute-aged specimen. It is important to note that the heat-treatment conditions used in this study result in only a small amount of precipitates at grain boundaries. For these heat-treatment conditions, approximately 1-percent grain-boundary precipitation coverage was estimated (Payer, et al., 2002). The chemical compositions of the grain-boundary precipitates and the regions adjacent to the precipitates were measured in the thin-foil specimens by spot analysis and are presented in Table 3-2. It is clearly seen in Table 3-2 that the measured concentrations of molybdenum and tungsten in the precipitates are much higher than the bulk content of these elements as listed in Table 3-1. In addition, composition at the regions adjacent to the precipitates is similar to the bulk composition of Alloy 22 with a slightly lower molybdenum content. Concentration profiles of nickel, chromium, molybdenum, iron, and tungsten were obtained across precipitate-matrix interfaces and along grain boundaries between precipitates. Several grain-boundary regions were examined on duplicate specimens with the same heat treatment. Representative concentration profiles are shown in Figures 3-9 through 3-11. All concentration profiles showed a smooth transition from the matrix to the precipitate. These results indicate that no significant depletion of chromium and molybdenum was detected in the matrix adjacent to the precipitates nor in the grain-boundary regions between precipitates.

Stainless steels and nickel-chromium-iron alloys with higher carbon contents are subjected to sensitization as a consequence of thermal exposure (Bruemmer, 1990; Was and Kruger, 1985). Sensitized stainless steels and nickel-chromium-iron alloys are susceptible to intergranular corrosion as a result of the formation of a narrow chromium-depleted zone adjacent to the chromium carbide precipitates in the grain-boundary regions. In view of the sensitization phenomenon for the development of chromium depletion in stainless steels and

Table 3-2. Measured Composition of Grain-Boundary Precipitates and the Vicinity in Weight Percent (± Indicates the 95-Percent Confidence Interval)

Probe Location	Nickel	Chromium	Molybdenum	Tungsten	Iron
Precipitate	26.53 ± 3.00	17.81 ± 3.81	44.33 ± 2.66	8.88 ± 1.17	2.34 ± 0.27
Adjacent to Precipitate	58.42 ± 0.15	22.43 ± 0.25	11.75 ± 0.38	2.54 ± 0.70	4.46 ± 0.15
Bulk Composition	57.8	21.40	13.60	3.00	3.08

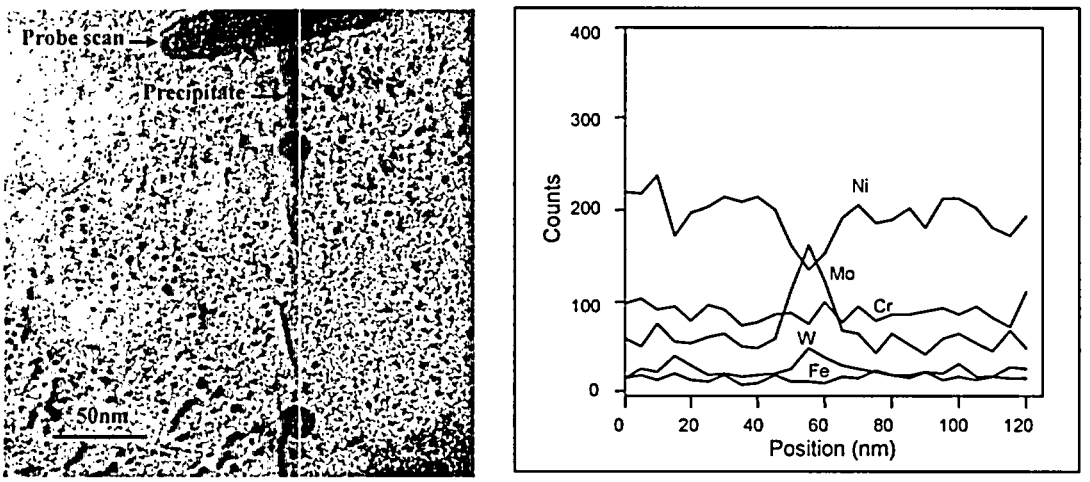

Figure 3-9. Grain-Boundary Microstructure and Concentration Profiles across a Grain Boundary of Alloy 22 after Aging at 870 °C [1,598 °F] for 5 Minutes

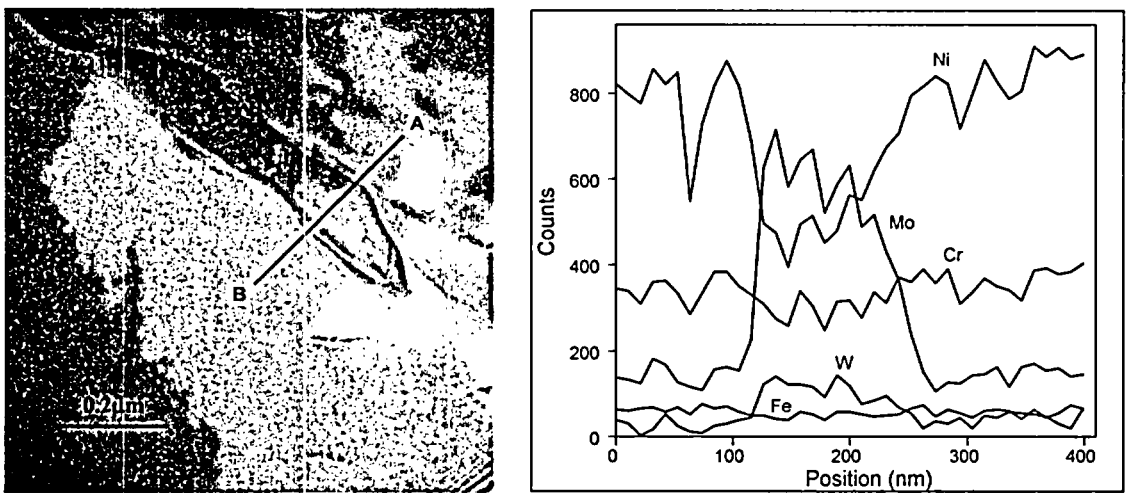

Figure 3-10. Grain-Boundary Microstructure and Concentration Profiles across a Grain Boundary of Alloy 22 after Aging at 870 °C [1,598 °F] for 30 Minutes

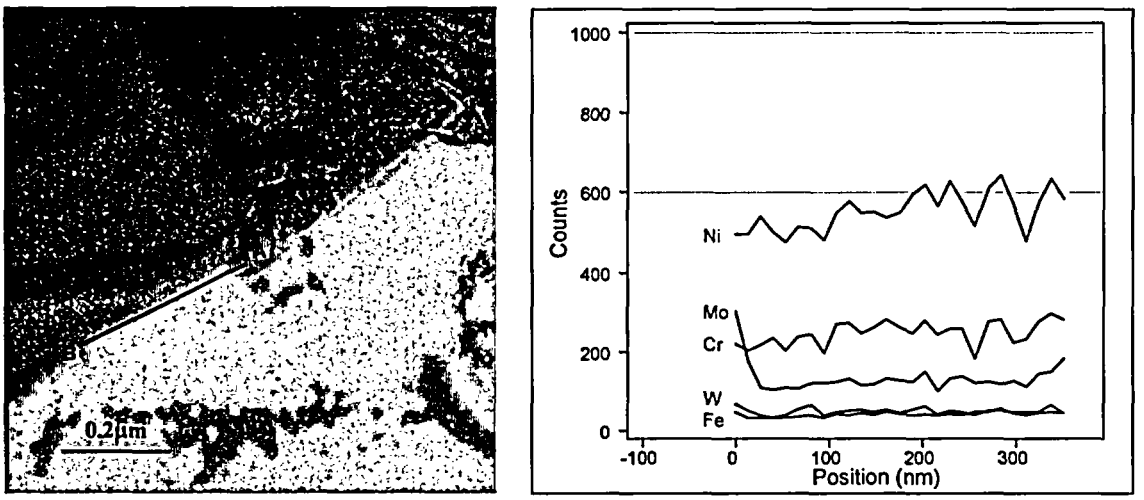

Figure 3-11. Grain-Boundary Microstructure and Concentration Profiles along a Grain Boundary of Alloy 22 after Aging at 870 °C [1,598 °F] for 30 Minutes

nickel-chromium-molybdenum alloys, it is generally expected that incorporation of molybdenum in the topologically close-packed phases is likely to induce the depletion of molybdenum in the matrix immediately adjacent to the precipitate. At present, the only data on alloying element depletion in nickel-chromium-molybdenum alloys have been reported by Tawancy (1996) using analytical electron microscopy spot analyses to measure the composition in the vicinity of a μ-phase in Alloy C-276 after aging at 870 °C [1,598 °F] for 1 hour. From the spectrum taken approximately 40 nm [1.6×10^{-6} in] from the μ-phase and compared with that from the precipitate, it was concluded by Tawancy (1996) that precipitation of μ-phase resulted in localized depletion of molybdenum. In the present study, however, multiple concentration profiles indicate that no significant depletion of precipitate-forming elements (i.e., chromium and molybdenum) occurred in the grain-boundary regions of the thermally aged Alloy 22 specimens. This discrepancy could be attributed to the presence of molybdenum-rich carbides adjacent to the μ-phase, as observed in Alloy C-276 (Tawancy, 1996).

Chromium depletion in sensitized stainless steels is widely accepted to be prompted by the precipitation and growth of chromium-rich carbides at grain boundaries because of the fast diffusion of carbon (compared with chromium) to the grain boundaries (Bruemmer, 1990). In contrast with the kinetics of carbide precipitation controlled by carbon diffusion, precipitation of the topologically close-packed phases is anticipated to be governed by substitutional element diffusion. As shown in Table 3-2, molybdenum, nickel, and chromium are the major elements forming the topologically close-packed phases and are expected to have comparable bulk diffusivities. For this reason, sharp depletion of chromium or molybdenum, if any depletion zone is present, should not be expected. Nevertheless, a conclusive determination of the absence of alloying element depletion in Alloy 22 is necessary. In addition, because the compositions of the various topologically close-packed phases are similar (Raghavan, et al., 1984), it is difficult to identify these phases using only x-ray microanalysis. Electron diffraction analysis is essential in identifying these phases.

3.2.2 Welded Material

The 38.1-mm- [1.5-in-] thick Alloy 22 welded plate used in this study was produced by Framatome ANP, Inc. for DOE using gas tungsten-arc welding with a double U-groove joint geometry. The appearance of half of the weldment is shown in Figure 3-12. Chemical compositions of the base Alloy 22 plate (Heat 059902LL2) and Alloy 622 weld filler (Heat XX2048BG) are provided in Table 3-3. Both aging and solution-annealing treatments of the as-received welded material were performed to verify the amount of precipitates reported by DOE and to evaluate the precipitation stability in the weld. While the aging treatments were conducted at 760 °C [1,400 °F] for 6 and 60 hours and at 870 °C [1,598 °F] for periods ranging from 5 minutes to 4 hours, solution annealing was conducted at 1,125 °C [2,057 °F] for periods ranging from 15 to 60 minutes. Metallurgical samples were prepared using standard polishing techniques and electrochemical etching in an oxalic acid solution similar to that used in the DOE aging studies. A short etching time of a few seconds was used so that removal of precipitates as a result of overetching could be minimized. Microstructure of these welded samples was analyzed using optical and scanning electron microscopy. The volume fraction of the precipitates was measured from optical micrographs using imaging analysis software.

Table 3-3. Bulk Composition of Base Alloy 22 and Alloy 622 Filler Materials (Weight Percent)*

Material	Ni	Cr	Mo	W	Fe	Co	Si	Mn	V	P	S	C
Alloy 22 Heat 059902LL2	59.58	20.35	13.85	2.63	2.85	0.01	0.05	0.16	0.17	0.007	0.0002	0.005
Alloy 622 Filler Heat XX2048BG	59.40	20.48	14.21	3.02	2.53	0.02	0.07	0.20	0.02	0.009	<0.001	0.001

*NOTES: Ni — nickel; Cr — chromium; Mo — molybdenum; W — tungsten; Fe — iron; Co — cobalt; Si — silicon; Mn — manganese; V — vanadium; P — phosphorus; S — sulfur; C — carbon

Figure 3-13 shows micrographs taken from the fusion zone of the welded material in the as-welded condition. On solidification, formation of a dendritic structure and precipitation of secondary phases are evident, as shown in Figure 3-13. It was noted, however, the microstructure adjacent to the fusion zone was not significantly altered, and a heat-affected zone was not clearly evident in the welded material. Because welds are prone to the segregation of alloying elements inside the fusion zone (Cieslak, et al., 1986), local compositions of both the dendrite cores and the interdendritic regions were determined using energy-dispersive x-ray spectroscopy analysis. Table 3-4 shows the mean and standard deviation chemical composition values of the dendrite cores and the interdendritic regions measured by spot analysis in the Alloy 22 welded specimen in the as-welded condition. It is clearly seen in Table 3-4 that molybdenum tends to segregate to the interdendritic regions as a consequence of nonequilibrium solidification because of its higher melting point in comparison with other major alloying elements (i.e., nickel and chromium). The measured molybdenum concentration is much higher than the bulk molybdenum content in the Alloy 22 base metal and in the Alloy 622 filler metal, as listed in Table 3-4. Cieslak, et al. (1986) analyzed the welding metallurgy of gas tungsten-arc welds of Alloy 22. The concentration profiles were obtained transverse to the dendritic growth direction using electron microprobe analysis. It was observed

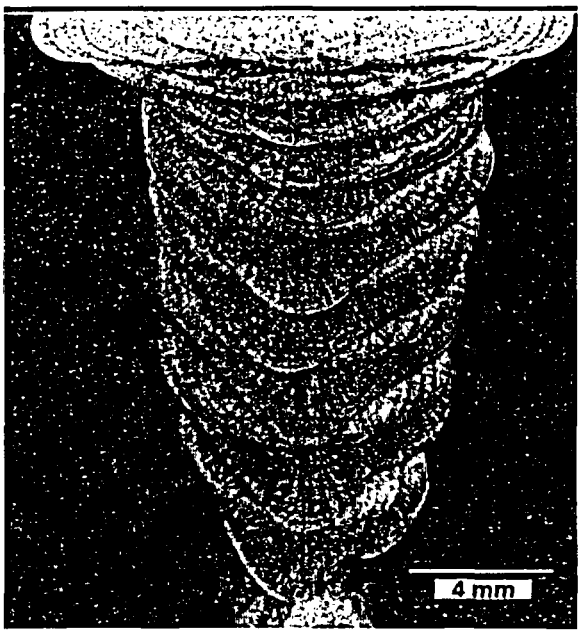

Figure 3-12. Photograph Showing the Fusion Zone Morphology That Covers Half the Thickness of the Alloy 22 Welded Plate

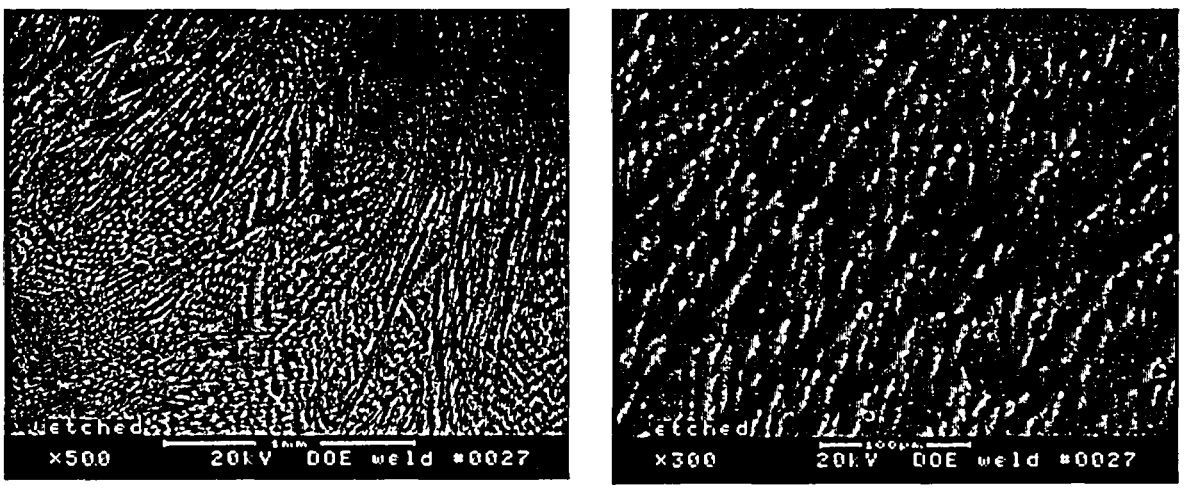

Figure 3-13. Scanning Electron Micrographs of Alloy 22 Welds in the As-Welded Condition Showing Dendrite Structure (Left) and Precipitates (White Spots on the Right) in the Fusion Zone

Table 3-4. Measured Chemical Compositions and Calculated P-Phase Solvus Temperatures in the Weld Fusion Zone						
	Chemical Content (Weight Percent)					
Location	Nickel	Chromium	Molybdenum	Iron	Tungsten	P-Phase Solvus Temperature
Dendrite Core	59.8 ± 1.3	21.8 ± 0.4	13.0 ± 1.1	2.75 ± 0.11	2.60 ± 0.09	1,024 °C [1,875 °F]
Interdendritic Region	54.4 ± 1.6	22.6 ± 0.2	18.0 ± 1.6	2.48 ± 0.07	2.48 ± 0.06	1,271 °C [2,320 °F]
Alloy 22 Base Metal	60.64	20.44	12.80	2.63	3.08	1,026 °C [1,879 °F]
Alloy 622 Filler	59.89	20.41	13.99	2.46	2.96	1,066 °C [1,951 °F]

that the dendrite core is enriched in nickel and depleted in molybdenum relative to the interdendritic region. The observed molybdenum segregation in the present study in the solidified Alloy 22 weld fusion zone is in agreement with the work of Cieslak, et al. (1986).

The amount of precipitates in the welded samples as a function of aging time and temperature is shown in Table 3-5. Multiple measurements were conducted along the centerline of the fusion zone for all thermally aged welded specimens. Additional analysis across the fusion zone of the specimen after aging at 760 °C [1,400 °F] for 6 hours was attempted to evaluate distribution of the precipitates. The measured volume percent values inside the fusion zone for both orientations are consistent. The large standard deviation values reported in Table 3-5 indicate an inhomogeneous distribution of the precipitates. It is apparent in Table 3-5 that the specimen in the as-welded condition has the lowest volume percent of precipitates, and a significant effect of aging treatment on precipitation of secondary phases is seen. The amount of precipitates increases with increasing aging time for the aging temperature of 870 °C [1,598 °F], whereas a decrease was observed for the aging temperature of 760 °C [1,400 °F]. Figures 3-14 and 3-15 show representative microstructures for aging temperatures of 760 °C [1,400 °F] and 870 °C [1,598 °F], respectively, at various aging times. It was observed that with aging at 870 °C [1,598 °F], the size of the precipitates increases with increasing aging time. In contrast, the precipitate morphology after a 60-hour treatment at 760 °C [1,400 °F] became coarse, but the number of precipitates per unit area decreases significantly, as shown in Figure 3-14(c). The low-volume fraction of precipitates measured for the welded sample aged at 760 °C [1,400 °F] for 60 hours can be attributed to a substantial grain growth in the fusion zone as a result of prolonged aging, as shown in Figure 3-14(d) at a low magnification. As discussed in Section 3.1.2, DOE reported an average value of 2.7 volume percent of precipitates in the as-welded condition, a factor approximately six times higher than that measured in this study. It is also noted that both precipitate volume percent values measured for the 760 °C [1,400 °F] aged Alloy 22 welded specimens in Table 3-5 are much lower than the values reported by DOE in Figure 3-7 (Summers, et al., 2002). Given that different Alloy 22 welds were used in these analyses, the observed discrepancies could be attributed to the effects of various welding process parameters on the resultant weld microstructure.

Table 3-5. Volume Fraction of Precipitates Measured on Alloy 22 Welds after Aging at 760 and 870 °C [1,400 and 1,598 °F] for Various Times	
Heat Treatment Condition	**Amount of Precipitates (Volume Percent)**
As-welded (centerline)	0.42 ± 0.24
760 °C [1,400 °F]/6-hour (centerline)	4.4 ± 0.6
760 °C [1,400 °F]/6-hour (lengthwise inside weld)	3.7 ± 0.6
760 °C [1,400 °F]/6-hour (lengthwise outside weld)	1.4 ± 0.4
760 °C [1,400 °F]/60-hour (centerline)	2.6 ± 0.7
870 °C [1,598 °F]/5-minute (centerline)	1.2 ± 0.2
870 °C [1,598 °F]/30-minute (centerline)	4.0 ± 0.9
870 °C [1,598 °F]/1-hour (centerline)	8.1 ± 1.6
870 °C [1,598 °F]/4-hour (centerline)	10.8 ± 1.5

Residual precipitates were observed for all solution annealing times at 1,125 °C [2,057 °F]. Representative micrographs of the solution annealed Alloy 22 welds are shown in Figure 3-16. There are 1.8 volume percent precipitates after a 15-minute heat treatment at 1,125 °C [2,057 °F], which is higher than in the as-welded condition. A long hold time up to 60 minutes does not significantly change the microstructure, as revealed in Figure 3-16. The influence of solution-annealing temperature on phase stability of Alloy 22 welds was also investigated. In addition to 1,125 °C [2,057 °F], solution heat treatments at 1,200, 1,250, and 1,300 °C [2,192, 2,282, and 2,372 °F] for 15 minutes followed by water quenching were applied. The microstructures inside the fusion zone of the solution treated specimens examined by scanning electron microscopy are shown in Figures 3-17 and 3-18 at 100 and 300 times magnification, respectively. As seen in these two figures, solution annealing at 1,125, 1,200, and 1,250 °C [2,057, 2,192, and 2,282 °F] results in homogenization of the fusion zone in comparison with that in the as-welded condition in Figure 3-13, and the extent of homogenization increases with increasing temperature. In contrast, after solution annealing at 1,300 °C [2,372 °F] for 15 minutes, dendrite structure in the fusion zone is completely dissolved and abnormal grain growth is observed with the majority of the precipitates located inside the grains, as shown in Figures 3-17(d) and 3-18(d). In all cases, the amount of precipitates per unit area seems to slightly decrease as the solution-annealing temperature increases. Nevertheless, the high-volume fraction of precipitates in the solution-annealed Alloy 22 welds indicates the solution-annealing conditions employed in this study promote precipitation of the secondary phases [compare Figures 3-16 and 3-17 with Figure 3-14(a)].

In the Waste Package Operations Fabrication Process Report (CRWMS M&O, 2001a), the current outer cylinder fabrication methods include annealing of the Alloy 22 outer cylinder at 1,150 °C [2,102 °F] for an unspecified time. Annealing at 1,121 °C [2,050 °F] for a minimum of 20 minutes, a general solution heat treatment for Alloy 22 from the alloy manufacturers, was also noted in the Waste Package Project FY–01 Closure Methods Report (CRWMS M&O,

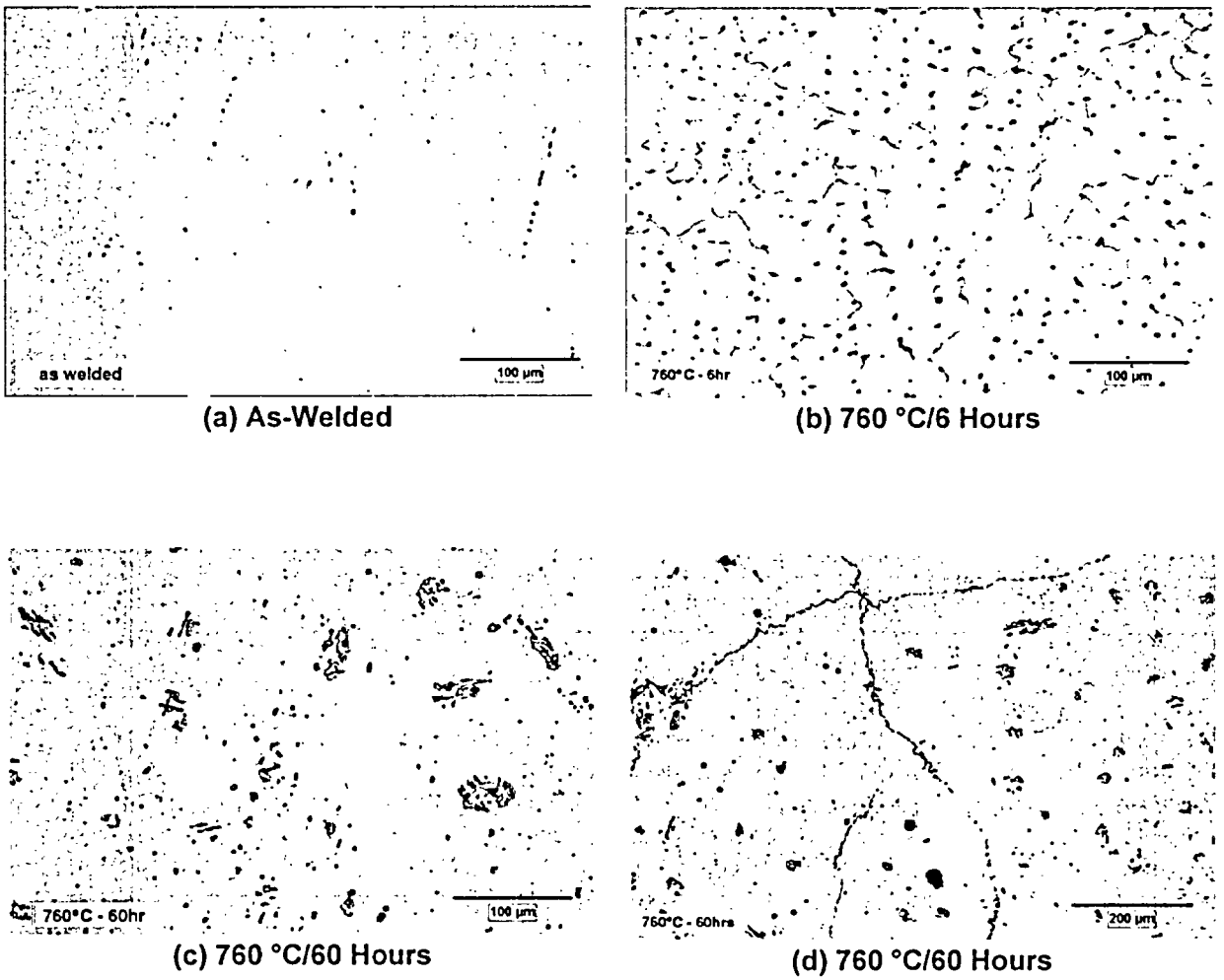

(a) As-Welded

(b) 760 °C/6 Hours

(c) 760 °C/60 Hours

(d) 760 °C/60 Hours

Figure 3-14. Photographs Showing Amount of Precipitates in Alloy 22 Welds in the As-Welded Condition and after Aging at 760 °C [1,400 °F] for 6 and 60 Hours

2001b). Because of the kinetics of topologically close-packed phases dissolution is sluggish and a high-annealing temperature may lead to undesirable grain growth, longer solution treatment times at intermediate temperatures, such as those proposed by DOE, may be required. The observed microstructural changes in the welded Alloy 22 material as a result of solution annealing warrant further evaluation in assessing the solution-annealing treatment.

3.2.3 Phase-Stability Modeling

Precipitation of topologically close-packed phases in Alloy 22 and the upper stability temperature of these phases (also known as solvus temperature), as influenced by alloy compositional variation, were evaluated using thermodynamic calculations. Theoretical calculations were performed using the Thermo-Calc Version N software program and the Ni-Data Version 5 database, a multicomponent database developed by Thermotech for nickel-base alloys. Figure 3-19 shows the predicted phase mole fraction versus temperature

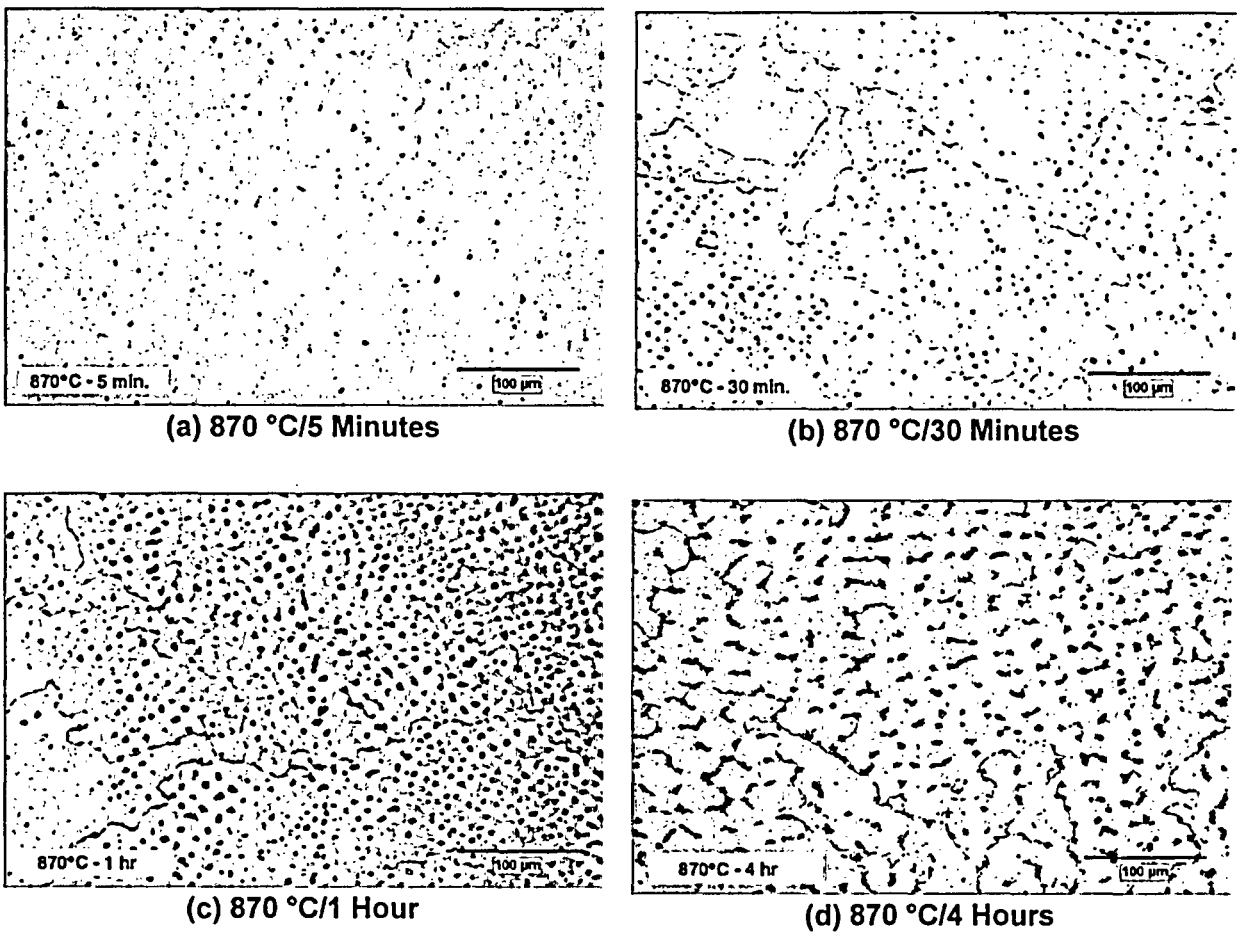

(a) 870 °C/5 Minutes

(b) 870 °C/30 Minutes

(c) 870 °C/1 Hour

(d) 870 °C/4 Hours

Figure 3-15. Photographs Showing Amount of Precipitates in Alloy 22 Welds after Aging at 870 °C [1,598 °F] for Various Times

diagrams using the Alloy 22 composition listed in Table 3-1. At the aging temperature of 870 °C [1,598 °F], the thermodynamic calculations predicted that P-phase would be the only equilibrium topologically close-packed phase. This result is contrary to that reported by the DOE (CRWMS M&O, 2001c) in which the σ-phase is predicted to be the only equilibrium phase at this temperature, as shown in Figure 3-5. The observed discrepancy in the thermodynamic calculations could have been caused by the use of different databases. The Ni-Data Version 5 database used in the current calculations has been extensively validated against experimental results reported for multicomponent nickel-base alloys. Additionally, this database has been used to predict topologically close-packed phase stability in various nickel-base alloys. The calculated phase contents and compositions at 870 °C [1,598 °F] are listed in Table 3-6. The calculated P-phase composition is consistent with the experimental values measured by analytical electron microscopy in Table 3-2.

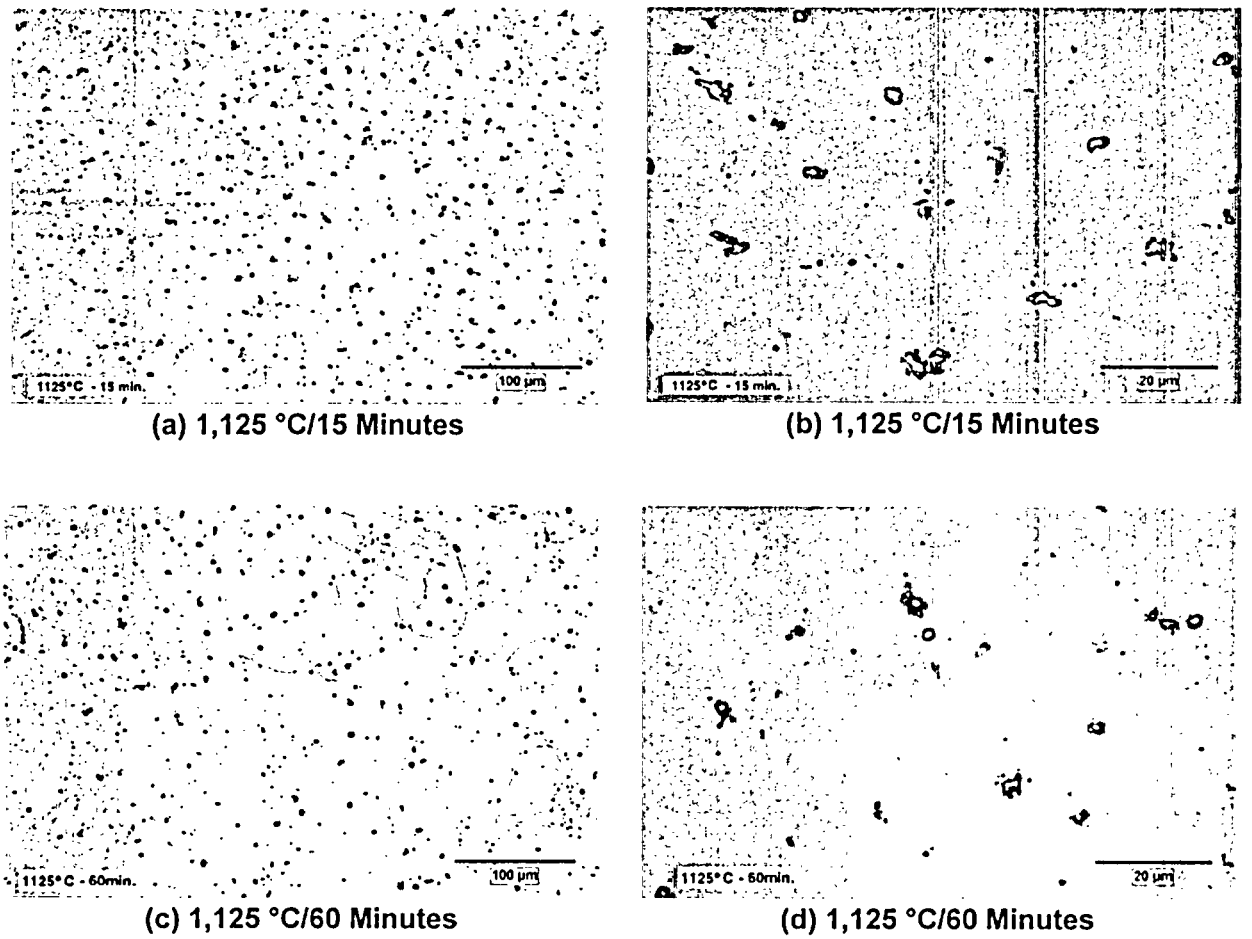

Figure 3-16. Photographs Showing Residual Precipitates in Alloy 22 Welds after Solution Annealing at 1,125 °C [2,057 °F] for 15 and 60 Minutes

Table 3-6. Calculated Phase Compositions at 870 °C [1,598 °F]

Phase	Amount		Chemical Content (Weight Percent)*							
	wt%	Mole%	Ni	Cr	Mo	W	Fe	Co	Si	C
γ	88.88	90.83	62.60	21.69	10.34	1.85	3.39	0.095	0.034	0.001
P	11.01	9.07	28.47	19.10	39.50	12.29	0.59	0.045	—	—
M_6C	0.11	0.10	25.08	14.47	52.12	4.80	0.93	0.016	0.001	2.58

*NOTES: Ni — nickel; Cr — chromium; Mo — molybdenum; W — tungsten; Fe — iron; Co — cobalt; Si — silicon; C — carbon

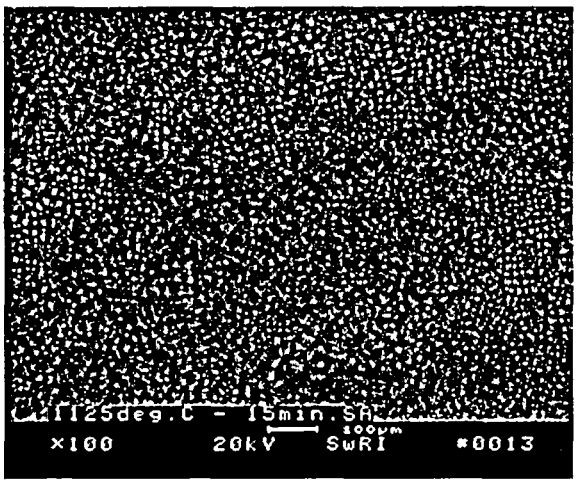

(a) 1,125 °C/15 Minutes

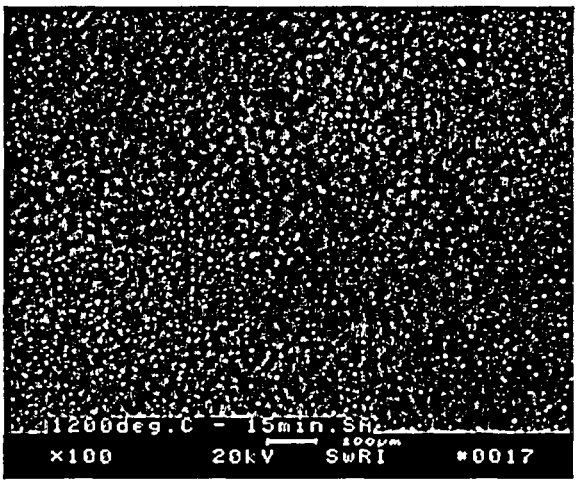

(b) 1,200 °C/15 Minutes

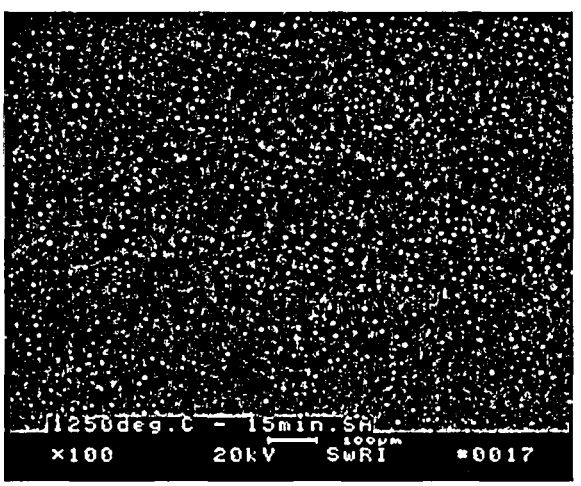

(c) 1,250 °C/15 Minutes

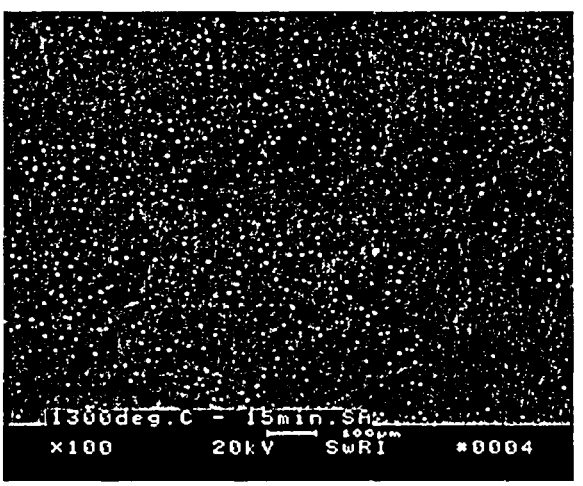

(d) 1,300 °C/15 Minutes

Figure 3-17. Scanning Electron Micrographs Showing Microstructural Changes in Alloy 22 Welds After Solution Annealing at Temperatures: 1,125; 1,200; 1,250; and 1,300 °C [2,057; 2,192; 2,282; and 2,372 °F] for 15 Minutes

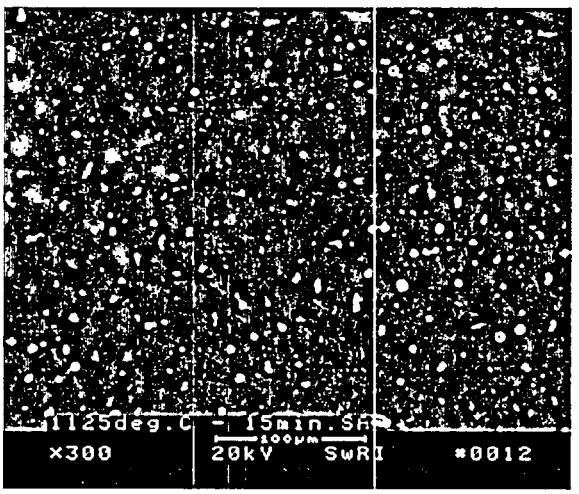

(a) 1,125 °C/15 Minutes

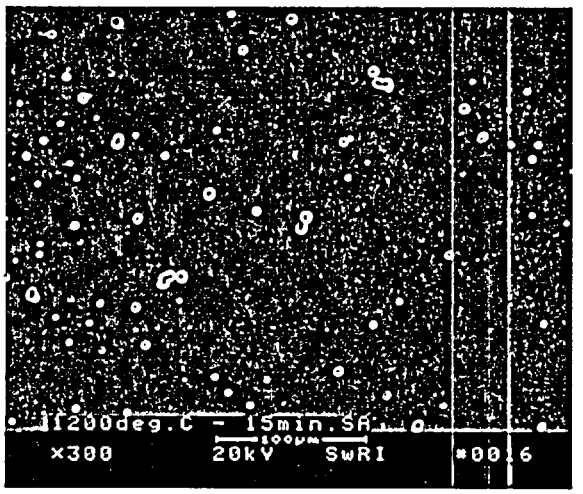

(b) 1,200 °C/15 Minutes

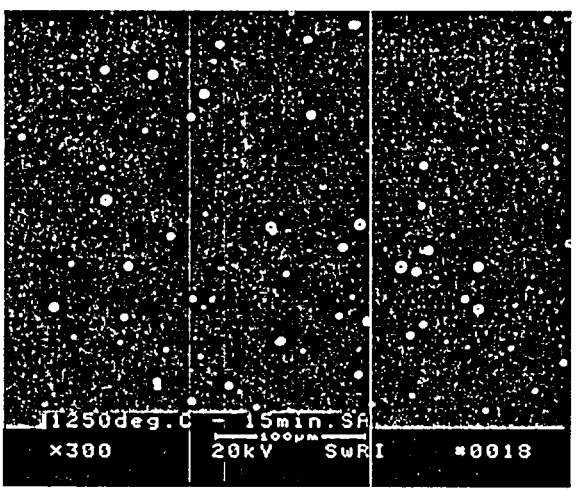

(c) 1,250 °C/15 Minutes

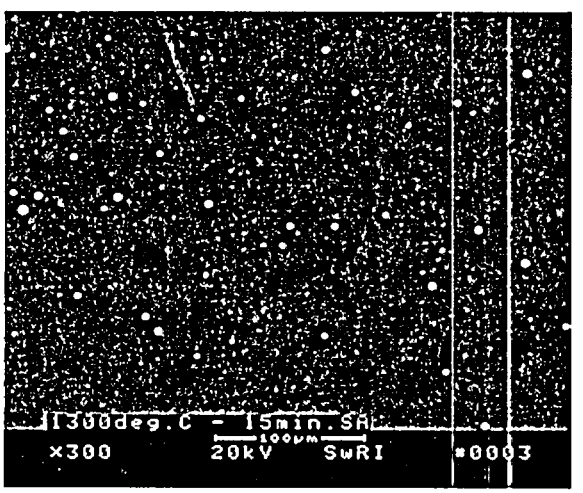

(d) 1,300 °C/15 Minutes

Figure 3-18. Scanning Electron Micrographs Showing the Detailed Microstructures in the Fusion Zone in Alloy 22 Welds After Solution Annealing at Temperatures: 1,125; 1,200; 1,250; and 1,300 °C [2,057; 2,192; 2,282; and 2,372 °F] for 15 Minutes

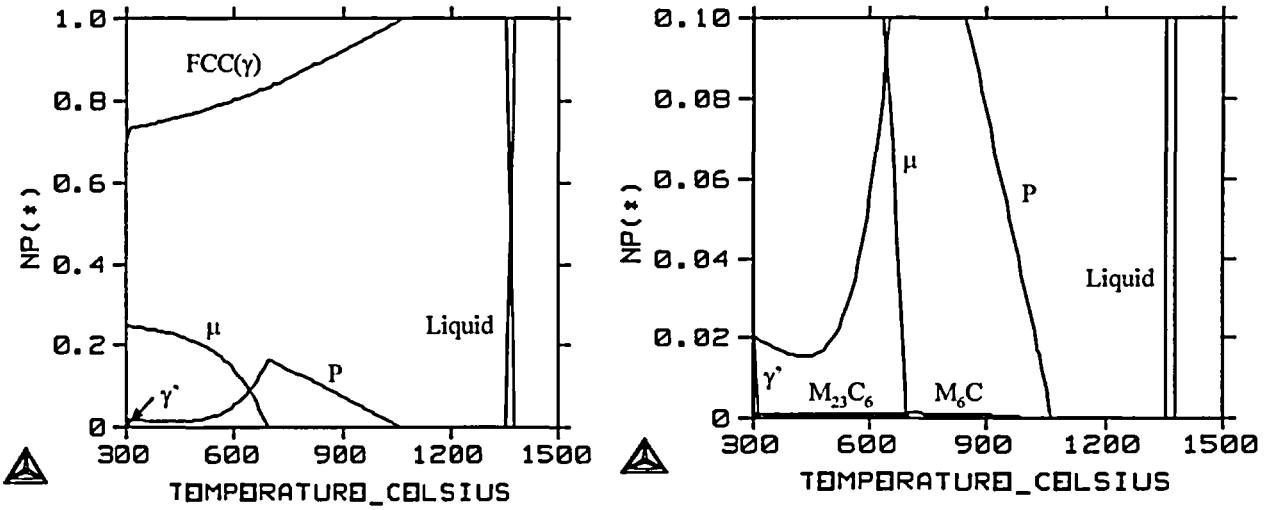

Figure 3-19. Predicted Phase Fraction Versus Temperature Diagrams. NP(✳) Represents Phase Fraction for Each Phase, and FCC Is Face-Centered-Cubic. NOTE: Temperature Provided in °C; for Conversion to °F use °F = 9/5 °C + 32.

Evaluation of the effect of compositional variation on the solvus temperature of P-phase was accomplished by varying the composition between the specified limits for each element, as listed in ASTM Standard Specification B575–99a (ASTM International, 2001a). The baseline Alloy 22 composition was assumed to be 21.2Cr-13.5Mo-4Fe-3W-2Co-0.08Si-0.01C-balance nickel in weight percent, the same composition used in the DOE calculations for Figure 3-5, except that manganese and vanadium were excluded because of their absence in the database. The predicted P-phase solvus temperatures, as each element is changed between its maximum and minimum limits, are shown in Figure 3-20. The thermodynamic calculation using the baseline composition predicted a solvus temperature for P-phase of 1,074 °C [1,965 °F]. Molybdenum, as the major topologically close-packed phase forming element, exhibits the greatest sensitivity to the upper stability temperature of the P-phase. Other P-phase forming elements (i.e., chromium and tungsten) also have a profound effect. It should be mentioned that the potent influence of iron is attributed to the largest variation between its maximum and minimum limits. These results indicate that heat-to-heat variations in the Alloy 22 composition may influence the formation and dissolution of topologically close-packed phases.

The effect of element segregation on the upper stability temperature of the P-phase in the weld was also evaluated. The calculated solvus temperatures for the P-phase are listed in Table 3-4 based on the measured compositions in the Alloy 22 weld (Table 3-4). The thermodynamic calculation predicted a solvus temperature for the P-phase at 1,271 °C [2,320 °F] in the interdendritic regions, suggesting that the P-phase is stable at temperatures up to 1,271 °C [2,320 °F]. This calculated solvus temperature in the interdendritic regions is higher than the solution-annealing temperature of 1,125 °C [2,057 °F] used in this study. Similar calculations were conducted using the compositions measured in the weld fusion zone by Cieslak, et al. (1986). The composition estimated from the microprobe profiles was about 62.2Ni-19.6Cr-10.9Mo-3.13Fe-2.75W in weight percent inside the dendrite core, and that of the interdendritic region was about 52.4Ni-21.1Cr-18.8Mo-2.90Fe-3.43W. From these composition values, the solvus temperatures for the P-phase are predicted to be 872 and 1,319 °C [1,602 and 2,406 °F]

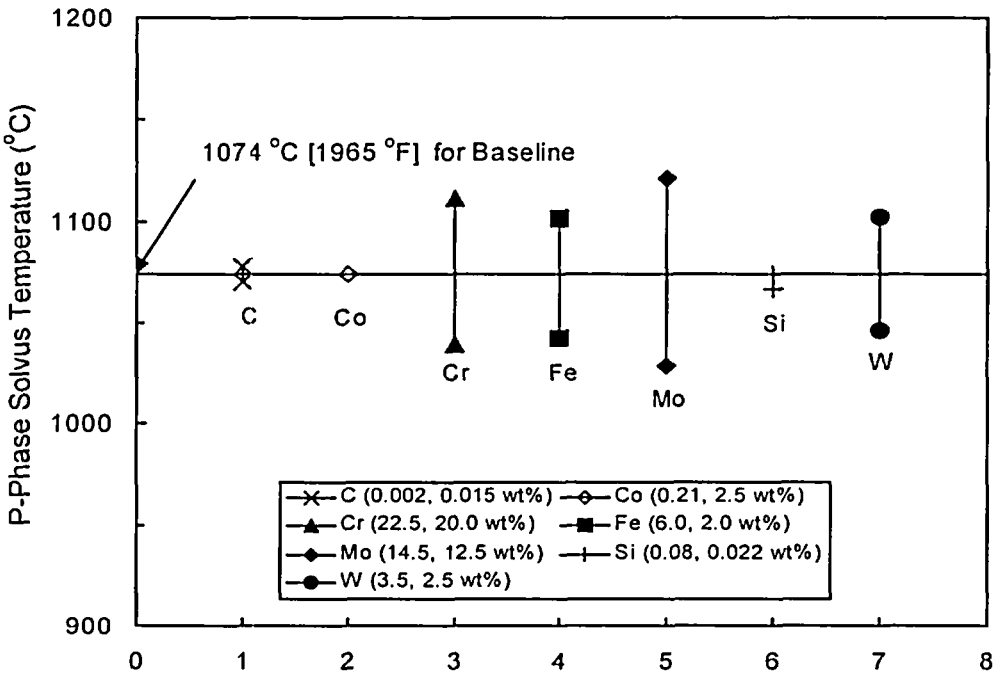

Figure 3-20. Variation in Calculated P-Phase Solvus Temperature by Varying Each Element in Alloy 22 within Its Composition Limits. The Baseline Composition is 21.2Cr-13.5Mo-4Fe-3W-2Co-0.08Si-0.01C-Balance Ni in Weight Percent.

in the dendrite core and the interdendritic region, respectively. These results imply that solution annealing of the Alloy 22 weld at the temperatures proposed by DOE (CRWMS M&O, 2001a,b) is inadequate to form a single phase solid solution by dissolving the topologically close-packed precipitates. This model prediction is consistent with experimental results showing that precipitates are observed in the Alloy 22 welded samples after various solution-annealing treatments, as discussed in Section 3.2.2. Results from both experiments and theoretical calculations suggest the proposed fabrication and closure processes may result in microstructural changes and thus adversely affect the lifetime of the waste package as a result of their influence on corrosion processes.

4 EFFECT OF FABRICATION PROCESSES ON CORROSION RESISTANCE

Multiple fabrication processes will be required to construct and seal the waste packages. As summarized in Chapter 2, these processes will include forming operations, cutting, machining, welding, postweld heat treatments, and postweld stress mitigation methods. As indicated in Chapter 3, thermal processes such as welding and postweld heat treatments can alter the microstructure of the welds and the base alloy. In the as-welded condition, Alloy 22 has been shown to contain topologically close-packed phases that have high concentrations of molybdenum and tungsten. In addition, short exposures to elevated temperatures can also result in the precipitation of topologically close-packed phases at the grain boundaries of mill-annealed Alloy 22. Formation of topologically close-packed phases may alter the corrosion resistance of the waste packages.

4.1 The DOE Investigations

The U.S. Department of Energy (DOE) investigated the uniform corrosion rate, localized corrosion susceptibility, and stress corrosion cracking resistance of Alloy 22. The effects of fabrication processes have been investigated using both welded and thermally aged material. The uniform corrosion rate has been evaluated using weight loss specimens exposed for periods ranging from 6 months to 5 years in test solutions derived from the composition of J–13 Well water. The compositions of the test solutions have been reviewed and reported by Brossia, et al. (2001). The compositions of simulated dilute water, simulated concentrated water, simulated acidified water, and simulated saturated water are provided in Table 4-1. Localized corrosion susceptibility of the mill-annealed alloy has been evaluated using standardized tests such as cyclic potentiodynamic polarization (ASTM International, 2001b) in the J–13 Well water based test solutions and in other solutions such as those containing concentrated calcium chloride. Evaluation of the effects of fabrication on localized corrosion susceptibility are limited to immersion and electrochemical tests in the J–13 Well water based solutions. Localized corrosion propagation rates are based on pit propagation rates obtained from literature reports using boiling concentrated oxidizing acid chloride solutions and are limited to the mill-annealed alloy. Stress corrosion cracking susceptibility had been evaluated using a variety of test methods. Studies on the effects of fabrication processes on stress corrosion cracking susceptibility were limited to single U-bend, slow-strain-rate, constant-load tests.

4.1.1 Uniform Corrosion of Mill-Annealed Alloy 22

General corrosion rates of Alloy 22 have been calculated using the measured weight loss of specimens exposed to the J–13 Well water based test solutions (CRWMS M&O, 2000c,d). A review of the data (6-month, 1-, and 2-year exposures) obtained from the long-term corrosion test facility at Lawrence Livermore National Laboratory was previously reported (Brossia, et al., 2001). The corrosion tests included both mill-annealed and welded specimens. Based on weight loss measurements, there were no significant differences in the corrosion rates for mill-annealed and welded specimens. Corrosion rates decreased with exposure time and were not found to be dependent on the composition of the test solution within the range studied. For an exposure time of 2 years, the corrosion rates were -31 to 37 nm/yr [-1.2×10^{-3} to 1.5×10^{-3} mpy] for specimens with no crevices and -9 to 73 nm/yr [-3.5×10^{-4} to 2.9×10^{-3} mpy] with crevices. Negative corrosion rates were attributed to the accumulation of

Table 4-1. The Composition of Several Aqueous Solutions Used for Corrosion Testing*								
	Concentration							
Ion	Simulated Dilute Water		Simulated Concentrated Water		Simulated Acidified Water		Simulated Saturated Water	
	60 and 90 °C		60 and 90 °C		60 and 90 °C		100 °C	
	mg/L	mM	mg/L	mM	mg/L	mM	mg/L	mM
K	34	0.87	3,400	87	3,400	87	142,000	3,632
Na^+	40	17.8	40,900	1,780	40,900	1,780	487,000	21,182
Mg^{2+}	1	0.04	<1	20.04	1,000	41	0	0.00
Ca^{2+}	0.5	0.01	<1	20.01	1,000	25	0	0.00
F	14	0.74	1,400	74	0.00	0.00	0	0.00
Cl	67	1.89	6,700	189	24,250	684	128,000	3,610
NO_3	64	1.03	6,400	103	23,000	371	1,313,000	21,175
SO_4^2	167	1.74	16,400	174	38,000	396	0	0.00
HCO_3	947	15.52	70,000	1,148	0.00	0.00	0	0.00
Si	27 (60 °C) 49 (90 °C)	—	27 (60 °C) 49 (90 °C)	—	27 (60 °C) 49 (90 °C)	—	—	—

*Civilian Radioactive Waste Management System Management and Operating Contractor. "Environment on the Surfaces of the Drip Shield and Waste Package Outer Barrier." ANL–EBS–MD–000001. Rev. 00 ICN 01. Las Vegas, Nevada: DOE, Office of Civilian Radioactive Waste Management. 2000.

NOTE: Temperature Provided in °C; for Conversion to °F use °F = 9/5 °C + 32.

silica scale on the test specimens. Tests conducted for shorter periods yielded higher corrosion rates. The maximum corrosion rate was 731 nm/year [2.9×10^{-9} mpy] and was observed after a 6-month exposure. Average corrosion rates were 50 nm/yr [2.0×10^{-3} mpy] for the specimens exposed for 6 months, 30 nm/yr [1.2×10^{-3} mpy] after 1 year, and 10 nm/yr [3.9×10^{-4} mpy] for specimens exposed for 2 years. Tests at Lawrence Livermore National Laboratory have been conducted for 5 years. Although detailed results of the 5-year test specimens have not been published, it was reported that the corrosion rate of 56 specimens exposed for 5 years was typically less than 25 nm/yr [9.8×10^{-4} mpy].[1] For the 5-year test specimens, greater corrosion

[1]Farmer, J. "Chemical Environment Evolution on Alloy 22." *Presentation to Nuclear Waste Technical Review Board January 28, 2003.* Las Vegas, Nevada. 2003.

rates were also observed for specimens with crevice formers.[2] Without crevice formers, the corrosion rates varied from 0 to 12 nm/yr [0 to 4.7×10^{-4} mpy]. Specimens with crevice formers had corrosion rates of 2 to 23 nm/yr [7.8×10^{-5} to 9.1×10^{-4} mpy], however, crevice corrosion was not observed. Composition of the test solutions and temperature {60 or 90 °C [140 or 194 °F]} did not have a significant effect on corrosion rate for either the creviced or uncreviced test specimens.

The corrosion rate of Alloy 22 has also been determined using electrochemical methods (Lian, et al., 2003; Meck, et al., 2003). The linear polarization resistance method with a scan rate of 0.0167 mV/s was used to determine the corrosion rate of Alloy 22 in simulated acidified water at 90 °C [194 °F]. The test specimens were maintained at anodic potentials of 0.4 and 0.65 volts versus the saturated Ag/AgCl reference electrode (V_{SSC}), which has a potential of -199 mV versus the standard hydrogen electrode (0 mV_{SHE} = -199 mV_{SSC}) and differs by 43 mV from the saturated calomel electrode. The polarization resistance varied from 6.5×10^5 to 1.4×10^6 ohms. Assuming an anodic Tafel slope of ∞ and a cathodic Tafel slope of 30 mV/decade, the corresponding corrosion rate based on the polarization resistance method ranges from 7.8×10^{-4} to 3.6×10^{-4} mm/yr [3.1×10^{-2} to 1.4×10^{-2} mpy]. Data reported by Lian, et al. (2003) are summarized in Table 4-2. The polarization resistance of specimens

Table 4-2. Passive Corrosion Rates for Alloy 22 in Simulated Acidified Water at 90 °C [194 °F]*

Test Method		Potentiostatic at 0.4 V_{SSC}		Potentiostatic at 0.65 V_{SSC}	
		Before Potentiostatic Test	After Potentiostatic Test	Before Potentiostatic Test	After Potentiostatic Test
Linear Polarization Resistance	R_p	6.5×10^5	1.4×10^6	9.1×10^5	1.1×10^6
	Corrosion rate, mm/yr	7.9×10^{-4}	3.6×10^{-4}	5.6×10^{-4}	4.6×10^{-4}
	Corrosion rate, mpy	3.1×10^{-2}	1.4×10^{-2}	2.2×10^{-2}	1.8×10^{-2}
Electrochemical Impedance Spectroscopy	$R_{Barrier\ Oxide}$	1.7×10^5	1.1×10^6	6.9×10^5	5.4×10^5
	Corrosion rate, mm/yr	3.0×10^{-3}	4.6×10^{-4}	7.4×10^{-4}	9.5×10^{-4}
	Corrosion rate, mpy	1.2×10^{-1}	1.8×10^{-2}	2.9×10^{-2}	3.7×10^{-2}

*Lian, T., J.C. Estill, G.A. Hust, and R.B. Rebak. "Passive and Transpassive Dissolution of Alloy 22 in Simulated Repository Environments." Proceedings of the CORROSION 2003 Conference. Paper No. 694. Houston, Texas: NACE International. 2003.

[2]Wong, L.L., D.V. Fix, J.C. Estill, R.D. McCright, and R.B. Rabak. "Characterization of the Corrosion Behavior of Alloy 22 After Five Years Immersion in Multi-Ionic Solutions." Scientific Basis for Nuclear Waste Management XXVI. R. Finch and D. Bullen, eds. Symposium Proceedings 757. Pittsburgh, Pennsylvania: Materials Research Society. In press. 2003.

increased slightly after short-term potentiostatic testing. Rebak[3] also measured the corrosion rate of Alloy 22 in simulated acidified water at several temperatures between 30 and 90 °C [86 and 194 °F] using polarization resistance with a scan rate of 0.167 mV/s. Corrosion rates were calculated assuming anodic and cathodic Tafel slopes of 120 mV/decade. The corrosion rate was found to be a function of temperature with a calculated activation energy between 17.1 and 23.3 kJ/mol [4.1 and 5.6 kcal/mol]. At 30 °C [86 °F], the corrosion rate varied from 3×10^{-4} to 8×10^{-4} mm/yr [1.2×10^{-2} to 3.1×10^{-2} mpy], whereas, at 90 °C [194 °F], the corrosion rate varied from 1×10^{-3} to 2×10^{-4} mm/yr [3.9×10^{-2} to 7.9×10^{-2} mpy].

Electrochemical impedance spectra obtained for a frequency range of 10^{-3} to 10^{5} Hz were analyzed using the equivalent circuit model shown in Figure 4-1 (Lian, et al., 2003). The resistance of the barrier layer varied from 1.7×10^{5} to 1.1×10^{6} ohms (Table 4-2), which was similar to the measured values of polarization resistance. For tests at 0.4 V_{SSC}, the resistance of the barrier layer increased after potentiostatic polarization indicating either a thickening of the oxide or a change in oxide composition or structure. The increased resistance of the oxide layer after potentiostatic polarization suggests the alloy is not susceptible to localized corrosion or transpassive dissolution for the conditions tested.

Polarization resistance tests on several alloys including Alloys 22, 2000, 59, and 625 in chloride, fluoride, and chloride plus fluoride solutions were conducted by Meck, et al. (2003). Details of the test conditions and parameters (e.g., Tafel slopes) used to calculate the corrosion rates

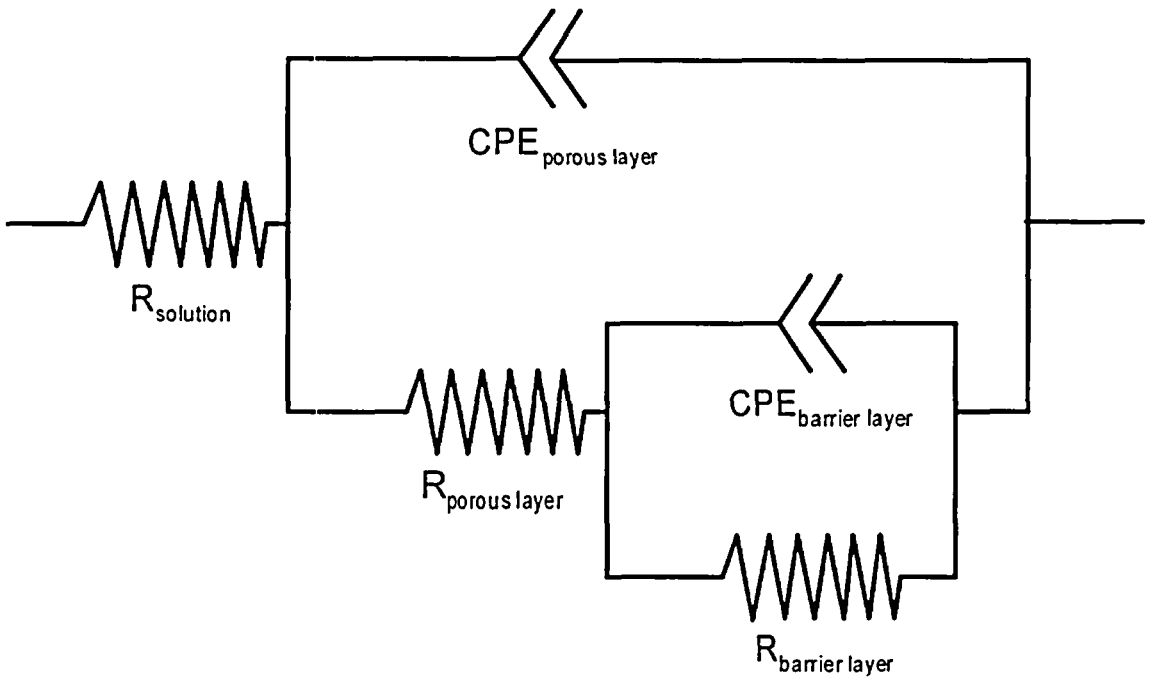

Figure 4-1. Analog Circuit Model for Analysis of Electrochemical Impedance Spectroscopy Data (Lian, et al., 2003)
NOTE: R—Resistance; CPE—Constant Phase Element

[3]Rebak, R.B. "Passive and Localized Corrosion Resistance of Alloy 22." *Presentation at the 5th Nickel Development Institute Workshop on the Fabrication, Welding, and Corrosion of Nickel Alloys and Other Materials for Radioactive Waste Containers October 16–17, 2002.* Las Vegas, Nevada. 2002.

from the measurements were not provided, although the tests were apparently conducted using scan rates of 0.5 mV/s, which may not yield valid polarization resistance values (Silverman, 2000). The average, corrosion rates for Alloy 22 obtained from six measurements are shown in Table 4-3. It is apparent the corrosion rate was dependent on both the solution composition and temperature. The greatest corrosion rate occurred in 1 M NaCl at 90 °C [194 °F]. Decreasing the temperature from 90 °C [194 °F] to 60 °C [140 °F] reduced the average corrosion rate from 3.04×10^{-3} to 9.2×10^{-4} mm/yr [1.2×10^{1} to 3.6×10^{-2} mpy]. The lowest corrosion rates were observed in solutions of 0.5 M NaCl + 0.5 M NaF and were typically five times less than the corrosion rates observed in 1 M NaCl.

Potentiostatic anodic current density measurements were also obtained for mill-annealed Alloy 22 in simulated acidified water (Lian, et al., 2003). The anodic current density was observed to decrease with time according to the expression

$$i\left(\frac{A}{cm^2}\right) = A(t)^n \qquad (4\text{-}1)$$

The parameters reported by Lian, et al. (2003) are shown in Table 4-4 for Alloy 22 in deaerated simulated acidified water and deaerated simulated concentrated water at 90 °C [194 °F]. For an applied potential of 100 mV_{SSC} to 650 mV_{SSC}, the initial value of n was between -0.48 and -0.816, indicating the current rapidly decreased with time. After 1 hour, the value of n was determined to be -0.368 for a potential of 0.1 V_{SSC} and -0.267 using an applied potential of 0.4 V_{SSC}. The change in the value of n indicates an initial rapid decrease in the current density followed by a slow decay in current density. Rebak[4] also reported the anodic current density decreased with time under potentiostatic conditions. Based on 24-hour tests, for potentiostatic

Table 4-3. Alloy 22 Corrosion Rates Determined Using Linear Polarization Resistance*

Test Solution	Temperature (°C) [°F]	Average Corrosion Rate	
		mm/yr	mpy
1 M NaCl	60 [140 °F]	9.2×10^{-4}	3.6×10^{-2}
	90 [194 °F]	3.04×10^{-3}	1.2×10^{-1}
1 M NaF	60 [140 °F]	9.2×10^{-4}	3.6×10^{-2}
	90 [194 °F]	1.68×10^{-3}	6.6×10^{-2}
0.5 M NaCl + 0.5 M NaF	60 [140 °F]	1.6×10^{-4}	6.3×10^{-3}
	90 [194 °F]	4.7×10^{-4}	1.8×10^{-2}

*Meck, N.S., P. Crook, S.D. Day, and R.B. Rebak. "Localized Corrosion Susceptibility of Nickel Alloys in Halide Containing Environments." Proceedings of the CORROSION 2003 Conference. Paper No. 682. Houston, Texas: NACE International. 2003.

[4]Ibid.

Table 4-4. Alloy 22 Passive Current Density Parameters Determined Using Potentiostatic Tests*					
Test Solution	Potential mV_{SSC}	Rapid Decay *n*	Gradual Decay *n*	Final Dissolution Rate After 24 Hours A/cm²	
				A/cm²	A/ft²
Deaerated Simulated Acidified Water 90 °C [194 °F]	100	-0.816	-0.368	5.33×10^{-8}	4.95×10^{-5}
	400	-0.816	-0.267	8.10×10^{-8}	7.53×10^{-5}
	650	-0.489	-0.055	1.92×10^{-6}	1.78×10^{-3}
Deaerated Simulated Concentrated Water 90 °C [194 °F]	100	-0.750	-0.368	1.43×10^{-7}	1.32×10^{-4}
	300	not reported	not reported	1.13×10^{-7}	1.05×10^{-4}
	600	-0.690	not reported	6.90×10^{-7}	6.4×10^{-4}

*Lian, T., J.C. Estill, G.A. Hust, and R.B. Rebak. "Passive and Transpassive Dissolution of Alloy 22 in Simulated Repository Environments." Proceedings of the CORROSION 2003 Conference. Paper No. 694. Houston, Texas: NACE International. 2003.

conditions in simulated concentrated water, the value of *n* was -0.497 at an applied potential of 100 mV_{SSC} and -0.412 at 400 mV_{SSC}.[5] The values reported by Rebak[6] were determined for the test duration and fall in the range of the values of *n* reported by Lian, et al. (2003).

4.1.2 Localized Corrosion of Mill-Annealed Alloy 22

The DOE approach to evaluate the susceptibility of Alloy 22 and other nickel-base candidate container alloys to localized corrosion has been previously reviewed (Brossia, et al., 2001). Immersion tests with creviced specimens have been conducted for 5 years in solutions based on J–13 Well water. Although weight loss measurements indicate the creviced specimens had greater corrosion rates than uncreviced specimens, no localized corrosion was observed on any of the Alloy 22 specimens. The localized corrosion susceptibility of Alloy 22 was evaluated by comparing the corrosion potential (E_{corr}) to the critical potential for localized corrosion ($E_{critical}$) measured in short-term tests also conducted in aerated solutions based on J–13 Well water. Values of the critical potential were based on several features observed in cyclic potentiodynamic polarization curves. The evaluation of Alloy 22 was conducted using only the base alloy without welds or thermal processing to simulate waste package fabrication effects. The results of comparisons of the critical potential and the corrosion potential suggest that in simulated acidified water, the critical potential is at least 600 mV greater than the corrosion potential. In simulated saturated water and basic saturated water, the critical potential is at least 400 mV greater than the corrosion potential (CRWMS M&O, 2000c,d).

[5]Ibid.

[6]Ibid.

The localized corrosion susceptibility of Alloy 22 in concentrated chloride solutions with and without the additions of nitrate have been reported by Rebak[7] and Farmer.[8] The results of cyclic potentiodynamic polarization in 9 M $CaCl_2$ with and without the addition of 0.9 M $Ca(NO_3)_2$ suggest that localized corrosion can occur even with the addition of nitrate when the corrosion potential exceeds the critical potential. The corrosion potential, however, was reported to be less than the critical potential (defined as the repassivation potential for pitting corrosion) for temperatures less than 140 °C [284 °F], with or without the addition of nitrate. The corrosion potential reported was obtained from the cyclic polarization scan, which does not represent steady-state corrosion potentials and does not account for long-term changes in corrosion potentials as a result of passive film aging. In 5 M $CaCl_2$ solutions at 90 °C [194 °F], crevice corrosion was observed after cyclic potentiodynamic polarization tests. The addition of 0.5 M $Ca(NO_3)_2$ was observed to inhibit localized corrosion even with creviced test specimens.

Recently, Meck, et al. (2003) examined the localized corrosion susceptibility of Alloys 22, 2000, 59, and 625 in chloride, fluoride, and chloride plus fluoride solutions. The tests were conducted using a scan rate of 0.5 mV/s, which may be too fast for the valid measurement of either the crevice corrosion initiation potential or the repassivation potential. In these tests, the critical potential (E20) was determined by the minimum potential at which the current density exceeded 20 $\mu A/cm^2$. The corrosion potential was also measured but the test solutions were deaerated, a standard practice to avoid measuring current associated with the oxygen reduction reaction. Despite these limitations, the tests may provide a useful assessment of the effects of solution chemistry on the localized corrosion susceptibility of the nickel-chromium-molybdenum alloys. The critical potentials for Alloy 22 are shown in Table 4-5. Localized corrosion was only observed in solutions containing 0.5 M NaF + 0.5 M NaCl, however, a hysteresis in the cyclic polarization curve was observed in tests with 1 M NaCl suggesting localized corrosion was possible. The maximum potential was typically 0.8 V_{SSC}, which is clearly in the region of transpassive dissolution. No localized corrosion was observed in 1 M NaF solutions, however, transpassive dissolution was observed at lower potentials compared with either the 1 M NaCl or the 0.5 M NaF + 0.5 M NaCl solutions.

4.1.3 Stress Corrosion Cracking of Mill-Annealed Alloy 22

The results of the DOE stress corrosion cracking susceptibility tests for Alloy 22 and the model abstraction for stress corrosion cracking have been reviewed recently (Pan, et al., 2003). Stress corrosion cracking of Alloy 22 has been observed in slow-strain-rate tests in simulated concentrated water at anodic potentials (Estill, et al., 2002; King, et al., 2002). The severity of cracking was shown dependent on both the test temperature and the applied potential (Estill, et al., 2002; King, et al., 2002). Stress corrosion crack propagation rates for mill-annealed Alloy 22 reported by Andresen, et al. (2001) and Estill, et al. (2002) were dependent on material condition and stress intensity. The crack propagation rates for Alloy 22 in basic saturated water at 110 °C [230 °F] were estimated to be 1×10^{-9} to 2×10^{-9} mm/s [4×10^{-11} to 8×10^{-11} in/s] at a stress intensity of 30 $MPa \cdot m^{1/2}$ [27 $ksi \cdot in^{1/2}$]. The crack propagation rate was similar for a material with 20-percent cold work tested at 30 $MPa \cdot m^{1/2}$ [27 $ksi \cdot in^{1/2}$] and for the mill-annealed material tested at 45 $MPa \cdot m^{1/2}$ [41 $ksi \cdot in^{1/2}$]

[7]Ibid.

[8]Farmer, J. "Chemical Environment Evolution on Alloy 22." Presentation to Nuclear Waste Technical Review Board January 28, 2003. Las Vegas, Nevada. 2003.

Table 4-5. Results of Cyclic Potentiodynamic Polarization Tests with Alloy 22*						
Test Solution	Temperature (°C) [°F]	Critical Potential, E20, mV_{SSC}			Localized Corrosion Observed	Hysteresis Observed
		Average	Minimum	Maximum		
1 M NaCl	60 [140 °F]	-221	-210	-231	No	Yes
	90 [194 °F]	-264	-251	-277	No	Yes
1 M NaF	60 [140 °F]	311	208	413	No	No
	90 [194 °F]	442	441	442	No	No
0.5 M NaCl + 0.5 M NaF	60 [140 °F]	529	523	535	Yes	No
	90 [194 °F]	389	349	429	Yes	No

*Meck, N.S., P. Crook, S.D. Day, and R.B. Rebak. "Localized Corrosion Susceptibility of Nickel Alloys in Halide Containing Environments." Proceedings of the CORROSION 2003 Conference. Paper No. 682. Houston, Texas: NACE International. 2003.

(Andresen, et al., 2001). Estill, et al. (2002) reported crack propagation rates of 2×10^{-10} to 5×10^{-9} mm/s [8×10^{-12} to 2×10^{-11} in/s] in simulated acidified water at 95 °C [203 °F] for mill-annealed Alloy 22 with an applied stress intensity of 45 $MPa \cdot m^{1/2}$ [41 $ksi \cdot in^{1/2}$] for static loading conditions. Higher crack propagation rates were reported for cyclic loading conditions (Andresen, et al., 2001; Estill, et al., 2002).

4.1.4 Effect of Fabrication Processes on Uniform and Localized Corrosion

The effect of fabrication processes on the uniform corrosion rate of Alloy 22 was assessed by measuring the weight loss welded specimens and the anodic polarization response of specimens thermally aged for 10 and 173 hours at 700 °C [1,292 °F] (CRWMS M&O, 2000d). The approach used by DOE to assess the effects of thermal aging have been reviewed and reported (Brossia, et al., 2001). Weight-loss measurements suggest the corrosion rate of the welded material was similar to the mill-annealed material. Anodic current density measurements obtained for potentiodynamic conditions suggest the corrosion rate of the thermally aged material was approximately 2.5 times that of the base alloy.

The localized corrosion susceptibility of thermally aged Alloy 22 was evaluated using potentiodynamic polarization in simulated acidified water and simulated concentrated water at 90 °C [194 °F] and in basic saturated water at 110 °C [230 °F]. In both simulated acidified water and basic saturated water, the critical potential was determined by the potential at which the anodic current increases significantly and is no longer independent of potential. In simulated acidified water, the critical potential was approximately 650 mV_{SSC} for the 173-hour aged material and close to the value measured for the base alloy without thermal aging. In basic saturated water, the critical potential was reduced to 350 mV_{SSC} for the 173-hour aged material. The anodic current densities were similar for both the thermally aged material and the base alloy. The anodic behavior of Alloy 22 is different in simulated concentrated water and the

anodic polarization scan is characterized by an anodic peak that occurs in the range 200–400 mV_{SSC}. For the thermally aged specimens in simulated concentrated water, the critical potential was again similar to the base metal, and the anodic current densities were similar for both the thermally aged material and the base alloy.

The effect of fabrication processes has been evaluated using standard test methods such as ASTM International G28A (2001c) in which a boiling ferric sulfate/50-percent sulfuric acid solution is used and boiling 2.5-percent hydrochloric acid as the test solution (Rebak, et al., 2000, 2002; Summers, et al., 2000, 2002). Results of the standardized tests are shown in Figures 4-2 and 4-3. The results of ASTM G28A tests shown in Figure 4-2 suggest thermal aging at a temperature of 760 °C [1,400 °F] results in an increased susceptibility to corrosion for exposure times greater than 1 hour. At lower temperatures, longer aging times are required to obtain a measurable increase in corrosion rate. At 593 °C [1,100 °F], an aging time of 1,000 hours is required before an increase in corrosion rate is observed. The results plotted in Figure 4-2 also suggest there is little difference in performance of the mill-annealed and aged material compared with the welded and aged material, especially for aging times less than 10 hours.

The results of tests performed in boiling 2.5 percent HCl are shown in Figure 4-3. In contrast to the ASTM G28A tests shown in Figure 4-2, significant increases in the corrosion rate were observed after aging at 760 °C [1,400 °F] for less than 1 hour. The difference in the corrosion rates measured for the mill-annealed and aged material compared with the welded and aged material was a function of both aging time and temperature. At 593 °C [1,100 °F], the corrosion rate of the mill-annealed and welded materials are very similar for all aging times. At 760 °C [1,400 °F], the difference in the corrosion rates after aging for the mill-annealed compared with

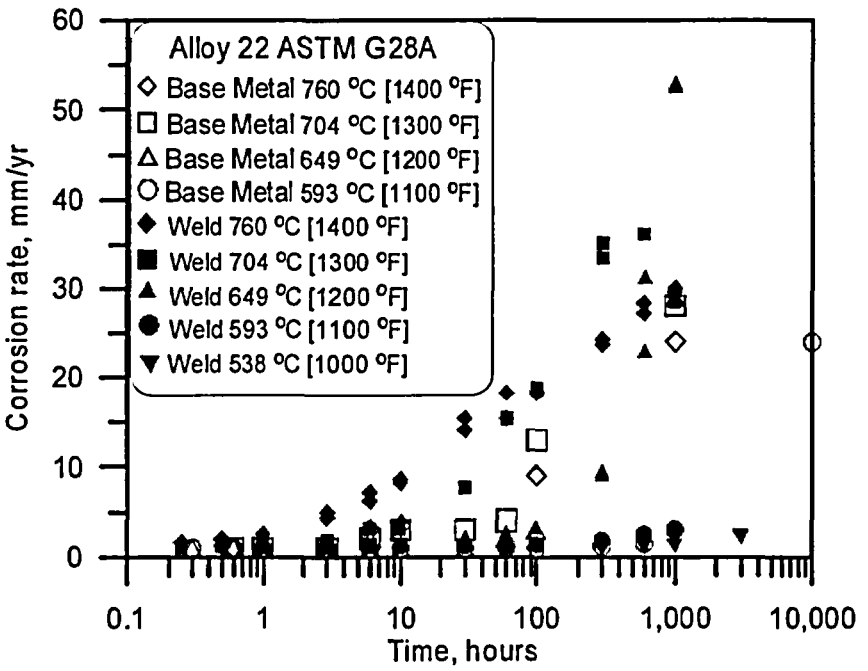

Figure 4-2. Results of Alloy 22 ASTM G28A Tests (Rebak, et al., 2002; Summers, et al., 2000)

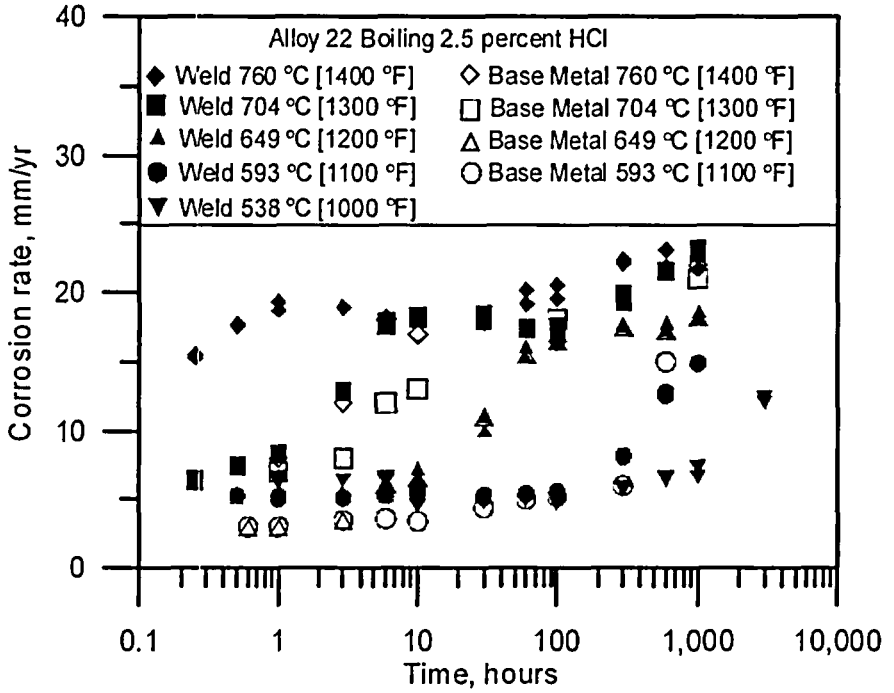

Figure 4-3. Results of Alloy 22 Corrosion Tests in Boiling Hydrochloric Acid (Rebak, et al., 2002; Summers, et al., 2000)

the welded material was evident after short exposures. The mill-annealed alloy, corrosion rates in excess of 15 mm/yr [591 mpy] were observed after an exposure of 10 hours or more. For the welded material, however, corrosion rates in excess of 15 mm/yr [591 mpy] were observed after 0.25 hours.

The effects of postweld heat treatment on the corrosion rate of Alloy 22 in both test solutions after thermal aging are shown in Figures 4-4 and 4-5. For the ASTM G28A tests (Figure 4-4), the corrosion rates for the welded, welded and solution annealed, and mill-annealed material are similar after thermal aging at 649 °C [1,200 °F] for aging times less than 100 hours (Rebak, et al., 2002; Summers, et al., 2000). For longer aging times, the welded and solution annealed material had the lowest corrosion rate. Similar results were obtained in boiling 2.5-percent hydrochloric acid (Figure 4-5) with the exception that the differences in the corrosion rates of the specimens were noticeable after aging for more than 6 hours.

4.1.5 Effect of Fabrication Processes on Stress Corrosion Cracking Susceptibility

Recent results reported by Andresen, et al. (2003) suggest the stress corrosion crack propagation rate in basic saturated water at 110 °C [230 °F] is influenced by cold work and thermal aging. The results of crack propagation rates for various test conditions are summarized in Table 4-6. Under cyclic loading, the stress corrosion crack propagation rate was 5.2×10^{-9} to 3.3×10^{-8} mm/s [2×10^{-10} to 1.3×10^{-9} in/s] at a stress intensity of 30 MPa·m$^{1/2}$ [27 ksi·in$^{1/2}$]. During static loading, the crack ceased to propagate. With a higher stress intensity, the crack propagation rate decreased with the length of the hold time for static

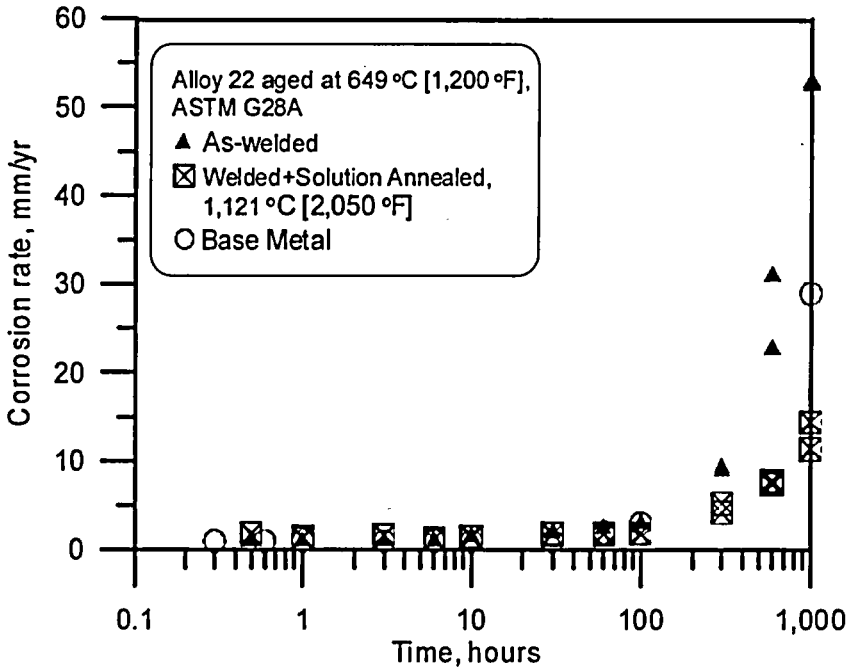

Figure 4-4. Comparison of Alloy 22 Corrosion Rates in ASTM G28A Tests (Rebak, et al., 2002)

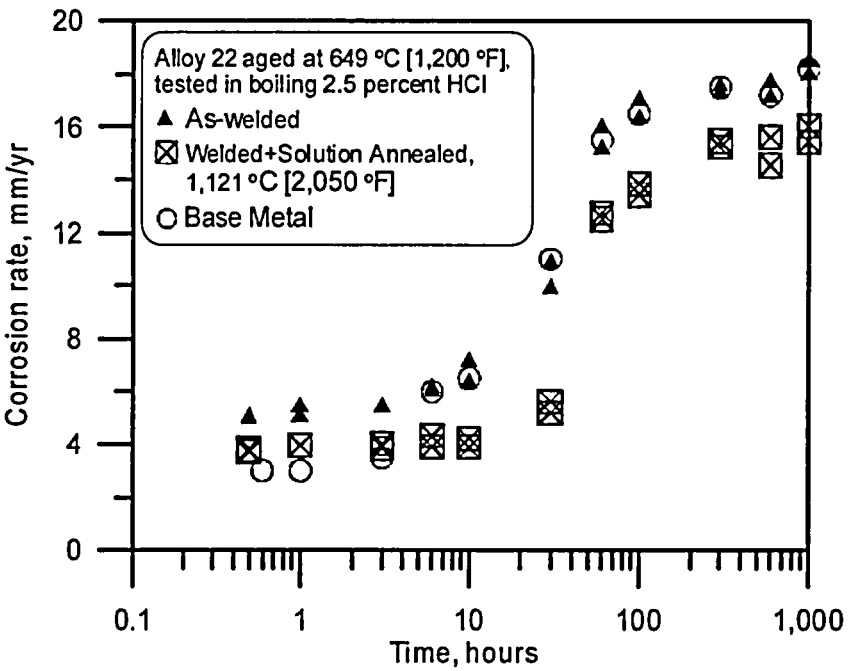

Figure 4-5. Comparison of Alloy 22 Corrosion Rates in Boiling Hydrochloric Acid (Rebak, et al., 2002)

Table 4-6. Crack Propagation Rates for Alloy 22 in Basic Saturated Water*						
		Static		Cyclic		
Material Condition	Stress Intensity, $MPa \cdot m^{1/2}$	Crack propagation Rate, mm/s	Hold Time Under Static Load	Crack Propagation Rate, mm/s	R Ratio	Cyclic Frequency, Hz
Mill-annealed	30	0	3,000 seconds	5.2×10^{-9}	0.7	0.001
	30	—	—	3.3×10^{-8}	0.6	0.003
	45	7×10^{-9}	3,000 seconds	2.3×10^{-7}	0.7	0.01
	45	1.3×10^{-9}	9,000 seconds	2.3×10^{-8}	0.7	0.001
	45	4×10^{-10}	85,400 seconds	2.2×10^{-9}	0.7	0.001
Mill-annealed plus 20-percent cold work	30	5×10^{-10}	~800 hours	1.5×10^{-8}	0.7	0.003
	30	2×10^{-10}	~1,800 hours	5.3×10^{-9}	0.7	0.001
Thermally aged 175 hours at 700 °C [1,292 °F]	16.5	—	—	2.0×10^{-8}	0.7	0.001
	16.5	—	—	6.4×10^{-8}	0.5	0.001
	24.2	1.3×10^{-9}	~400 hours	3.4×10^{-7}	0.5	0.001
	24.2	8×10^{-10}	~1,000 hours	5×10^{-7}	0.5	0.001

*Andresen, P.L., P.W. Emigh, L.M. Young, and G.M. Gordon. "Stress Corrosion Cracking Growth Rate Behavior of Alloy 22 (UNS N06022) in Concentrated Groundwater. "Proceedings of the CORROSION 2003 Conference. Paper No. 683. Houston, Texas: NACE International. 2003.

NOTES: English equivalents for $MPa \cdot m^{1/2}$, mm/s, and Hz are as follows: $MPa \cdot m^{1/2} \times 0.9091 = ksi\ in^{1/2}$ and mm/s × 0.039 = in/s; no conversion for Hz.

conditions. For a 3,000-second hold time at 45 $MPa \cdot m^{1/2}$ [41 $ksi \cdot in^{1/2}$], the crack propagation rate was 7×10^{-9} mm/s [2.8×10^{-10} in/s] and decreased to 4×10^{-10} mm/s [1.6×10^{-11} in/s] during an 85,400-second static hold.

Andresen, et al. (2003) also tested mill-annealed material with 20-percent cold work and reported the crack propagation rate to be 2×10^{-10} to 5×10^{-10} mm/s [8×10^{-12} to 2×10^{-11} in/s] for static loading at a stress intensity of 30 $MPa \cdot m^{1/2}$ [27 $ksi \cdot in^{1/2}$]. Thermally aged Alloy 22 {700 °C [1292 °F] for 175 hours}, tested at a stress intensity of 24.2 $MPa \cdot m^{1/2}$ [22.0 $ksi \cdot in^{1/2}$], had a measured crack propagation rate of 8×10^{-10} to 1.3×10^{-9} mm/s [3.1×10^{-11} to 5.1×10^{-11} in/s] for static conditions. The crack propagation rate for the cold-worked material was similar to the mill-annealed material tested for similar conditions. However, the thermally aged material appeared to be much more susceptible to stress corrosion cracking compared with the mill-annealed material.

The susceptibility of Alloy 22 to stress corrosion cracking has been evaluated also using tensile specimens for constant load in simulated concentrated water (Young, et al., 2003). Various material conditions were examined including (i) as-received (mill-annealed), (ii) thermally aged

at 700 °C [1,292 °F] for 175 hours to produce topologically close-packed phases, (iii) thermally aged at 520 °C [968 °F] for 175 hours to produce long-range ordering, and (iv) as-welded. Selected specimens were tested with the addition of a crevice former on the reduced specimen thickness, and notches were machined in some specimens to promote stress corrosion cracking. Ductile failure was noted for as-received specimens tested at 2.5 times the yield strength. No ductile failures or evidence of stress corrosion cracking were observed for specimens tested at an applied stress that was 1.7 to 2.2 times the yield strength of the material after more than 8,500 hours of testing in simulated concentrated water at 105 °C [221 °F]. It should be noted that the Type 304 SS test fixtures were severely corroded. Because the test specimens were not electrically isolated from the Type 304 SS test fixtures, the potential of the test specimens was likely decreased as a result of the localized corrosion of the stainless steel. Localized corrosion of the stainless steel may have galvanically protected the Alloy 22 test specimens and prevented the initiation of stress corrosion cracking.

4.2 Assessment of the DOE Approach

DOE used an assortment of standardized tests to demonstrate that waste package fabrication will not have a significant effect on the uniform corrosion rate, localized corrosion susceptibility, or the stress corrosion cracking resistance of Alloy 22. Several important concerns exist with respect to the tests performed by DOE. These concerns include the selection of test methods, test environments, interpretation of results, and the selection of material conditions tested.

Uniform corrosion rates have been determined using several methods including weight loss measurements and electrochemical methods. The confounding effects of silica deposition has been previously reported and is the subject of an agreement between the U.S. Nuclear Regulatory Commission and DOE. Assessment of fabrication processes on the uniform corrosion rate of Alloy 22 has been performed using only weight loss measurements and potentiodynamic polarization in solutions based on the J–13 Well water compositions (CRWMS M&O, 2000d). The limitations of gravimetric methods to determine corrosion rate, including the resolution of the weight loss measurement to assess the corrosion rate of welded material, have been discussed (Pensado, et al., 2002).

The assessment of the uniform corrosion rate using electrochemical methods may provide better resolution than the weight-loss measurements. An assessment of the electrochemical test methods to determine uniform corrosion rates of passive metals was reviewed recently by Pensado, et al. (2002). Electrochemical tests performed by DOE to measure the passive corrosion rate include polarization resistance, electrochemical impedance spectroscopy, and potentiodynamic and potentiostatic tests. The results of all the electrochemical test methods are consistent and suggest low passive corrosion rates for Alloy 22. The polarization resistance was performed using scan rates that were likely too fast, however, for a high-impedance, chromium-oxide-rich passive film (Silverman, 2000). In addition, selection of some electrochemical parameters such as Tafel slopes is not well justified. Potentiostatic tests were conducted for 24 hours to obtain parameters to predict long-term evolution of the passive dissolution rate (Lian, et al., 2003). Results of the relatively short tests suggest the passive current density continually decreases with time. Potentiostatic tests conducted for more than 100 hours indicate the passive current density does not continually decrease with time and reaches a steady-state value (Dunn and Brossia, 2002). In addition, long-term measurements indicate the corrosion potential reaches a steady-state value after a period of a few weeks (Dunn, et al., 2003; Estill, et al., 2003). Because the corrosion potential is a mixed potential that

is dependent on both the anodic dissolution and reduction reaction kinetics, a continual decrease in the anodic dissolution rate should result in a continual increase in the corrosion potential. Modeling of the passive behavior of Alloy 22 also suggests that a steady-state current density should be reached (Pensado, et al., 2002).

The assessment of localized corrosion susceptibility using electrochemical tests has used several values of $E_{critical}$ including the breakdown or pitting potential, the repassivation potential, and the potentials based on arbitrary values of anodic current density. The $E_{critical}$ is the lowest threshold potential at which localized corrosion, in particular crevice corrosion, can be initiated and propagated in the long term (hundred to thousands of years). Justification or demonstration that the potentials selected as $E_{critical}$ are actually critical potentials for the initiation of localized corrosion has not been provided. In addition, although the electrochemical tests have been used to evaluate the localized corrosion susceptibility of mill-annealed Alloy 22, electrochemical test results for either thermally aged or welded specimens have not been reported.

The measured corrosion rates shown in Figures 4-2 and 4-3 indicate the test methods used to evaluate the effect of fabrication processes do not have the same sensitivity. The ASTM G28A test, which uses a solution of ferric sulfate and sulfuric acid, was not as sensitive as boiling 2.5 percent hydrochloric acid solution. An alternative to the ASTM G28A test, defined in the standard as procedure G28B (ASTM International, 2001c), uses an oxidizing acidic chloride solution and may provide better sensitivity to evaluate the effects of fabrication processes that alter the microstructure of the alloy. None of the standard test methods, however, is particularly useful in determining the effects of fabrication processes on the expected lifetime of the waste packages.

Thermal aging temperatures and aging times investigated for uniform corrosion rate, localized corrosion susceptibility, and stress corrosion cracking resistance do not appear to reflect the plausible sequence of fabrication processes such as cold work and thermal cycles likely to occur during fabrication of the disposal containers and closure of the waste packages. The basis for the selection of thermal aging parameters was to determine an activation energy for the formation of secondary phases necessary to create a measurable change in the corrosion rate or mechanical properties of Alloy 22. Temperatures chosen, however, were only those below the nose of the time temperature transformation diagram for the precipitation of topologically close-packed phases for Alloy 22. Effects of short-term exposures at temperatures near the nose of the time temperature transformation diagram that may be relevant for heat-affected zones and weld repairs have not been evaluated. In addition, assessment of the effects of solution annealing in the disposal container fabrication welds has not been reported.

Test environments used for crack growth rates for Alloy 22 are limited to solutions based on J–13 Well water. All solutions have nitrate to chloride concentration ratios similar and close to 1.0. Nitrate is known to be a strong inhibitor of localized corrosion, and it is not clear if low nitrate to chloride ratios would increase crack propagation rates. In addition to the inhibiting effect of nitrate, the presence of fluoride may be significant for the stress corrosion cracking of Alloy 22 observed in slow-strain-rate tests (Estill, et al., 2002). Tests to determine the effect of fluoride concentration on the crack propagation rate, however, have focused on a limited range of solution compositions.

Constant load tests were used to assess stress corrosion crack initiation for Alloy 22 in the mill-annealed, as-welded, and thermally aged condition. Although the results of these tests

suggest Alloy 22 is resistant to stress corrosion crack initiation in simulated concentrated water, the tests were performed using specimens not electrically isolated from the Type 304L SS test fixtures. Hence, the results of these tests are confounded by the galvanic interaction of the specimens with the test fixture. Previous results of Estill, et al. (2002) show a strong effect of potential on the stress corrosion cracking susceptibility of Alloy 22 in simulated concentrated water. Reducing the corrosion potential of the test specimens resulted in a decrease in the stress corrosion cracking susceptibility of Alloy 22. Corrosion potentials of the Alloy 22 specimens throughout the duration of the tests were not reported, however. Because localized corrosion was initiated on the Type 304 SS test fixtures, it is likely the corrosion potential of the test specimens was significantly reduced and controlled by the active corrosion of the test fixtures rather than the reduction of oxygen and passive dissolution of Alloy 22. Contact between the Alloy 22 test specimens and the Type 304 SS test fixtures resulted in the galvanic protection of the test specimens that may have prevented the initiation of stress corrosion cracking.

4.3 The CNWRA Investigations

Independent investigations are conducted at the Center for Nuclear Waste Regulatory Analyses (CNWRA) to assess the performance predictions reported by DOE, including the effects of fabrication processes on the corrosion resistance of waste package materials. The results of electrochemical tests using mill-annealed, thermally treated, and welded specimens can be used to determine the effect of fabrication processes on the long-term performance of waste packages. Investigation of the uniform corrosion rate, localized corrosion susceptibility, and stress corrosion cracking resistance of mill-annealed Alloy 22 has been addressed in previous CNWRA reports (Pan, et al., 2002; Pensado, et al., 2002; Brossia, et al., 2001; Cragnolino, et al., 1999).

Two standardized tests—(i) ASTM G28 method B (ASTM International, 2001c) immersion in a boiling mixed acid-oxidizing solution (23 % H_2SO_4 + 1.2 % HCl + 1 % $FeCl_3$ + 1 % $CuCl_2$) for 24 hours and (ii) immersion in boiling 2.5-percent hydrochloric acid for 24 hours—were used to evaluate the intergranular corrosion susceptibility of Alloy 22. Susceptibility to intergranular corrosion was evaluated by calculating an average corrosion rate during a 24-hour immersion test period.

Chemical compositions of the Alloy 22 heats and weld filler metals used in this study are provided in Table 4-7 (Dunn, et al., 2003). Results of tests conducted on the as-received material in the mill-annealed condition (Heat 2277-8-3175) are included to provide a comparison with both thermally aged and welded material. The mill-annealed material was thermally aged at temperatures up to 870 °C [1,598 °F] for times ranging from 5 minutes to 240 hours. Welded specimens were obtained from plate with a gas tungsten-arc weld with either a double V-groove {12.7-mm- [0.5-in-] thick material, Heat 2277-8-3235, filler metal Heat XX1045BG11} or a double U-groove {38.1-mm- [1.5-in-] thick material Heat 059902LL2, filler metal Heat XX2048BG} joint geometry.

The geometry and dimensions of specimens used in this study are shown in Figure 4-6. Cylindrical rod specimens were used to determine the passive dissolution rate in potentiostatic polarization and electrochemical impedance tests. The cylindrical specimens were machined to 6.3 mm (0.25 in) in diameter and 48.6 mm (1.9 in) in length. Flat specimens with an exposed surface area of approximately 20 cm^2 [3.1 in^2] and fitted with two polytetrafluoroethylene crevice

Table 4-7. Composition of Alloy 22 Heats and Alloy 622 Filler Metal*												
Material	Ni	Cr	Mo	W	Fe	Co	Si	Mn	V	P	S	C
Heat 2277-8-3175 12.7-mm thick	57.8	21.40	13.60	3.00	3.80	0.09	0.030	0.12	0.15	0.008	0.002	0.004
Alloy 22 Heat 2277-8-3235 12.7-mm thick	56.5	21.40	13.47	2.87	3.94	1.31	0.023	0.24	0.17	0.00	0.001	0.003
622 Filler Heat XX1045BG11	58.5	20.73	14.13	3.15	3.05	0.09	0.060	0.24	0.01	0.007	0.001	0.006
Alloy 22 Heat 059902LL2 38.1-mm thick	59.6	20.35	13.85	2.63	2.85	0.01	0.05	0.16	0.17	0.00	0.000	0.005
622 Filler Heat XX2048BG	59.4	20.48	14.21	3.02	2.53	0.02	0.07	0.20	0.02	0.009	<0.001	0.001

*NOTES: Ni — nickel; Cr — chromium; Mo — molybdenum; W — tungsten; Fe — iron; Co — cobalt; Si — silicon; Mn — manganese; V — vanadium; P — phosphorus; S — sulfur; C — carbon

Information provided in millimeters; for conversion, use inch = mm × 0.039.

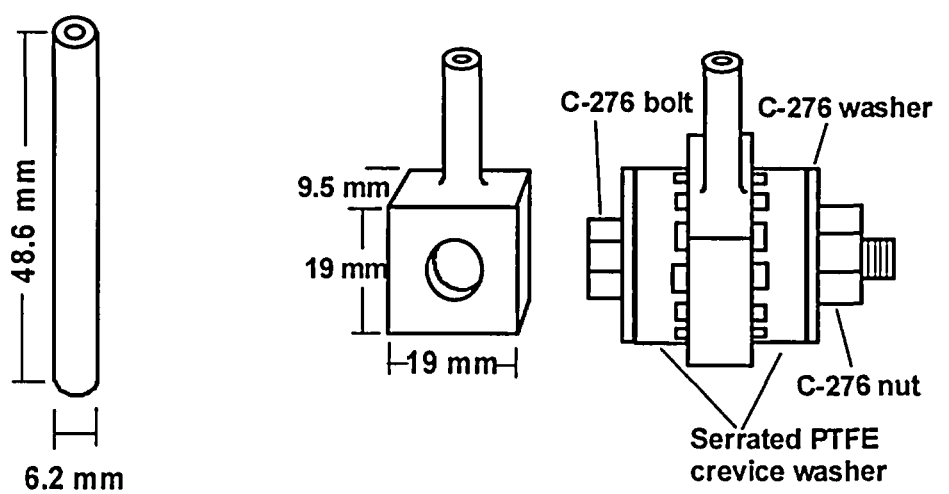

Figure 4-6. Alloy 22 Corrosion Test Specimens
NOTE: Measurements Provided in Millimeters; for Conversion Use Inch = mm × 0.039; PTFE—Polytetrafluoroethylene

forming washers held with insulated Alloy C-276 hardware were used for the localized corrosion studies. All specimens were polished to a 600-grit finish, cleaned ultrasonically in detergent, rinsed in deionized water, ultrasonically cleaned in acetone, and dried. At the completion of each test, the specimens were rinsed in deionized water and dried. Most specimens were cleaned ultrasonically in an inhibited hydrochloric acid solution that contained 2-butyne-1,4-diol as an inhibitor. Posttest examination was performed with an optical microscope and a scanning electron microscope.

Passive dissolution rates were measured in sodium chloride solutions using potentiostatic polarization and electrochemical impedance spectroscopy. Tests were conducted in a 2-L [0.53 gal] glass cell with a polytetrafluoroethylene lid. The cells were fitted with a water-cooled Allihn-type condenser and a water trap to minimize solution loss at elevated temperatures and air intrusion. A saturated calomel electrode was used as a reference electrode in all experiments. The standard calomel electrode was connected to the solution through a water-cooled Luggin probe with a porous silica tip so the reference electrode was maintained at room temperature. A platinum flag was used as a counter electrode. All solutions were deaerated with high-purity nitrogen (99.999 percent) for a period of at least 24 hours prior to start of the tests. The anodic current density was measured in potentiostatic tests where the specimens were maintained at potentials ranging from -200 to 800 mV_{SCE}. The resolution of the system was determined to be 1.25×10^{-10} A/cm^2 [1.16×10^{-7} A/ft^2]. At the conclusion of the test, the specimens were reweighed and examined microscopically for signs of corrosion. Corrosion rates were calculated using Eq. (4-2).

$$\text{Corrosion Rate}\left(\frac{\text{mm}}{\text{yr}}\right) = \frac{K i_{corr} EW}{\rho} \tag{4-2}$$

where

i_{corr} — passive corrosion current density in A/cm^2
EW — equivalent weight
K — conversion factor (3,270 mm • g·A^{-1} • cm^{-1} • yr^{-1})
ρ — density in g/cm^3

For Alloy 22, ρ is 8.69 g/cm^3 [543 lb/ft^3]. Assuming congruent dissolution of the major alloying elements as Ni^{2+}, Cr^{3+}, Mo^{3+}, Fe^{2+}, and W^{4+} within the potential range of -200 to 400 mV_{SCE}, the equivalent weight for Alloy 22 is 26.04 (ASTM International, 2001d).

Electrochemical impedance spectra were obtained at open circuit for a frequency range of 20,000 to 0.001 Hz in chloride-containing solutions at temperatures ranging from 25 to 95 °C [77 to 203 °F]. The spectra were fit to an analog-equivalent circuit that included components for both a porous outer oxide layer and an inner barrier oxide layer. The resistive component of the analog circuit was used as polarization resistance to calculate the corrosion rate using the approach originally proposed by Stern and Geary (1957) where the polarization resistance, R_p, is related to the corrosion current density, i_{corr}, using Eq. (4-3).

$$R_p = \left(\frac{dE}{di}\right)_{E_{corr}} = \frac{\beta_a \beta_c}{2.303(\beta_a + \beta_c)\, i_{corr}} \tag{4-3}$$

where β_a and β_c are the anodic and cathodic Tafel slopes. For passive metals, the anodic Tafel slope can be assumed to be infinite (Epelboin, et al., 1981), and the corrosion current density is calculated according to Eq. (4-4).

$$i_{corr} = \frac{\beta_c}{2.303 R_p} \tag{4-4}$$

The corrosion rate then can be calculated using Eq. (4-2).

Localized corrosion susceptibility was determined by measuring the crevice corrosion repassivation potential using both cyclic potentiodynamic polarization (ASTM International, 2001b) and back scanning potentiodynamic polarization after a potentiostatic hold (Dunn, et al., 2003). Cyclic potentiodynamic polarization tests of creviced specimens were conducted at temperatures ranging from 95 to 175 °C [203 to 347 °F] in a Type 316L SS autoclave with a polytetrafluoroethylene liner. The autoclave was equipped with a platinum counter electrode and an internal Ag/AgCl (0.1 M KCl) reference electrode. For comparison, all potential values were converted to the standard calomel electrode scale at 25 °C [77 °F]. At the conclusion of each test, the Ag/AgCl reference electrode was checked versus a standard calomel electrode to monitor the reference electrode performance. Tests were conducted in deaerated solutions containing 0.5, 1.0, and 4.0 M NaCl with 1.24 mM bicarbonate (HCO_3^-), 0.20 mM sulfate (SO_4^{2-}), 0.16 mM nitrate (NO_3^-), and 0.10 mM fluoride (F^-) added as sodium salts. Standard glass test cells with platinum counter electrodes and saturated calomel reference electrodes were used for tests conducted at 60, 80, and 95 °C [140, 176, and 203 °F]. The cyclic potentiodynamic polarization scans were initiated 100 mV below the corrosion potential. The potential of the specimens was increased at a rate of 0.167 mV/s and at current density of 5 mA/cm^2 [4.6 A/ft^2], the scans were reversed. The cyclic potentiodynamic polarization scans were terminated at 200 mV below the initial corrosion potential. For test conditions where crevice corrosion was observed, the crevice corrosion repassivation potential was determined by the potential where the current density remained below 2×10^{-6} A/cm^2 [1.9×10^{-3} A/ft^2] as previously described by Cragnolino, et al. (2001).

Repassivation tests conducted in glass test cells were used to compare the crevice corrosion resistance of as-received and thermally aged material (heat 2277-8-3175) at temperatures less than 100 °C [212 °F] in chloride only or chloride and nitrate solutions. Potentiodynamic scans were used to obtain the crevice corrosion repassivation potential. Scans were initiated at 100 mV_{SCE}, and the potential of the specimens were increased to a preset value in the range of 400 to 700 mV_{SCE} at a rate of 0.1 mV/s. On reaching the preset maximum potential, the specimen was held potentiostatically to allow localized corrosion propagation. After a period of 5 to 8 hours, the potential was decreased at a rate of either 0.0167 or 0.167 mV/s to a potential of -500 mV_{SCE} where the test was terminated. The faster scan rates were used in the initial tests conducted in the glass test cells. Although differences in the values of crevice corrosion repassivation potential measured with the different scan rates were not observed, slower scan rates were adopted as a precaution against overly conservative crevice corrosion repassivation potential measurements. The criterion for determining the crevice corrosion repassivation potential was identical to that used in tests conducted in the autoclaves and defined as the potential where the current density remained below 2×10^{-6} A/cm^2 [1.9×10^{-3} A/ft^2].

4.3.1 Passive Dissolution of Mill-Annealed Alloy 22

An analysis of the passive dissolution of Alloy 22 in the mill-annealed condition was reported by Pensado, et al. (2002). Steady-state potentiostatic anodic current density measurements in deaerated test solutions were used to determine the effect of temperature on the passive dissolution rate. In 0.028 M NaCl at 95 °C [203 °F], the anodic current density was measured to be 1×10^{-8} A/cm^2 [9×10^{-6} A/ft^2], which gives a corrosion rate of 1×10^{-4} mm/yr [4×10^{-3} mpy]. The temperature was decreased to values in the range of 1×10^{-10} to 1×10^{-9} A/cm^2 [9×10^{-7} to 9×10^{-8} A/ft^2] corresponding to corrosion rates of 1×10^{-6} to 1×10^{-5} mm/yr [4×10^{-5} to 4×10^{-4} mpy]. The activation energy for the passive dissolution rate was determined to be 44.7± 5.5 kJ/mol [10.7 ± 1.3 kcal/mol] (Pensado, et al., 2002).

Passive dissolution rates were determined using electrochemical impedance spectroscopy. The impedance spectra were analyzed using the analog model shown in Figure 4-7, which has components for the solution resistance, a porous outer oxide layer and an inner barrier oxide layer. Results for Alloy 22 in the mill-annealed condition in solutions containing 0.028 M NaCl are shown in Figure 4-8. The corrosion rate is clearly a function of temperature and varies from 5.5×10^{-6} mm/yr [2.2×10^{-4} mpy] at 25 °C [77 °F] to 1.9×10^{-4} mm/yr [7.5×10^{-3} mpy] at 95 °C [203 °F]. Error bars for the corrosion rate were determined using the error in the resistance of the barrier layer. For comparison with the investigation of Lian, et al. (2003), the impedance spectra were fit to the analog circuit model shown in Figure 4-1. Although the analog circuit is different, the calculated corrosion rate was similar when the impedance spectra were analyzed using either the model (Figure 4-1) used by Lian, et al. (2003) or the analog circuit shown in Figure 4-7.

Tests were conducted in concentrated $MgCl_2$ solutions to reach temperatures above 100 °C [212 °F] at atmospheric pressure. In 35-percent $MgCl_2$ solutions, the corrosion rates for mill-annealed Alloy 22 were more than one order of magnitude greater than those measured in the more dilute 0.028 M NaCl solution (Figure 4-9) for the temperature range of 25 to 95 °C [77 to 203 °F]. The calculated activation energy (Figure 4-10) is 46.3 kJ/mol [11.1 kcal/mol] for the temperature range 25–95 °C [77–203 °F] in 0.028 M NaCl. The activation energy for the corrosion rate as a function of temperature in the $MgCl_2$ was 37.2 kJ/mol [8.9 kcal/mol]. Although the value of activation energies for the 0.028 M NaCl and the more concentrated magnesium chloride solution were similar, it is apparent from Figure 4-9 that the corrosion rates in magnesium chloride at 120 °C [248 °F] deviate substantially from the trend observed at lower temperatures. In addition, initial measurements conducted at 20 °C [68 °F] also seem to deviate from the established trend. Considering only the data from 40 to 120 °C [104 to 248 °F], the activation energy increases to 49.6 kJ/mol [11.8 kcal/mol].

4.3.2 Localized Corrosion of Mill-Annealed Alloy 22

In the cyclic potentiodynamic polarization tests conducted in autoclaves, localized corrosion was initiated by progressively increasing the potential of the test specimen until breakdown of the passive film occurred, which was marked by a significant increase in the anodic current density. A representative of the cyclic potentiodynamic polarization scan conducted in 4.0 M Cl^- at 95 °C [203 °F] is shown in Figure 4-11. A small anodic peak was observed at approximately 400 mV_{SCE} followed by the breakdown of the passive film at 700 mV_{SCE}. Based on a current density value of 2×10^{-6} A/cm^2 [1.9×10^{-3} A/ft^2] as the criterion for repassivation, the E_{rcrev} measured in this test was -57 mV_{SCE}. The crevice corrosion repassivation potential versus

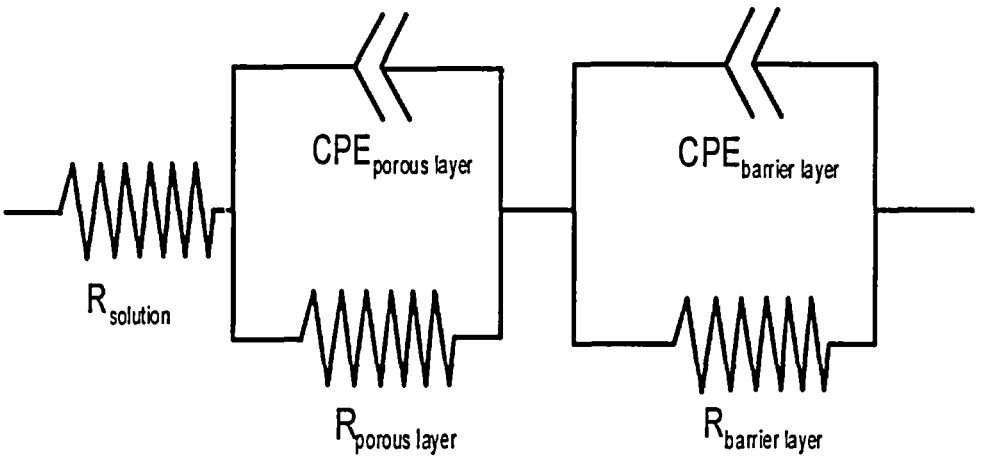

Figure 4-7. Analog Circuit Model for Electrochemical Impedance Spectroscopy Data
NOTE: R—Resistance; CPE—Constant Phase Element

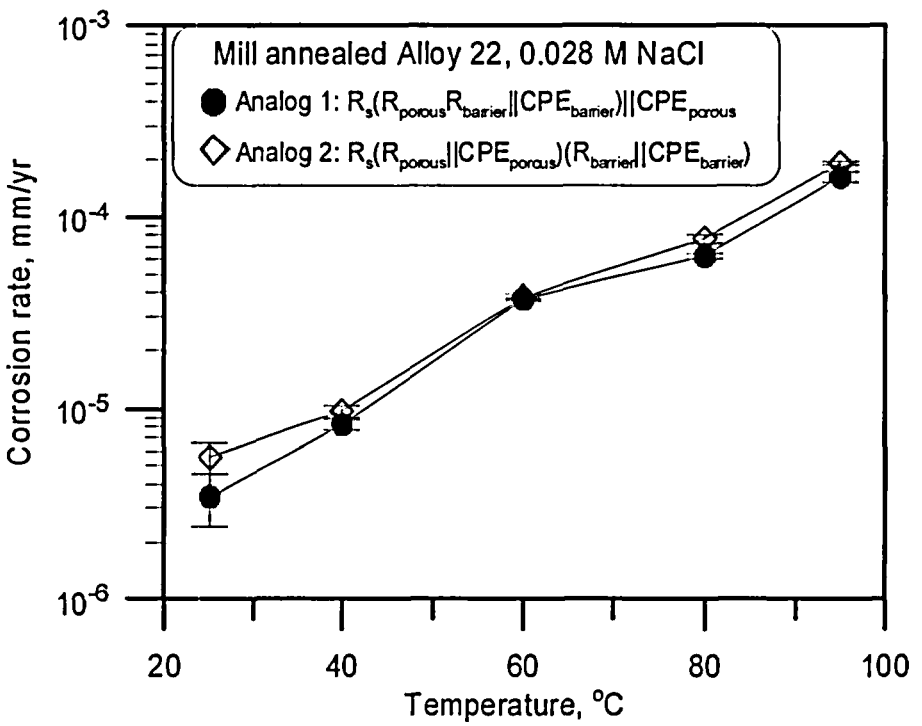

Figure 4-8. Alloy 22 Corrosion Rates Obtained Using Electrochemical Impedance Spectroscopy. Analog 1 Proposed by Lian, et al. (2003). Analog 2 Shown in Figure 4-7.
NOTES: Temperature Provided in °C; for Conversion Use °F = 9/5 °C + 32; R—Resistance; CPE—Constant Phase Element

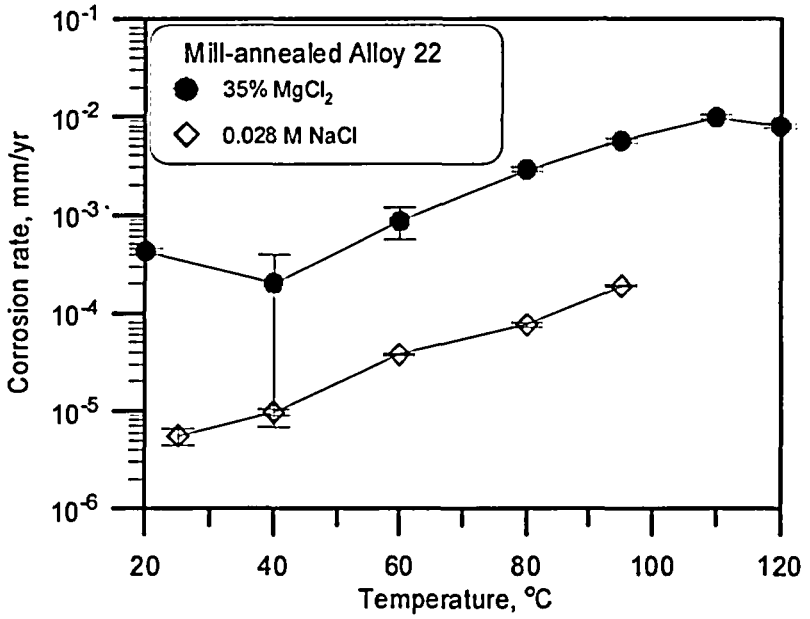

Figure 4-9. Corrosion Rates for Alloy 22 in 0.028 M NaCl and 35-Percent $MgCl_2$ Obtained Using Electrochemical Impedance Spectroscopy
NOTE: Temperature Provided in °C; for Conversion Use °F = 9/5 °C + 32.

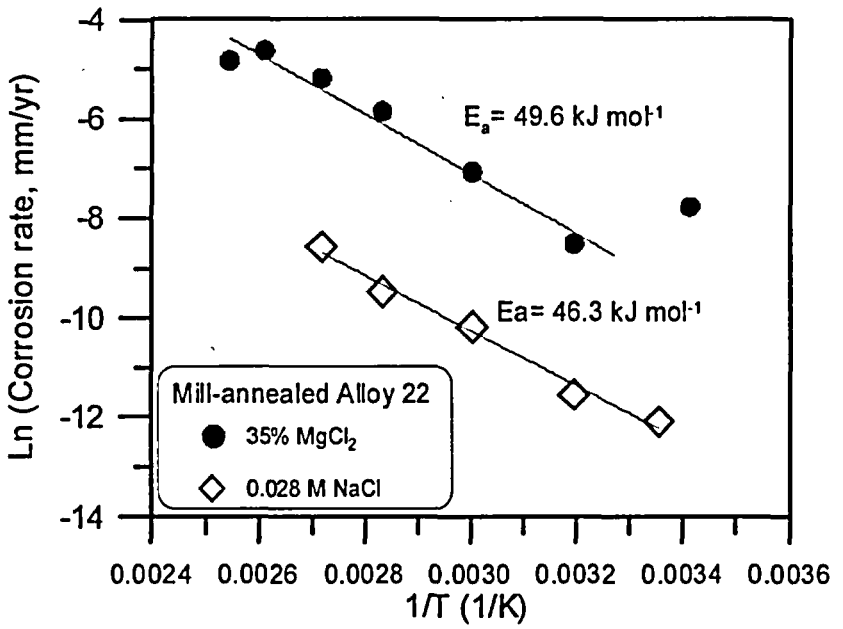

Figure 4-10. Activation Energy for Alloy 22 Corrosion Rates Measured in 0.028 M NaCl and 35-Percent $MgCl_2$

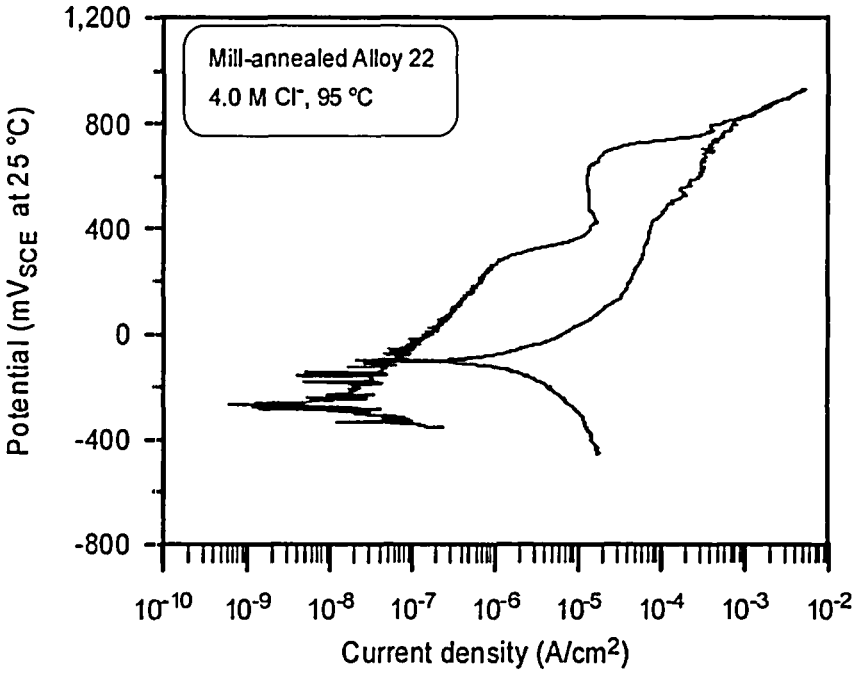

Figure 4-11. Cyclic Potentiodynamic Polarization Curve for Alloy 22 in 4 M NaCl at 95 °C [203 °F]

chloride concentration plots for all as-received Alloy 22 test specimens measured at temperatures ranging from 80 to 150 °C [176 to 302 °F] is shown in Figure 4-12. No localized corrosion was observed on tests conducted at either 80 or 95 °C [176 or 203 °F] in 0.5 M Cl^-. The results in Figure 4-12 show that temperature has a strong influence on the crevice corrosion repassivation potential. It is also apparent the crevice corrosion repassivation potential at a given temperature decreases with chloride concentration. The largest decrease in crevice corrosion repassivation potential occurs as the temperature increases from 80 to 125 °C [176 to 257 °F]. For example, in a 1 M Cl^- solution, the crevice corrosion repassivation potential decreased by 400 mV from 250 mV_{SCE} to -150 mV_{SCE}.

The results of the repassivation potential tests conducted in autoclaves can be fit to an equation of the form

$$E_{rcrev} = E^0_{rcrev}(T) + B(T)\log[Cl^-] \quad (4\text{-}5)$$

where

$$E^0_{rcrev}(T) = A_1 + A_2(T) \quad (4\text{-}6)$$

and

$$B(T) = B_1 + B_2(T) \quad (4\text{-}7)$$

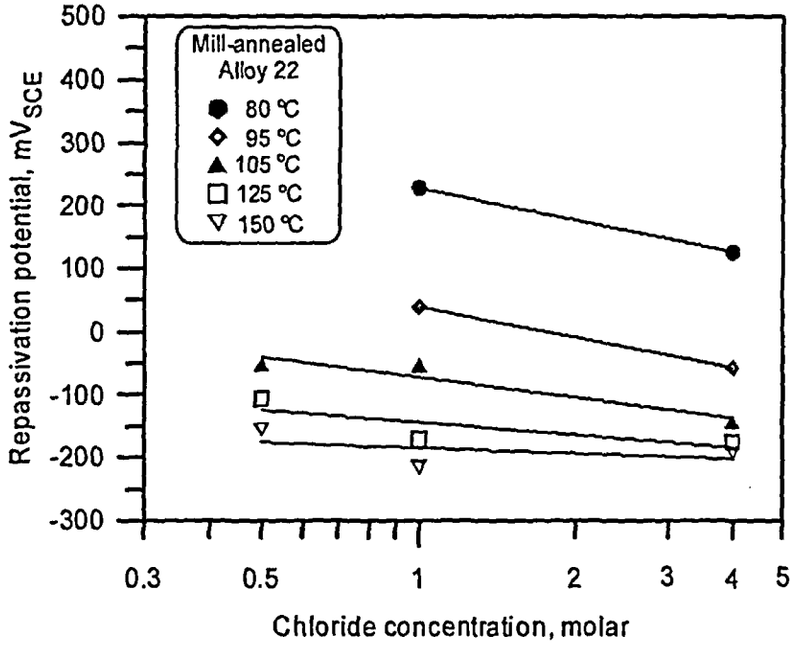

Figure 4-12. Crevice Corrosion Repassivation Potentials for Mill-Annealed Alloy 22 As a Function of Chloride Concentration and Temperature
NOTE: Temperature Provided in °C; for Conversion Use °F = 9/5 °C + 32.

Based on the results shown in Figure 4-12, Eq. (4-5) can be expressed as

$$E_{rcrev} = 1{,}300 - 13.1T + (-362.7 + 2.3T)\log[Cl^-] \quad (4\text{-}8)$$

which is valid from 80 to 105 °C [176 to 221 °F] and for chloride concentrations from 0.5 to 4.0 M.

Figure 4-13 shows an example of the crevice corrosion repassivation potential measurements conducted in glass cells using a backward potentiodynamic scan. The forward scan was initiated at 0 mV_{SCE}, and the potential of the specimen was increased to a value of 700 mV_{SCE}. After holding the specimen at this potential for 5 hour, the potential was decreased at a rate of 0.167 mV/s. The potential of the specimen was held constant for two periods when the current reached values of 1×10^{-5} and 2×10^{-6} A/cm^2 [9.3×10^{-3} and 1.9×10^{-3} A/ft^2]. During both short potentiostatic holds, the current density increased with time, indicating continued localized corrosion propagation. The measured current density decreased and remained below 2×10^{-6} A/cm^2 [1.9×10^{-3} A/ft^2] at a potential of -98 mV_{SCE}. At lower potentials, the current density rapidly decreased suggesting repassivation of localized corrosion. This value of the E_{rcrev} is close to the value of -57 mV_{SCE} measured using the cyclic potentiodynamic polarization test method in an autoclave for equivalent environmental conditions. Using a slower scan rate

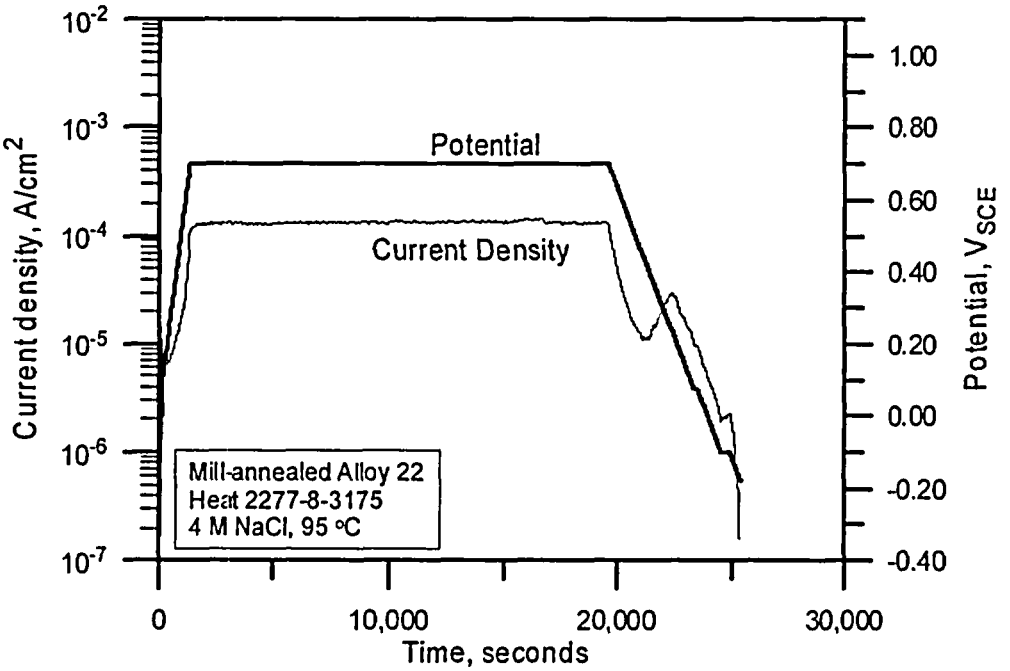

Figure 4-13. Crevice Corrosion Repassivation Potential Measurement for Mill-Annealed Alloy 22 Using Potentiostatic Hold Followed by Reverse Potential Sweep
NOTE: 95 °C = 203 °F

of 0.0167 mV/s, the measured crevice corrosion repassivation potential with the same 2×10^{-6} A/cm^2 [1.9×10^{-3} A/ft^2] criterion was -92 mV_{SCE} indicating the slower scan rate did not significantly alter the crevice corrosion repassivation potential value. Crevice corrosion was confirmed by posttest optical examination of the specimens.

Repassivation potentials of Alloy 22 in the mill-annealed condition as a function of chloride concentration are shown in Figure 4-14. The log linear relationship of the repassivation potential with chloride concentration [Eq. (4-5)] is not maintained at chloride concentrations below 0.5 M. This is differentiated in Figure 4-14 with a dashed line. At chloride concentrations of 0.5 M or less, the initiation of localized corrosion is not consistently observed. Results of tests where no localized corrosion was initiated are indicated in Figure 4-14 as open symbols. Also included in Figure 4-14 are repassivation measurements for Type 316L SS, Alloys 825 and 625. The solid lines represent the log linear repassivation potential dependence on chloride concentration previously reported (Cragnolino, et al., 2002a, 1999). These alloys behave similarly to Alloy 22, and for each alloy, there is a minimum chloride concentration for the relationship described by Eqs. (4-5) to (4-7). A key difference among Alloys 825, 625, and 22, which all contain approximately 21 weight percent chromium, is the molybdenum and tungsten concentration added to increase the localized corrosion resistance. As the concentration of molybdenum in the alloy increases, the repassivation potential at a given chloride concentration increases. In addition, the critical chloride concentration necessary to initiate localized corrosion also increases with the addition of molybdenum and tungsten.

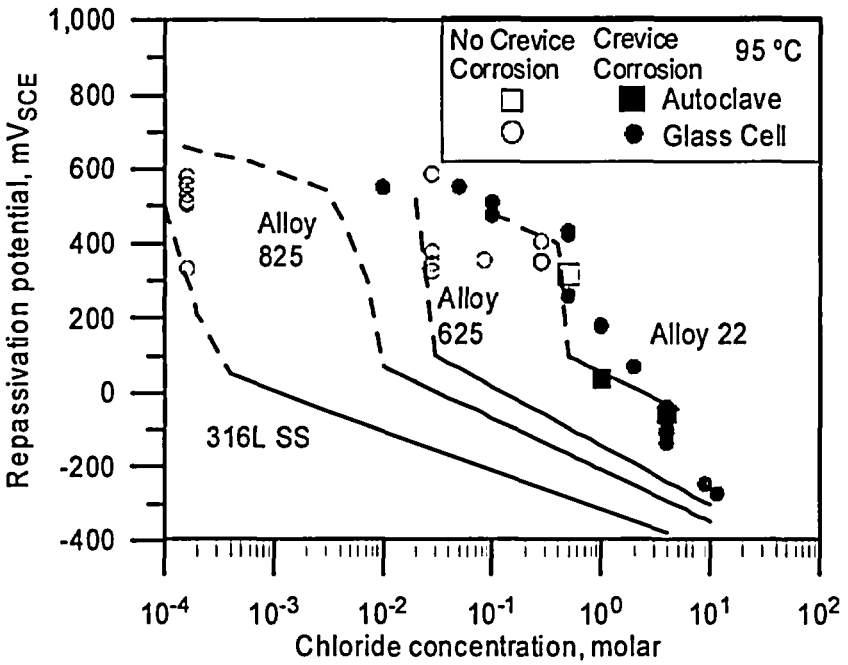

Figure 4-14. Repassivation Potentials for Type 316L SS and Alloys 825, 625, and 22 As a Function of Chloride Concentration at 95 °C [203 °F]

For all the as-received specimens where localized corrosion was observed, the attack was characterized by deep penetrations under the crevice formers with a smooth, electropolished appearance as shown in Figure 4-15. The attack did not follow metallurgical features such as grain or twin boundaries. When localized corrosion was not observed, the specimen surface typically had a bright gold color and often exhibited a light etching of grain boundaries that was attributed to transpassive dissolution. Pitting on the open surfaces was never observed.

The results shown in Figures 4-12 and 4-14 were obtained in solutions consisting of pure chloride or chloride with low concentrations of potentially inhibitive anions such as nitrate. Figure 4-16 shows the effects of a nitrate to chloride concentration ratio on the repassivation potential for localized corrosion. For nitrate to chloride ratios less than 0.1, the repassivation potential is not altered significantly, and localized corrosion was observed in all tests. When the nitrate to chloride ratio was increased and was greater than 0.1, the repassivation potential increased significantly. Localized corrosion was observed at a nitrate to chloride ratio of 0.12, however, the repassivation potential was 450 mV_{SCE}. For higher nitrate to chloride ratios, localized corrosion was not observed.

Short-term corrosion potential tests conducted simultaneously on three Alloy 22 specimens exposed in the same test cell are shown in Figures 4-17 and 4-18. The corrosion potential values in alkaline 0.028 M Cl^- for both polished and oxidized specimens are shown in Figure 4-17. For polished specimen, the E_{corr} was as low as -340 mV_{SCE} at the start of the test and subsequently increased and stabilized at values in the range of -200 mV_{SCE} to 0 mV_{SCE}. Oxidized specimens had much greater variability in the corrosion potential compared with the

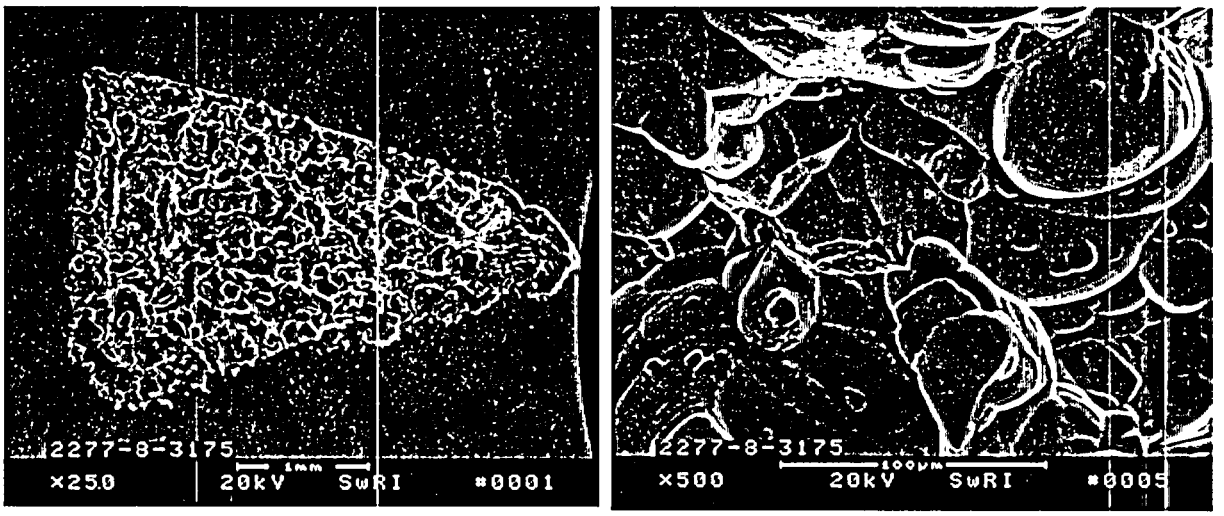

Figure 4-15. Scanning Electron Microscope Images of Mill-Annealed Alloy 22 Crevice Corrosion After Testing in 4 M Cl^- at 95 °C [203 °F]

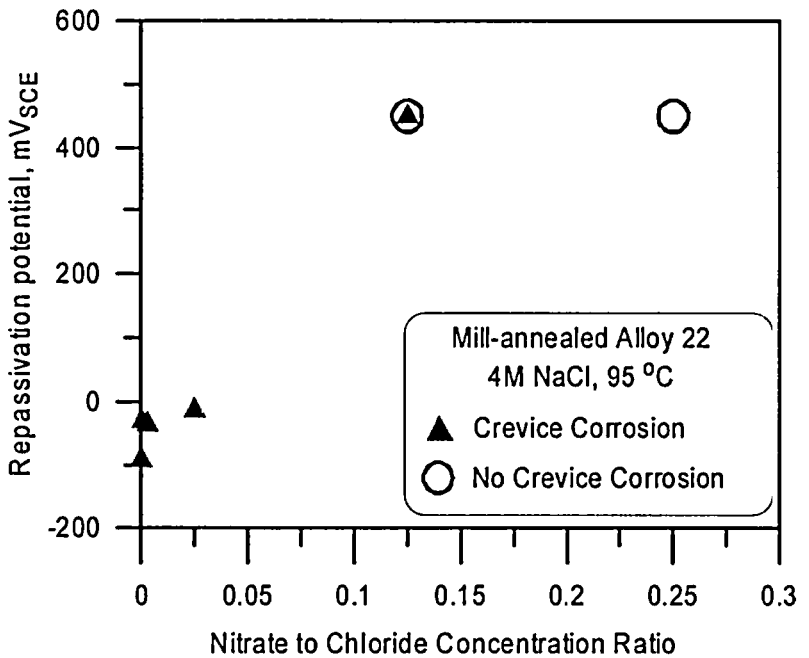

Figure 4-16. Repassivation Potential of Mill-Annealed Alloy 22 in 4 M Cl^- at 95 °C [203 °F] As a Function of Nitrate to Chloride Concentration Ratio

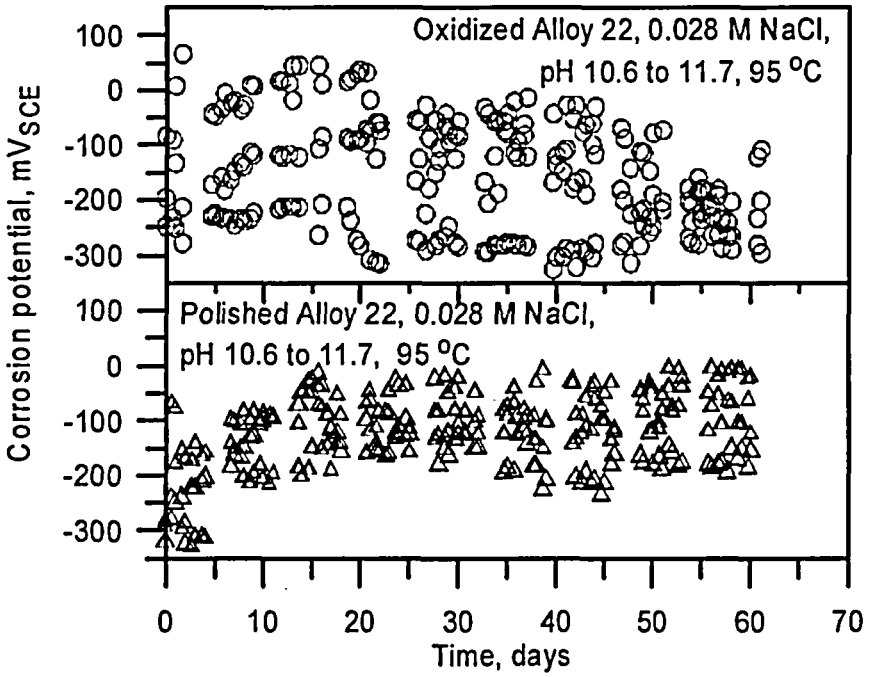

Figure 4-17. Corrosion Potential of Mill-Annealed Alloy 22 in 0.028 M Cl^- at 95 °C [203 °F]. Thermal Oxidation of Test Specimens Was Conducted in an Oven at 200 °C [392 °F] for 30 Days.

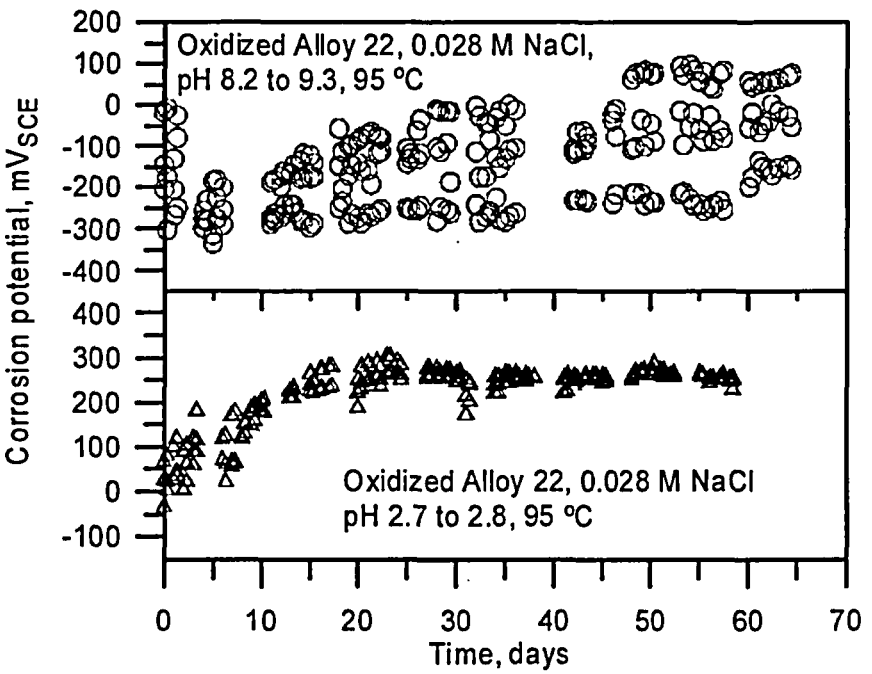

Figure 4-18. Corrosion Potential of Mill-Annealed and Thermally Oxidized {200 °C [392 °F] for 30 Days} Alloy 22 in 0.028 M Cl^- at 95 °C [203 °F] As a Function of Solution pH

polished specimens. Initial values of the corrosion potential were as high as 65 mV_{SCE} and, unlike the polished specimens, decreased with time. Initial variations and a general decrease in the oxide film thickness may contribute to the specimen-to-specimen variation and the general decrease in the corrosion potential. The corrosion potential values for oxidized specimens at acidic and slightly alkaline conditions are shown in Figure 4-18. The results obtained for slightly alkaline conditions were also characterized by large specimen-to-specimen variations, however, the corrosion potential tended to increase with time. In acidic conditions, as shown in Figure 4-18, the corrosion potential of the oxidized specimens increased from initial values in the range of -40 to 60 mV_{SCE} and stabilized near 250 mV_{SCE}. The specimen-to-specimen variation for acidic conditions was typically less than 50 mV. Similar values of corrosion potentials were obtained with polished specimens in acidic solutions with 4 M Cl^-. A summary of the corrosion potentials measured for all conditions is shown in Figure 4-19. The error bars indicate one standard deviation of the measured corrosion potential for each specimen. In alkaline solutions, the corrosion potential does not appear to be a function of solution pH or chloride concentration. In addition, with the exception of the larger variation in the corrosion potential observed in 0.028 M Cl^- at pH 8.2, the corrosion potential was not dependent on the surface condition of the Alloy 22 specimens. These solutions contained chloride and additions of sodium bicarbonate and sodium carbonate to alter the solution pH. Carbonate and bicarbonate salts are common in groundwater and do not act as oxidizing or reducing agents. As previously noted, the corrosion potential in acidic solutions was more than 300 mV greater than the corrosion potential in alkaline solutions and was not dependent on chloride concentration.

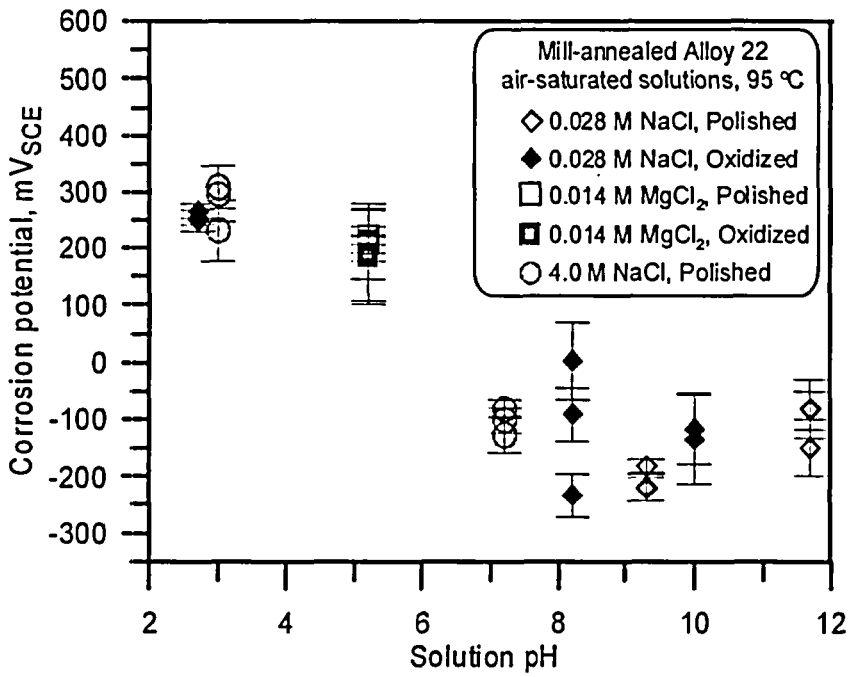

Figure 4-19. Corrosion Potential of Mill-Annealed Alloy 22 in Chloride Solutions As a Function of Solution pH and Surface Condition

4.3.3 Stress Corrosion Cracking Susceptibility of Mill-Annealed Alloy 22

The stress corrosion cracking susceptibility of mill-annealed Alloy 22 has been reported recently (Cragnolino, et al., 2003; Pan, et al., 2002). Results of tests conducted using fracture mechanics-type test specimens, including fatigue precracked double cantilever beam and compact tension, did not indicate any chloride stress corrosion cracking. Tests conducted at 95 °C [203 °F] in concentrated 9.1 M LiCl at applied potentials above the measured repassivation potential for crevice corrosion for high-stress intensities for a period of more than 3,000 hours revealed crevice corrosion of the specimen, but no evidence of stress corrosion cracking. The application of cyclic loading also did not promote stress corrosion cracking.

Tests conducted in simulated concentrated water using high stress intensities were initiated following the report of Estill, et al. (2002), which revealed that stress corrosion cracking of Alloy 22 was observed in slow-strain-rate tests. Tests conducted using fatigue precracked compact tension specimens for cyclic loading conditions did not reveal stress corrosion cracking. Although tests with the mill-annealed material are continuing, no evidence of stress corrosion cracking has been observed in either pure chloride or solutions that simulate concentrated groundwater that may evolve at the proposed repository at Yucca Mountain (Cragnolino, et al., 2003).

4.3.4 Effect of Fabrication Processes on Passive Dissolution and Localized Corrosion

The results of immersion tests using ASTM G28 method B tests (ASTM International, 2001c) using boiling 23 % H_2SO_4 + 1.2 % HCl + 1 % $FeCl_3$ + 1 % $CuCl_2$ for 24 hours and immersion tests in boiling 2.5-percent hydrochloric acid for 24 hours are shown in Table 4-8. High corrosion rates, ranging from 2.61 to 2.94 mm/yr [103 to 116 mpy], were measured for all specimen conditions tested in boiling 2.5-percent hydrochloric acid solutions, independent of thermal aging. The ASTM G28 method B tests resulted in low corrosion rates of 0.08 to 0.10 mm/yr [3 to 4 mpy], except for the specimen aged at 870 °C [1,598 °F] for 30 minutes that had a corrosion rate of 1.16 mm/yr [46 mpy], approximately 11 times greater than that for the mill-annealed specimen and the specimens aged for shorter times. Optical microscopic examination of the specimens after immersion testing revealed a combination of general

Table 4-8. Results of Immersion Corrosion Tests of Alloy 22 Aged at 870 °C [1,598 °F]

Aging Time (min)	ASTM G28 Method B		Boiling 2.5% HCl	
	Corrosion Rate (mm/yr)	Normalized Rate	Corrosion Rate (mm/yr)	Normalized Rate
0	0.10	1.00	2.76	1.00
3	0.09	0.90	2.61	0.94
5	0.08	0.80	2.67	0.97
30	1.16	11.60	2.94	1.06

NOTE: Information provided in millimeters per year; for conversion use mpy = mm/yr × 0.0254.

corrosion and grain-boundary attack on the surfaces of the specimens tested in boiling 2.5-percent hydrochloric acid. In contrast, pitting corrosion was observed at the grain boundaries of the thermally aged specimens used in the ASTM G28 method B tests. Severe pitting attack was observed in the 30-minute aged specimen. The step function increase in corrosion rate, as influenced by heat treatment, and the associated mode of attack observed in the ASTM G28 method B tests in an oxidizing, acid solution are in agreement with the work of Manning (1985) in evaluating the susceptibility of Alloy C-276 to intergranular corrosion.

Despite the absence of significant alloy depletion in the grain-boundary regions, as discussed in Chapter 3, thermally aged Alloy 22 was more susceptible to intergranular corrosion than the mill-annealed material. This detrimental effect could be because of preferential dissolution of the topologically close-packed phases. Another possibility is a galvanic effect between the molybdenum-rich, grain-boundary precipitates and the adjacent matrix. Laycock and Newman (1997) observed that molybdenum alloying increases the corrosion potential and decreases the corrosion current density in pit-like environments by inhibiting the anodic reaction. As a result of this effect of molybdenum, topologically close-packed phases, which are rich in molybdenum, may act as cathodes relative to the adjacent matrix in establishing a galvanic couple because of the difference in molybdenum content between the precipitates and the matrix. Thus, the adjacent matrix may corrode preferentially, causing pitting at the grain boundaries.

The passive dissolution of mill-annealed, thermally aged, and welded Alloy 22 has been reported for Alloy 22 as a function of temperature, solution chemistry, and potential (Pensado, et al., 2002; Brossia, et al., 2001). Corrosion rates were calculated based on anodic current transients measured for potentiostatic conditions. A comparison of the passive corrosion rates for mill-annealed and welded Alloy 22 based on anodic current transients obtained for potentiostatic conditions for a period of 24 hours is shown in Figure 4-20. At potentials less than 600 mV_{SCE} the anodic current densities for the welded specimens are in the range of 2×10^{-8} to 4×10^{-8} A/cm^2 [2×10^{-5} to 4×10^{-5} A/ft^2] and are quite similar to the anodic current density measured for the base alloy. The anodic current density of the welded specimen tested in 4 M Cl^- adjusted to pH 2.7 is slightly greater than that measured in the alkaline solutions. At 600 mV_{SCE}, the anodic current densities of specimens tested in solutions adjusted to pH 2.7 and 11.0 increase substantially, and, at 800 mV_{SCE}, the anodic current density measured in all solutions is greater than 10^{-4} A/cm^2 [0.1 A/ft^2]. Posttest examination of the specimen revealed preferential attack in the weld region that exposed the weld microstructure; however, no intergranular corrosion was observed.

Thermally aged specimens have been shown to have passive dissolution rates similar to the mill-annealed specimens at low potentials. At high potentials, however, long-term thermal aging {870 °C [1,598 °F] for 4 hours} was shown to have a detrimental effect on the anodic dissolution rate. Passive dissolution current densities of 1×10^{-8} A/cm^2 [9×10^{-6} A/ft^2] were observed for thermally aged Alloy 22 at a potential of -200 mV_{SCE} (Dunn, et al., 2000). At potentials of 200 mV_{SCE}, however, severe intergranular corrosion was noted. The low anodic dissolution current density at low potentials suggests the passive dissolution rate is not affected by the precipitation of topologically close-packed phases. The topologically close-packed phases are rich in molybdenum (Cragnolino, et al., 1999; Raghavan, et al., 1984, 1982) as discussed in Chapter 3, however, the passive dissolution rate is dependent on chromium (Kirchheim, et al., 1989). Because the topologically close-packed phases are not significantly enriched or depleted in chromium, formation of these phases does not result in chromium-depleted regions

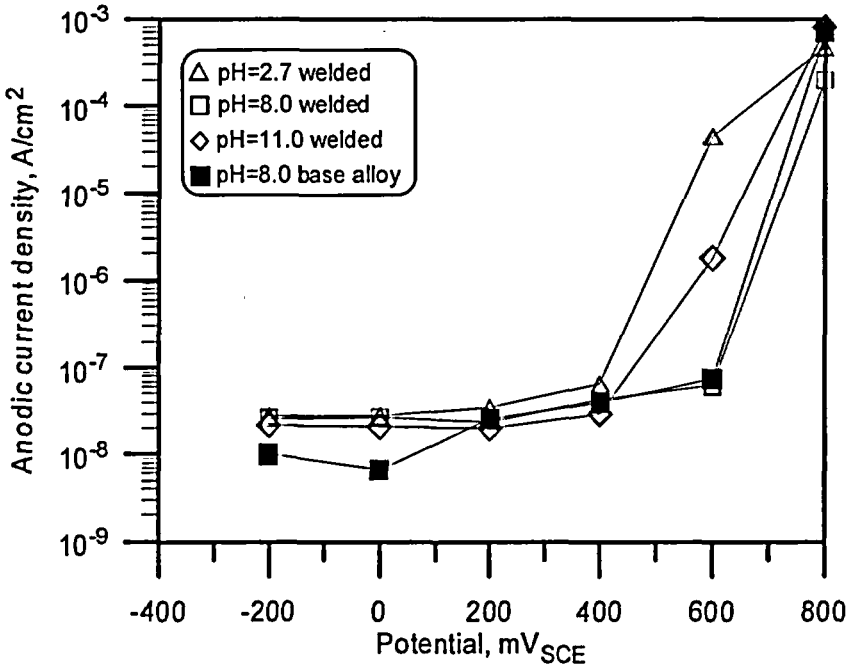

Figure 4-20. Anodic Current Density for Mill-Annealed and As-Welded Alloy 22

that may increase the passive dissolution rate. The high concentration of molybdenum in the topologically close-packed phases, which preferentially form at grain boundaries, may create molybdenum depletion in the grain-boundary regions that increases the intergranular corrosion susceptibility. As discussed in Chapter 3, however, depletion of molybdenum was not observed for thermally-aged specimens. Nevertheless, the formation of topologically close-packed phases at grain boundaries does not appear to alter the passive dissolution rate.

Figure 4-21 shows the passive corrosion rates for mill-annealed, thermally aged {870 °C [1,598 °F] for 5 minutes}, and welded Alloy 22 determined using electrochemical impedance spectroscopy. The corrosion rates were calculated based on the resistance of the inner barrier oxide layer determined by fitting the impedance spectra to the analog circuit shown in Figure 4-7. The corrosion rates shown in Figure 4-21 for the mill-annealed material are comparable to the corrosion rates calculated from the anodic current transients (Pensado, et al., 2002). In addition, it is apparent the corrosion rates for the welded material and the thermally aged material are similar to, but higher than, those for the mill-annealed alloy. At 25 °C [77 °F], the corrosion rates for the as-welded and thermally aged materials were approximately twice that of the mill-annealed material. Larger differences were observed at 95 °C [203 °F]. The corrosion rate was determined in a relatively dilute chloride concentration. Although the results of the electrochemical impedance spectroscopy tests are consistent with rates determined from potentiostatic anodic current density transients, additional environments should be tested to evaluate the effects of fabrication processes on the passive dissolution rate of Alloy 22.

Previous evaluations of the effects of fabrication processes on the localized corrosion susceptibility of Alloy 22 showed that short-term thermal aging {870 °C [1598 °F] for 5 minutes} significantly reduced localized corrosion resistance (Cragnolino et al., 2002b; Dunn, et al.,

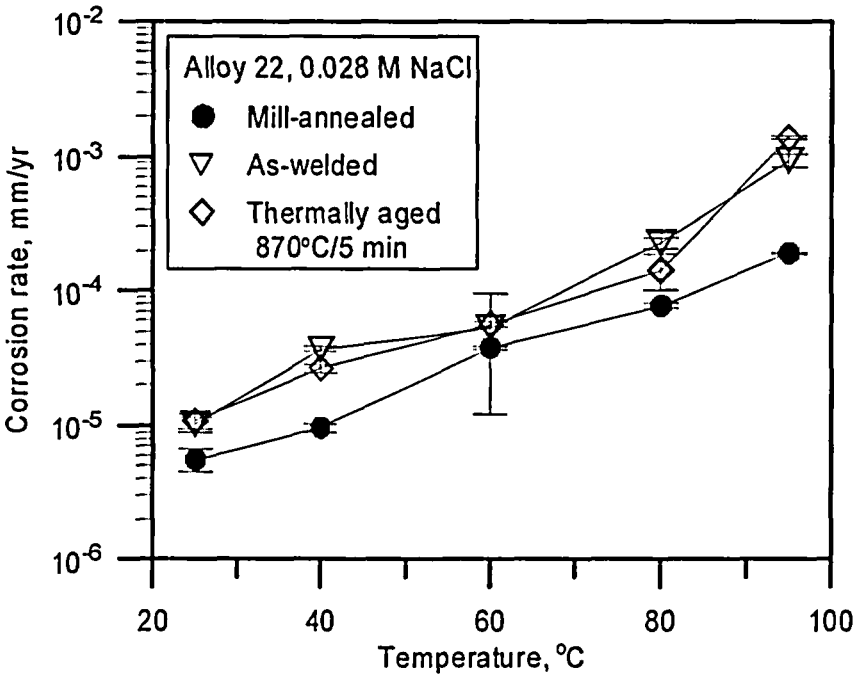

Figure 4-21. Corrosion Rates of Mill-Annealed, As-Welded, and Thermally Aged Alloy 22 As a Function of Temperature in 0.028 M Cl^-
NOTE: Temperature Provided in °C; for Conversion Use °F = 9/5 °C + 32.

2000). In 4 M Cl^- at 95 °C [203 °F], the crevice corrosion repassivation potential for the as-received material was in the range -57 to -98 mV_{SCE}; whereas, the welded material had a crevice corrosion repassivation potential of -159 mV_{SCE}. Much lower repassivation potentials were observed for thermally aged specimens. After aging for 5 minutes at 870 °C [1,598 °F], the repassivation potential decreased to -260 mV_{SCE} in 4 M Cl^- at 95 °C [203 °F]. Increasing the thermal aging time did not result in lower repassivation potentials. A greater difference in the localized corrosion susceptibility was observed at lower chloride concentrations. Intergranular corrosion on creviced specimens was observed at chloride concentrations as low as 0.005 M at 95 °C [203 °F] (Dunn, et al., 2003). Repassivation potentials as a function of chloride concentration at 95 °C [203 °F] for specimens thermally aged for 5 minutes at 870 °C [1,598 °F] were similar to the repassivation potentials measured for the as-welded specimens (Dunn and Brossia, 2002).

Figure 4-22 shows the effect of thermal aging {5 minutes at 870 °C [1598 °F]} on the crevice corrosion repassivation potential as a function of chloride concentration at temperatures ranging from 60 to 95 °C [140 to 203 °F]. Also included are crevice corrosion repassivation potential measurements for the welded material listed in Table 4-7 at 95 °C [203 °F]. Regression lines for the thermally aged specimens are plotted, and results show the crevice corrosion repassivation potential decreases with temperature and chloride concentration. It is also apparent the critical chloride concentration for localized corrosion of thermally aged specimens is dependent on temperature. At 60 °C [140 °F], the critical chloride concentration was 0.25 M and decreased to 0.05 M at 80 °C [176 °F] and to 0.01 M at 95 °C [203 °F]. The regression

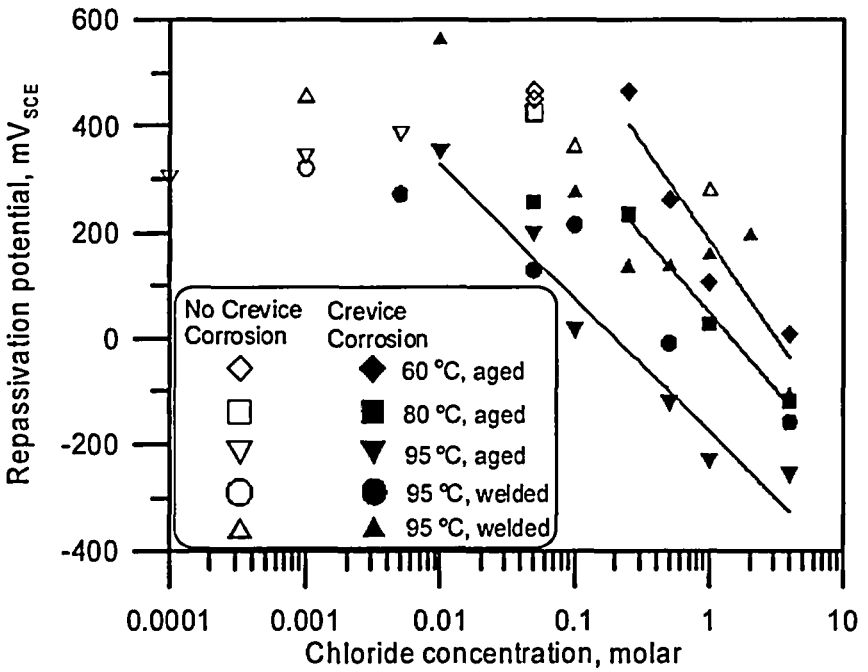

Figure 4-22. Crevice Corrosion Repassivation Potential for Alloy 22 in the Thermally Aged and As-Welded Conditions NOTE: Temperatures Provided in °C; for Conversion Use °F = 9/5 °C + 32.

parameters for the thermally aged material are provided in Table 4-9. Parameters of the mil-annealed alloy are also listed for comparison. The repassivation potential intercept A_1 decreased from 1,300 mV for the mill-annealed material to 800 mV for the thermally aged material. In addition, a stronger dependence on the chloride concentration was observed for the thermally aged material. As indicated in Table 4-9 , the temperature-dependent coefficient in the slope of the repassivation potential regression was -584 mV for the thermally aged material compared to -362 mV for the mill-annealed material. The repassivation potentials for the as-welded specimens at 95 °C [203 °F] were similar to those of the thermally aged specimens, although the repassivation data for the as-welded specimens exhibit greater variability.

The chemistry of the environment contacting the waste package may also have a significant effect on the localized corrosion resistance of the waste package material. The effect of nitrate to chloride concentration ratio on the crevice corrosion repassivation potential of welded Alloy 22 is shown in Figure 4-23 (Dunn and Brossia, 2002). In pure 0.5 M NaCl,, the crevice corrosion repassivation potential of welded Alloy 22 is 0 mV_{SCE}. The E_{rcrev} of welded Alloy 22 is not significantly altered in 0.5 M Cl^- with the addition of 0.05 M NO_3^-. With 0.5 M Cl^- and nitrate concentrations of 0.1 M or greater, no localized corrosion was initiated in short-term tests (shown by open circles in Figure 4-23). An additional test was also conducted to determine the effect of nitrate on active localized corrosion by initiating crevice corrosion in a solution containing only 0.5 M Cl^- and measuring the crevice corrosion repassivation potential after the addition of nitrate to the solution. As shown in Figure 4-23, the addition of nitrate increased the

Table 4-9. Coefficients of the Crevice Repassivation Potential Expressions						
Alloy	T (°C)	$[Cl^-]_{crit}$ (M)	A_1 (mV_{SCE})	A_2 (mV/°C)	B_2 (mV)	B_2 (mV/°C)
Alloy 22 Heat 2277-8-3175 as-received/ mill-annealed	80 to 125 °C [176 to 257 °F]	0.5	1,300	-13.1	-362.7	2.3
Alloy 22 Heat 2277-8-3175 Thermally aged 5 minutes at 870 °C	60 to 95 °C [140 to 203 °F]	0.25 to 0.001	800	-10.0	-584.2	3.7

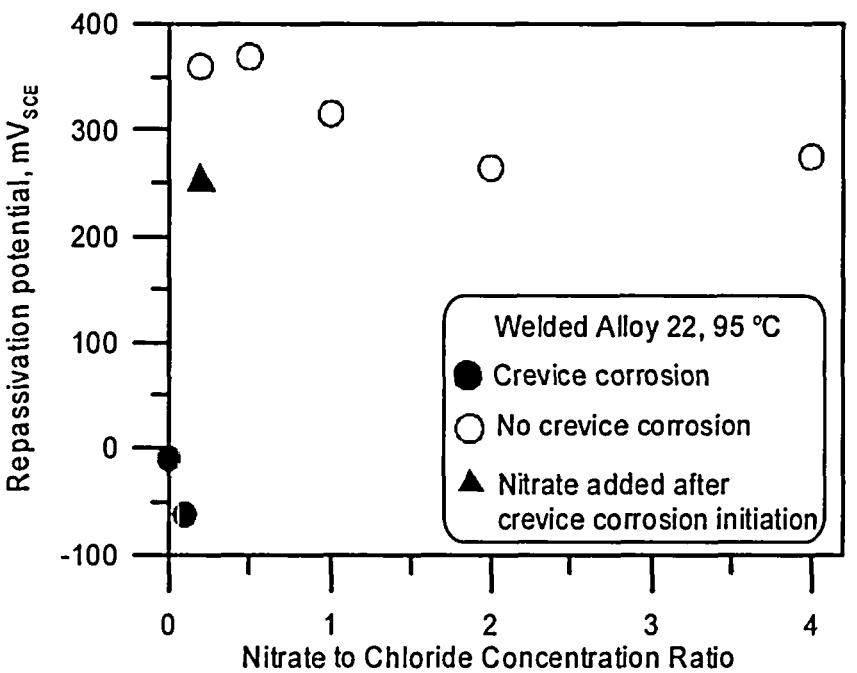

Figure 4-23. Crevice Corrosion Repassivation Potential for As-Welded Alloy 22 in 0.5 M Cl^- at 95 °C [203 °F] As a Function of Nitrate to Chloride Concentration Ratio

crevice corrosion repassivation potential of welded Alloy 22 by more than 200 mV, indicating that nitrate has a significant effect on the inhibition of localized corrosion initiation and also promotes repassivation of localized corrosion during the growth stage.

Figure 4-24 shows the effect of welding and postweld solution annealing on the repassivation potential for localized corrosion. The solid-dashed line is included to represent the results of repassivation tests with Alloy 22 Heat 2277-8-3175 at 95 °C [203 °F] shown in Figure 4-14. Although the repassivation potential data for Alloy 22 Heat 059902LL2 in the mill-annealed condition were obtained by testing material cut from a plate that was welded, the specimens were cut from a section of the plate located approximately 90 mm [3.5 in] from the centerline of the weld. The repassivation potential of these specimens was similar to that measured for the Heat 2277-8-3175. Figure 4-24 also shows data for as-welded specimens contain weld metal and adjacent base metal. The greater variability observed for the as-welded material may be attributed to the heterogeneous microstructure created by the multipass weld. In the as-welded condition, the repassivation potential was similar to the mill-annealed alloy in solutions where chloride concentration was greater than or equal to 0.1 M. Localized corrosion was observed at lower chloride concentrations for the as-welded material, however, the repassivation potential was above 550 mV_{SCE}. Although the critical chloride concentration for localized corrosion was lower for the alloy in the as-welded condition, the results shown in Figure 4-24 suggest that the welding slightly reduced the localized corrosion resistance of the material. After solution annealing at 1,125 °C [2,057 °F], the repassivation potential for localized corrosion was again similar to the mill-annealed material at high chloride concentrations. In solutions with less than 0.5 M chloride the repassivation potentials for the welded+solution annealed specimens were reduced by at least 200 mV compared with the mill-annealed material. Crevice corrosion was

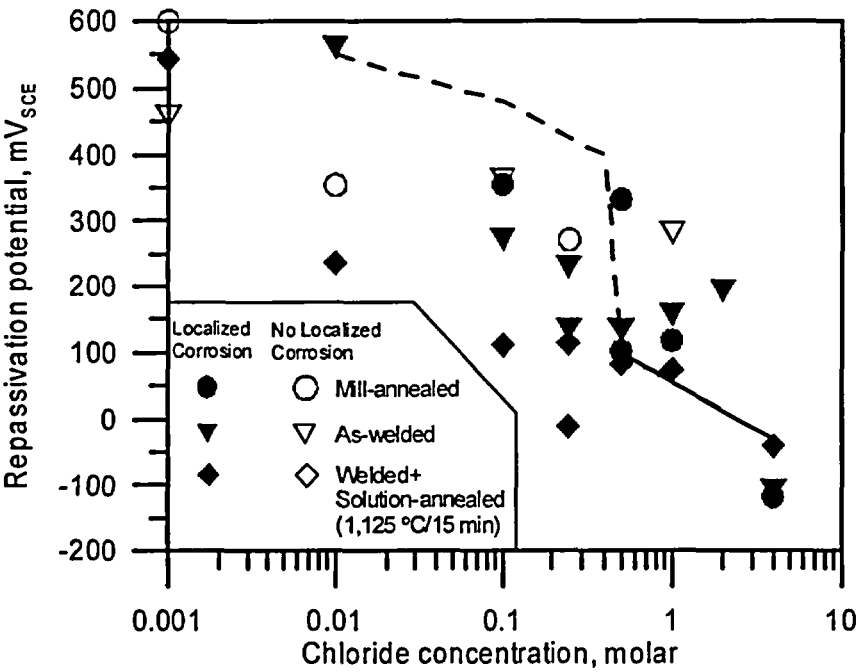

Figure 4-24. Crevice Corrosion Repassivation Potential at 95 °C [203 °F] for Mill-Annealed, As-Welded, + Solution-Annealed {1,125 °C [2,057 °F] for 15 Minutes} Alloy 22

observed in a 0.001 M Cl^- solution with the welded+solution annealed material. For the mill annealed material, no crevice corrosion was observed in solutions with less than 0.1 M Cl^-. The results shown in Figure 4-24 suggest that postweld solution annealing may actually be detrimental to the localized corrosion resistance of welded Alloy 22. The repassivation potentials for the welded+solution annealed material are comparable to the repassivation potentials for the thermally aged material shown in Figure 4-22.

The effect of solution annealing of material from the heat affected zone is shown in Figure 4-25. The heat-affected zone specimens, which did not contain weld metal, had repassivation potentials similar to the mill-annealed material in solutions containing greater than 0.25 M Cl^-. At lower chloride concentrations, the heat-affected zone material may be slightly more susceptible to localized corrosion compared with the mill-annealed material. After short-term thermal aging at 870 °C [1,598 °F] for 5 minutes followed by solution annealing at 1,125 °C [2,057 °F] for 15 minutes, the localized corrosion resistance was not reduced and may have improved slightly compared with the heat-affected zone material. Comparing the results shown in Figures 4-24 and 4-25, it is apparent the effect of solution annealing is different for the weld metal and the thermally aged base metal. Differences in the response of the weld and thermally aged material are likely related to stability of the topologically close-packed phases that form during solidification and thermal aging. Although the mechanism for is not well established, the presence of topologically close-packed phases can significantly decrease localized corrosion resistance of Alloy 22. The welded microstructure is known to have topologically close-packed phases in the interdendritic regions where compositional variations occur during solidification. The composition of the interdendritic region was shown (Chapter 3) to be enriched in molybdenum and tungsten, which stabilize topologically close-packed phases. The reduced

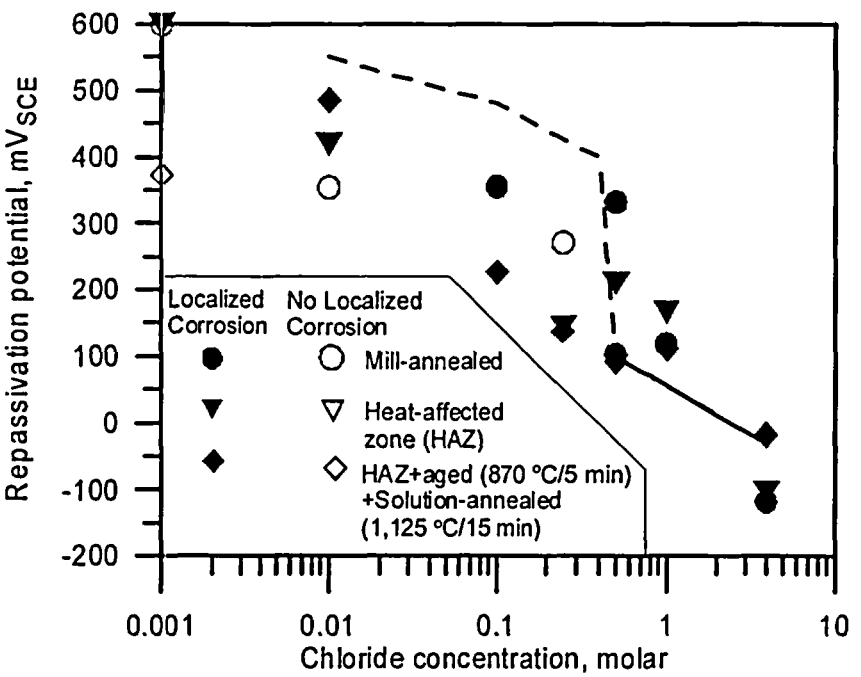

Figure 4-25. Crevice Corrosion Repassivation Potential at 95 °C [203 °F] for Mill-Annealed Alloy 22 Compared with Material from the Heat-Affected Zone (HAZ)

localized corrosion resistance for the welded+solution annealed material is consistent with the microstructural alteration of the welded material after solution annealing. Increased concentrations of molybdenum in the interdendritic regions stabilizes the topologically close-packed phases that in turn, reduce the localized corrosion resistance of the welded+solution annealed material compared with the mill-annealed alloy. In contrast, detrimental effects of topologically close-packed phases and, if present, any alloying element depletion zone associated with formation of the secondary phases in the grain boundaries of the base alloy appear to be partially mitigated by solution annealing the heat affected zone.

Effects of the microstructure on the change in localized corrosion resistance after solution annealing are shown in Figure 4-26. Whereas, the mill-annealed material had a corrosion morphology consistent with an electropolished appearance, localized attack on the welded material exhibited preferential attack in the weld filler metal exposing the cast microstructure and intergranular attack in the adjacent heat-affected zone. Attack on the thermally aged specimens was also characterized by intergranular corrosion that resulted in deep penetrations along the grain boundaries. After solution annealing, localized corrosion was still observed on the welded specimens, however, the severity of the intergranular attack on the thermally aged material was reduced. The severity of localized corrosion in the weld region, however, was not altered by solution annealing.

The susceptibility of Alloy 22 to localized corrosion can be evaluated by comparing the corrosion potential and the repassivation potential for crevice corrosion. Figure 4-27 shows the corrosion potential values as a function of pH from Figure 4-19. Also included are the repassivation potential at 95 °C [203 °F] for the mill-annealed alloy and the thermally aged material (Table 4-9). The repassivation potentials shown are for a pure chloride solution and do not consider the inhibitive effects of anions such as nitrate or the possible detrimental effects of other species. It is apparent the corrosion potential exceeds the repassivation potential for the mill-annealed material in acidic solutions when the chloride concentration is greater than 0.5 M. For the thermally aged material, which tends to bound the behavior of the welded material, the repassivation potential and the critical chloride concentration necessary for localized corrosion are significantly reduced. The corrosion potential may exceed the repassivation potential of the welded or thermally altered material at lower chloride concentrations. The reduction in the repassivation potential and critical chloride concentration as a consequence of fabrication processes increase significantly the range of possible environmental conditions where localized corrosion is possible in the absence of inhibitive species such as nitrate.

4.3.5 Effect of Fabrication Processes on Stress Corrosion Cracking

Limited testing has been performed to evaluate the effects of fabrication processes on the stress corrosion cracking susceptibility of Alloy 22. Welded specimens have not been tested because of the lack of available material. The effect of thermal aging on the stress corrosion cracking resistance of Alloy 22 was evaluated in a test conducted with a compact tension specimen thermally treated for 5 minutes at 870 °C [1,598 °F]. This specimen was tested for more than 1,600 hours at an initial stress intensity of 47 $MPa \cdot m^{1/2}$ [43 $ksi \cdot in^{1/2}$] in a deaerated 4 M NaCl solution at 95 °C [203 °F]. A potential of -220 mV_{SCE} was applied because this potential is just above the crevice corrosion repassivation potential measured for a similarly thermally aged specimen in the same NaCl solution. In this environment, intergranular attack inside the creviced area occurred in unstressed samples, and it was expected that intergranular attack may facilitate the initiation of stress corrosion cracks. The current density increased

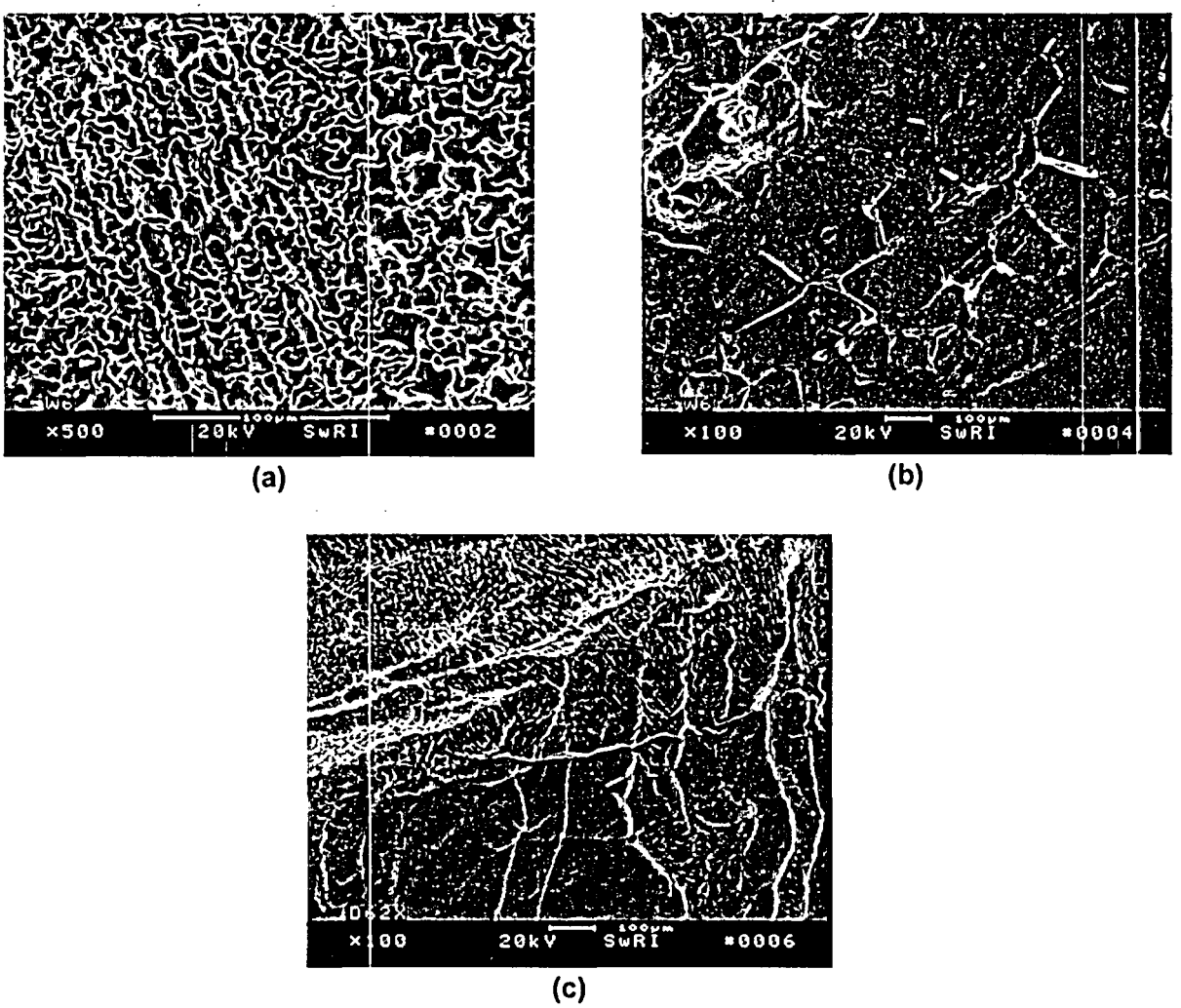

Figure 4-26. Localized Corrosion of As-Welded Alloy 22 after Testing in 0.25 M NaCl at 95 °C [203 °F] (a) in the Fusion Zone, (b) in the Heat-Affected Zone, and (c) after Postweld Solution Annealing

during the course of the test, reaching values close to 1.0×10^{-6} A/cm^2 [9.2×10^{-4} A/ft^2]. An increase in the crack opening displacement was detected during the test, however, the compliance ratio was constant. Although intergranular corrosion was observed on the side surfaces of the specimen, no crack growth was detected beyond the tip of the precrack (Cragnolino, et al., 2003).

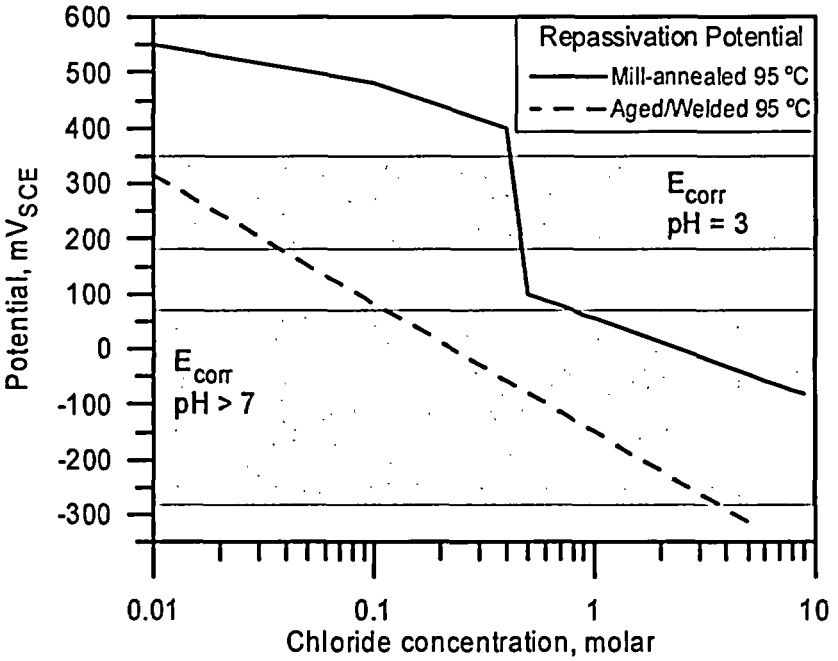

Figure 4-27. Comparison of the Crevice Corrosion Repassivation Potential at 95 °C [203 °F] and Corrosion Potential for Mill-Annealed and Thermally Aged or Welded Alloy 22

5 SUMMARY, CONCLUSIONS, AND RECOMMENDATIONS

Corrosion and stress corrosion cracking of the Alloy 22 outer container are considered important degradation processes that may strongly influence the lifetimes of waste packages. Fabrication processes that lead to microstructural alteration may promote these degradation processes. Several deficiencies and limitations are identified in the current U.S. Department of Energy (DOE) approach and in the technical bases provided for evaluating the effects of fabrication processes on the microstructure, uniform corrosion rate, localized corrosion susceptibility, and stress corrosion cracking resistance of the Alloy 22 outer container. These deficiencies are related to the effects of certain environmental factors, appropriate test methods, the effects of compositional variations of the materials, and an assessment of the complete range of fabrication processes that will be used to construct and close the waste packages.

5.1 Waste Package Fabrication, Closure, and Stress Mitigation

In the current DOE waste package design, Alloy 22 has been selected as the outer container material to provide corrosion resistance in the range of environments expected in the emplacement drifts. Structural strength will be provided by a thick inner container fabricated from Type 316 nuclear grade stainless steel. Fabrication processes used in the production of the waste packages include a variety of cold-forming and machining operations. Handling events may also impart cold work to the container during fabrication closure and emplacement operations. The rolled cylinders will be welded to construct the cylinder of the Alloy 22 disposal container. Welding will also be used to attach the bottom lid to the cylinder of the Alloy 22 disposal container. After the welding operations are completed, the disposal containers will be solution annealed and water quenched to remove residual stresses. Dual closure lids will be installed and welded to the disposal container after waste package loading. Following nondestructive examination, the residual stresses in the closure lid welds may be mitigated using several possible methods, which are being developed. The combination of cold work associated with the forming operations, welding, and postweld stress mitigation methods may alter the microstructure and reduce the corrosion resistance of the Alloy 22 waste package outer barrier. Characterization of the effects of the entire fabrication sequence on the microstructure and corrosion resistance is necessary to assess performance of the waste packages. DOE agreed to provide additional information to address the effects of fabrication closure and stress mitigation processes on the microstructure, corrosion resistance, and stress corrosion cracking susceptibility of the Alloy 22 outer container in CLST agreements 1.02, 1.09, 1.10, 1.12, 1.13, 1.15, 1.16, 2.04, 2.05, 2.07, and 2.08.

5.2 Effects of Fabrication Processes on Microstructure

DOE considered microstructural changes resulting from fabrication processes and possible degradation mechanisms that may strongly influence performance of the waste package. DOE evaluated the phase stability of Alloy 22 assuming the precipitation of secondary topologically close-packed phases and carbides and long-range ordering. The kinetics of phase transformations were determined based on aging data measured from samples treated in accelerated, high-temperature conditions and several assumptions involved in predicting phase stability for repository-relevant conditions. Extrapolation of the short-term data showed bulk precipitation of topologically close-packed phases and long-range ordering in the Alloy 22 base metal are predicted not to occur in 10,000 years at 300 °C [572 °F]. For Alloy 22 welds, the

most recent extrapolated temperatures to give a 10,000-year life for the formation of 5- and 10-volume percent topologically close-packed phases are above 300 °C [572 °F]. Review of the DOE approach for the phase stability of Alloy 22 indicated the assumptions of the same precipitation kinetics for all secondary phases and the temperature-independent precipitation mechanism need to be evaluated further for Alloy 22. Reliance on the limited aging data also may lead to a large uncertainty in the extrapolation of the short-term, high-temperature results. Furthermore, the possible effects of compositional variation, cold work, and weld thickness on the kinetics of phase transformations in Alloy 22 have not been evaluated. On the other hand, the DOE theoretical modeling of phase transformations was based on simplified alloy systems and phases. Additional evaluations are necessary to assess databases and validate the model predictions.

The Center for Nuclear Waste Regulatory Analyses (CNWRA) performed a limited analysis to evaluate the effect of thermal aging on the microstructure of the mill-annealed and welded Alloy 22 and to model the phase stability of the alloy as influenced by compositional variations. Thermal exposure of the mill-annealed Alloy 22 at 870 °C [1,598 °F] for only 5 minutes, a situation that may occur during fabrication of waste packages, resulted in formation of topologically close-packed phases at grain boundaries; however, no significant alloy depletion was detected in the grain-boundary regions. All aging and solution annealing treatments of the welded material conducted in this work promoted precipitation of the secondary phases. Results from both experiments and theoretical calculations indicated that heat-to-heat variations in the base metal and element segregation in the weld may affect significantly the stability of topologically close-packed phases as a consequence of the proposed fabrication and closure processes.

Microstructural analyses indicated the precipitation of topologically close-packed phases in the mill-annealed and welded Alloy 22 specimens after thermal aging. Solution annealing of the welded materials was unable to redissolve these precipitates into a solid solution because of segregation of molybdenum in the interdendritic regions. Based on these results, the proposed fabrication and closure processes may result in phase instability and adversely affect the lifetime of the waste package as a result of enhanced corrosion. This issue has not been adequately considered by DOE. According to agreements CLST 2.04 and 2.05, DOE will provide additional information on the effects of the entire fabrication sequence on phase instability of Alloy 22. The aging testing program will be expanded to include a wide range of Alloy 22 base metal and welded specimens to address the effects of aging at lower temperatures, cold work, solution annealing, welding operations, and stress mitigation treatments. Theoretical modeling will enhance confidence in extrapolating aging data to repository thermal conditions and time scale.

5.3 Effects of Fabrication Processes on Corrosion Processes

DOE evaluated the effects of welding and thermal aging on the uniform corrosion rate, localized corrosion, and stress corrosion cracking resistance of Alloy 22 using a combination of electrochemical and standardized immersion tests. The uniform corrosion rate of welded Alloy 22, measured using weight loss specimens exposed to simulated groundwaters based on variations of J–13 Well water, was determined to be indistinguishable from the corrosion rate of the alloy in the mill-annealed condition. Based on the results of short-term electrochemical tests, thermal aging was found to increase slightly the uniform corrosion rate of Alloy 22. The localized corrosion susceptibility of mill-annealed Alloy 22 was characterized using

electrochemical tests in simulated groundwaters and in solutions containing high chloride concentrations with and without nitrate. Because the simulated groundwater solutions contained significant concentrations of inhibitive species such as nitrate compared with aggressive species such as chloride, no localized corrosion was observed. In solutions that lacked significant concentrations of inhibitive species, the mill-annealed material was found susceptible to localized corrosion. Similar electrochemical tests have not been conducted for welded or welded and solution-annealed materials. The DOE characterization of the effects of fabrication processes on the localized corrosion of Alloy 22 has been limited to standardized tests in boiling acid solutions. The standard test methods selected rely on weight loss measurements and have low sensitivity for detecting increased localized corrosion susceptibility. Based on the results of these tests, DOE assessed the effect of fabrication processes will not significantly increase the localized corrosion susceptibility of the Alloy 22 waste package outer barrier. The effects of fabrication processes are modeled by DOE using an enhancement factor for the uniform corrosion rate that has a value distributed from 1 to 2.5. The approach used by DOE to assess the effects of fabrication processes on the uniform corrosion rate and localized corrosion susceptibility does not consider the metallurgical changes that may occur as a result of the entire fabrication sequence. In addition, evaluation of fabrication processes using standardized tests that rely on the measurement of weight loss is not likely to have sufficient resolution to detect meaningful changes to the localized corrosion susceptibility. The lack of any significant effect of fabrication processes on the corrosion rate of Alloy 22 measured in electrochemical tests can be attributed to the limited range of testing environments. It must be considered that exposure of welded or thermally aged Alloy 22 to groundwaters that have low concentrations of inhibitive species such as nitrate, which may evolve from pore waters, may lead to preferential attack in weld fusion zones or intergranular corrosion.

DOE evaluated the effects of fabrication processes on the stress corrosion cracking resistance of Alloy 22 using crack propagation rate tests and crack initiation tests in a limited range of environments. Results of tests conducted by DOE suggest that fabrication processes may increase the stress corrosion cracking susceptibility of Alloy 22 based on crack propagation rates for both cold-worked and thermally aged materials. Results of crack initiation tests in constant load conditions were likely compromised by galvanic protection of the test specimens caused by corrosion of the stainless steel test fixtures. The combination of residual stresses and enhanced stress corrosion cracking susceptibility associated with fabrication processes warrants additional investigation.

CNWRA independently evaluated the effects of fabrication processes on the uniform corrosion rate and localized corrosion susceptibility of Alloy 22. Uniform corrosion rates for either thermally aged or welding materials were similar to the mill-annealed material. Based on both potentiostatic and electrochemical impedance tests, corrosion rates for the welded material and the thermally aged alloy were typically three to five times larger than the corrosion rates measured for mill-annealed Alloy 22. Although welding and thermal aging had a marginal effect on the uniform corrosion rate, localized corrosion resistance was reduced significantly by either short-term thermal aging or welding. Severe intergranular corrosion was observed on mill-annealed Alloy 22 after thermal aging for times as short as 5 minutes at temperatures of 870 °C [1,598 °F]. Crevice corrosion repassivation potential measurements revealed an increased crevice corrosion susceptibility and a lower critical chloride concentration for localized corrosion on both thermally aged and welded Alloy 22. Intergranular corrosion also was observed in the heat-affected zone of welded material, together with preferential attack in the

fusion zone. Solution annealing was found beneficial for reducing the intergranular corrosion in the heat-affected zone but did not improve the localized corrosion resistance of the welded material. For both the mill-annealed and welded Alloy 22, nitrate was found an effective inhibitor of localized corrosion. Results of the localized corrosion tests can be represented by E_{rcrev} expressions with chloride and temperature-dependent parameters that can be used to model the effects of fabrication processes on the localized corrosion susceptibility of the Alloy 22 outer containers.

The CNWRA conducted a limited evaluation of the effects of fabrication processes on the stress corrosion cracking resistance of Alloy 22 using a precracked thermally aged specimen. No crack growth was observed, although intergranular corrosion in crevices has been observed. According to agreements CLST 1.09, 1.10, 1.12, and 1.15, DOE will conduct additional evaluations to reduce uncertainty and provide additional information on the effects of fabrication processes on the uniform corrosion rate, localized corrosion susceptibility, and stress corrosion cracking resistance of Alloy 22.

5.4 Future Work

Further evaluation of the effects of fabrication processes on the corrosion and stress corrosion cracking susceptibility of Alloy 22 is necessary to assess the lifetimes of the waste packages. The DOE assessment of fabrication effects is based on limited experimental work with materials that do not accurately represent the expected condition of the fabricated and sealed waste packages. Effects of the complete range of fabrication processes on the uniform corrosion rate, localized corrosion susceptibility, and stress corrosion cracking resistance need to be properly considered in responses to the DOE and the U.S. Nuclear Regulatory Commission agreements. Whereas most tests have been conducted with specimens subject to isothermal aging, it would be important to evaluate material exposed to cooling from the solution-annealing temperature. In addition, variations in the cooling cycles from the fusion temperature during closure welding, considering the range of decay heats generated for various wastes that will be contained within the waste packages should be examined. Additional experimental work and modeling should consider the range of expected repository environments, the complete sequence of fabrication processes, including cold work from forming and handling operations, postweld heat treatments, proposed stress mitigation methods, and variations in the alloy and filler metal composition.

Design of the waste packages has not been finalized, however, significant revisions to the design and the proposed fabrication processes occurred recently. Some processes such as laser peening and low-plasticity burnishing are still being evaluated. Changes to the waste package design and fabrication processes used in the construction of the disposal container and in closure and stress mitigation processes need to be assessed with respect to performance in the proposed repository. Significant changes to the waste package design or proposed fabrication processes will require a reevaluation of the effects of fabrication processes on the microstructure and susceptibility to corrosion and stress corrosion cracking.

6 REFERENCES

Anderson, M.J., N.R. Brown, J.D. Cloud, P.R.Z. Russell, and L.J. Trautner. "Waste Package Design for License Application." Proceedings of 10th High-Level Radioactive Waste Management Conference, Las Vegas, Nevada, March 30–April 3, 2003. La Grange Park, Illinois: American Nuclear Society. pp. 714–719. 2003.

Andresen, P.L., P.W. Emigh, L.M. Young, and G.M. Gordon. "Stress Corrosion Cracking Growth Rate Behavior of Alloy 22 (UNS N06022) in Concentrated Groundwater. " Proceedings of the CORROSION 2003 Conference. Paper No. 683. Houston, Texas: NACE International. 2003.

———. "Stress Corrosion Cracking of Annealed and Cold Worked Titanium Grade 7 and Alloy 22 in 110 °C Concentrated Salt Environments." Proceedings of the CORROSION 2001 Conference. Paper No. 01130. Houston, Texas: NACE International. 2001.

ASME International. "Rules for Construction of Nuclear Power Plant Components, Division 1, Subsection NB, Class 1 Components." *Section III of the 1995 ASME Boiler and Pressure Vessel Code.* New York City, New York: ASME International. 1995a.

———. "Nondestructive Examination." *Section V of the 1995 ASME Boiler and Pressure Vessel Code.* New York City, New York: ASME International. 1995b.

———. "Materials, Part C—Specifications for Welding Rods, Electrodes, and Filler Metals." *1995 Addenda: Section II of the 1995 ASME Boiler and Pressure Vessel Code.* New York City, New York: ASME International. 1995c.

———. "Qualification Standard for Welding and Brazing Procedures, Welders, Brazers, and Welding and Brazing Operators." *Section IX of the 1995 ASME Boiler and Pressure Vessel Code.* New York City, New York: ASME International. 1995d.

ASTM International. "Standard Specification for Low-Carbon Nickel-Molybdenum-Chromium, Low-Carbon Nickel-Chromium-Molybdenum, Low-Carbon Nickel-Chromium-Molybdenum-Copper, Low-Carbon Nickel-Chromium-Molybdenum-Tantalum, and Low-Carbon Nickel-Chromium-Molybdenum-Tungsten Alloy Plate, Sheet, and Strip." *ASTM B575–99a: Annual Book of Standards. Volume 3.02: Wear and Erosion—Metal Corrosion.* West Conshohocken, Pennsylvania: ASTM International. 2001a.

———. "Standard Test Method for Conducting Cyclic Potentiodynamic Polarization Measurements for Localized Corrosion Susceptibility of Iron-, Nickel- or Cobalt-Based Alloys." *ASTM G61-86: Annual Book of Standards Volume 3.02: Wear and Erosion—Metal Corrosion.* West Conshohocken, Pennsylvania: ASTM International. 2001b.

———. "Standard Test Methods of Detecting Susceptibility to Intergranular Attack in Wrought Nickel-Rich, Chromium Bearing Alloys." *ASTM G28-85: Annual Book of Standards Volume 3.02: Wear and Erosion—Metal Corrosion.* West Conshohocken, Pennsylvania: ASTM International. 2001c.

———. "Standard Practice for Calculation of Corrosion Rates and Related Information from Electrochemical Measurements." *ASTM G102-89: Annual Book of Standards Volume 3.02: Wear and Erosion—Metal Corrosion.* West Conshohocken, Pennsylvania: ASTM International. 2001d.

Brossia, C.S., L.B. Browning, D.S. Dunn, O.C. Moghissi, O. Pensado, and L. Yang. "Effect of Environment on the Corrosion of Waste Package and Drip Shield Materials." CNWRA 2001-003. San Antonio, Texas: CNWRA. 2001.

Bruemmer, S.M. "Quantitative Modeling of Sensitization Development in Austenitic Stainless Steel." *Corrosion.* Vol. 46. pp. 698–709. 1990.

Cieslak, M.J., T.J. Headley, and A.D. Romig, Jr. "The Welding Metallurgy of Hastelloy Alloys C-4, C-22, and C-276." *Metallurgical Transactions.* Vol. 17A. pp. 2,035–2,047. 1986.

Cragnolino, G.A., D.S. Dunn, and Y.-M. Pan. "Effects of Potential and Environment on the Stress Corrosion Cracking Susceptibility of Nickel-Chromium-Molybdenum Alloys." Proceedings of the CORROSION 2003 Conference. Paper No. 541. Houston, Texas: NACE International. 2003.

Cragnolino, G.A., O. Pensado, D.S. Dunn, C.S. Brossia, and N. Sridhar. "Lifetime Prediction of High-Level Radioactive Waste Containers Affected by Corrosion." Proceedings of the 15th International Corrosion Congress, National Centre for Metallurgical Research. Paper No. 416. Madrid, Spain: Spanish Council for Scientific Research. 2002a.

Cragnolino, G.A., D.S. Dunn, and Y.-M. Pan. "Localized Corrosion Susceptibility of Alloy 22 as a Waste Package Container Material." Scientific Basis for Nuclear Waste Management XXV. Symposium Proceedings 713. B.P. McGrail and G. A. Cragnolino, eds. Warrendale, Pennsylvania: Materials Research Society. pp. 53–60. 2002b.

Cragnolino, G.A., D.S. Dunn, Y.-M. Pan, and O. Pensado. "Corrosion Processes Affecting the Performance of Alloy 22 As a High-Level Radioactive Waste Container Material." Scientific Basis for Nuclear Waste Management XXIV. K.P. Hart and G.R. Lumpkin, eds. Symposium Proceedings 663. Warrendale, Pennsylvania: Materials Research Society. pp. 507–514. 2001.

Cragnolino, G.A., D.S. Dunn, C.S. Brossia, V. Jain, and K. Chan. "Assessment of Performance Issues Related to Alternate EBS Materials and Design Options." CNWRA 99-003. San Antonio, Texas: CNWRA. 1999.

CRWMS M&O. "Yucca Mountain Science and Engineering Report—Technical Information Supporting Site Recommendation Consideration." DOE/RW–0539–1. Rev. 1. Las Vegas, Nevada: DOE, Office of Civilian Radioactive Waste Management. 2002.

———. "Waste Package Operations Fabrication Process Report." TDR–EBS–ND–000003. Rev. 02. Las Vegas, Nevada: CRWMS M&O. 2001a.

———. "Waste Package Project FY–01 Closure Methods Report." TDR–EBS–ND–000006. Rev. 00. Las Vegas, Nevada: CRWMS M&O. 2001b.

———. "Supplemental Science and Performance Analysis—Report Volume 1 of 2." TDR–MGR–MD–000007. Rev. 00. Las Vegas, Nevada: CRWMS M&O. 2001c.

———. "Repository Safety Strategy: Plan to Prepare the Safety Case to Support Yucca Mountain Site Recommendation and Licensing Considerations." TDR–WIS–RL–000001. Rev. 04 ICN 01. Las Vegas, Nevada: CRWMS M&O. 2000a.

———. "Total System Performance Assessment for the Site Recommendation." TDR–WIS–PA–000001. Rev. 00 ICN 01. Las Vegas, Nevada: CRWMS M&O. 2000b.

———. "General Corrosion and Localized Corrosion of Waste Package Outer Barrier." ANL–EBS–MD–000003. Rev. 00. Las Vegas, Nevada: CRWMS M&O. 2000c.

———. "Waste Package Degradation Process Model Report." TDR–WDS–MD–000002. Rev. 00 ICN 01. Las Vegas, Nevada: CRWMS M&O. 2000d.

———. "Aging and Phase Stability of Waste Package Outer Barrier." ANL–EBS–MD–000002. Rev. 00. Las Vegas, Nevada: CRWMS M&O. 2000e.

———. "Waste Package Operations Fabrication Process Report." TDR–EBS–ND–000003. Rev. 01. Las Vegas, Nevada: CRWMS M&O. 2000f.

Dunn, D.S., L. Yang, Y.M. Pan, and G.A. Cragnolino. "Localized Corrosion Susceptibility of Alloy 22." Proceedings of the CORROSION 2003 Conference. Paper No. 697. Houston, Texas: NACE International. 2003.

Dunn, D.S. and C. S. Brossia. "Assessment of Passive and Localized Corrosion Processes for Alloy 22 As a High-Level Nuclear Waste Container Material." Proceedings of the CORROSION 2002 Conference. Paper No. 548. Houston, Texas: NACE International. 2002.

Dunn, D.S., G.A. Cragnolino, and N. Sridhar. "Passive Dissolution and Localized Corrosion of Alloy 22 High-Level Waste Container Weldments." Scientific Basis for Nuclear Waste Management XXIII. Symposium Proceedings 608. R.W. Smith and D.W. Shoesmith, eds Warrendale, Pennsylvania: Materials Research Society. pp. 89–94. 2000.

Epelboin, I., C. Gabrielli, M. Keddam, and H. Takenouti. "Alternating-Current Impedance Measurements Applied to Corrosion Studies and Corrosion-Rate Determination." *Electrochemical Corrosion Testing ASTM 727.* F. Mansfeld and U. Bertocci, eds. West Conshohocken, Pennsylvania: ASTM International. pp. 150–166. 1981.

Estill, J.C., G.A. Hust, and R.B. Rebak. "Long Term Corrosion Potential Behavior of Alloy 22 in Yucca Mountain Relevant Environments." Proceedings of the CORROSION 2003 Conference. Paper No. 688. Houston, Texas: NACE International. 2003.

Estill, J.C., K.J. King, D.V. Fix, D.G. Spurlock, G.A. Hurst, S.R. Gordon, R.D. McCright, R.B. Rebak, and G. M. Gordon. "Susceptibility of Alloy 22 to Environmentally Assisted Cracking in Yucca Mountain Relevant Environments." Proceedings of the CORROSION 2002 Conference. Paper No. 535. Houston, Texas: NACE International. 2002.

Floreen, S. "Composition Effects Within the Chemical Specification for Alloy 22." *Peer Review of the Waste Package Materials Performance—A Compilation of Special Topic Reports.* F.M.G. Wong and J.H. Payer, eds. Las Vegas, Nevada: DOE. pp. 3-4–3-8. 2002.

Goldstein, J.I., D.B. Williams, and G. Cliff. "Quantitative X-Ray Analysis." *Principles of Analytical Electron Microscopy.* D.C. Joy, A.D. Romig, and J.I. Goldstein, eds. New York City, New York: Plenum Press. pp. 155–217. 1986.

Heubner, U.L., E. Alepeter, M.B. Rockel, and E. Wallis. "Electrochemical Behavior and Its Relation to Composition and Sensitization of NiCrMo Alloys in ASTM G-28 Solution." *Corrosion.* Vol. 45. pp. 249–259. 1989.

Karmazin, L. "Lattice Parameter Studies of Structure Changes of Ni-Cr Alloys in the Region of Ni_2Cr." *Materials Science and Engineering.* Vol. 54. pp. 247–256. 1982.

King, K.J., J.C. Estill, and R.B. Rebak. "Characterization of the Resistance of Alloy 22 to Stress Corrosion Cracking." Proceedings of the Pressure Vessels and Piping Conference. Paper No. 03E–02. New York City, New York: American Society of Mechanical Engineers. 2002.

Kirchheim, R., B. Heine, H. Fischmeister, S. Hofmann, H. Knote, and U. Stoltz. "The Passivity of Iron-Chromium Alloys." *Corrosion Science.* Vol. 30, No. 7. pp. 899–917. 1989.

Lian, T., J.C. Estill, G.A. Hust, and R.B. Rebak. "Passive and Transpassive Dissolution of Alloy 22 in Simulated Repository Environments." Proceedings of the CORROSION 2003 Conference. Paper No. 694. Houston, Texas: NACE International. 2003.

Laycock, N.J. and R.C. Newman. "Localized Dissolution Kinetics, Salt Films, and Pitting Potentials." *Corrosion Science.* Vol. 39. pp. 1,771–1,790. 1997.

Manning, P.E. "An Improved Intergranular Corrosion Test for HASTELLOY Alloy C-276." *Laboratory Corrosion Tests and Standards.* ASTM STP 866. G.S. Haynes and R. Baboian, eds. West Conshohocken, Pennsylvania: ASTM International. pp. 437–454. 1985.

McCright, R.D. "An Annotated History of Container Candidate Material Selection." UCID–21472. Livermore, California: Lawrence Livermore National Laboratory. 1988.

Meck, N.S., P. Crook, S.D. Day, and R.B. Rebak. "Localized Corrosion Susceptibility of Nickel Alloys in Halide Containing Environments." Proceedings of the CORROSION 2003 Conference. Paper No. 682. Houston, Texas: NACE International. 2003.

Migala, T.S. and T.L. Jacobs. "Low Plasticity Burnishing: An Affordable, Effective Means of Surface Enhancement." Proceedings of the 13th International Federation for Heat Treatment and Surface Engineering Congress, Columbus, Ohio, October 7–10, 2002. Columbus, Ohio. 2002.

NRC. NUREG–1762, "Integrated Issue Resolution Status Report." Rev. 0. Washington, DC: NRC. August 2002.

———. "Issue Resolution Status Report, Key Technical Issue: Container Life and Source Term." Rev. 3b. Washington, DC: NRC. 2001.

Pan, Y.-M, D.S. Dunn, and G.A. Cragnolino. "Phase Stability and Corrosion of Alloy 22 As a High-Level Nuclear Waste Container Material." Proceedings of the Mike Meshii Symposium: Electron Microscopy—Its Role in Materials Science. J.R. Weertman, M. Fine, K. Faber, W. King, and P. Liaw, eds. Warrendale, Pennsylvania: The Minerals, Metals, and Materials Society. pp. 201–208. 2003.

Pan, Y.-M., C.S. Brossia, G.A. Cragnolino, D.S. Dunn, G.D. Gute, and L. Yang. "Stress Corrosion Cracking and Hydrogen Embrittlement of Container and Drip Shield Materials." CNWRA 2003-02. San Antonio, Texas: CNWRA. 2002.

Payer, J.H., J.A. Beavers, T.M. Devine, G.S. Frankel, R.H. Jones, R.G. Kelly, and R.M. Latanision. "Peer Review of the Waste Package Materials Performance Final Report." Las Vegas, Nevada: DOE. 2002.

Pensado, O., D.S. Dunn, and G.A. Cragnolino. "Passive Dissolution of Container Materials Modeling and Experiments." CNWRA 2003-01. San Antonio, Texas: CNWRA. 2002.

Prevey, P.S., J. Telesman, T.Gabb, and P. Kantzos. "FOD Resistance and Fatigue Crack Arrest in Low Plasticity Burnished IN718." Proceedings of the 5th National Turbine Engine High Cycle Fatigue Conference, Chandler, Arizona, March 7–9, 2000. Chandler, Arizona. 2000.

Raghavan, M., R.R. Mueller, G.A. Vaughn, and S. Floreen. "Determination of Isothermal Sections of Nickel Rich Portion of Ni-Cr-Mo System by Analytical Electron Microscopy." *Metallurgical Transactions.* Vol. 15A. pp. 783–792. 1984.

Raghavan, M., B.J. Berkowitz, and J.C. Scanlon. "Electron Microscopic Analysis of Heterogeneous Precipitates in Hastelloy C-276." *Metallurgical Transactions.* Vol 13A. pp. 979–984. 1982.

Rebak, R.B., T.S. Edgecumbe Summers, T. Lian, R.M. Carranza, J.R. Dillman, T. Corbin, and P. Crook. "Effect of Thermal Aging on the Corrosion Behavior of Wrought and Welded Alloy 22." Proceedings of the CORROSION 2002 Conference. Paper No. 542. Houston, Texas: NACE International. 2002.

Rebak, R.B., T.S.E. Summers, and R.M. Carranza. "Mechanical Properties Microstructure and Corrosion Performance of C-2 Alloy Aged at 260 °C to 800 °C." Scientific Basis for Nuclear Waste Management XXIII. Symposium Proceedings 608. R.W. Smith and D.W. Shoesmith, eds. Warrendale, Pennsylvania: Materials Research Society. pp. 109–114. 2000.

Silverman, D.C. "Practical Corrosion Prediction Using Electrochemical Techniques." *Uhlig's Corrosion Handbook.* 2nd Edition. R.W. Revie, ed. New York City, New York: John Wiley and Sons. pp. 1,197–1,225. 2000.

Sridhar, N., G.A. Cragnolino, D.S. Dunn, and H.K. Manaktala. "Review of Degradation Modes of Alternate Container Designs and Materials." CNWRA 94-010. San Antonio, Texas: CNWRA. 1994.

Sridhar, N., J.A. Kargol, and N.F. Fiore. "Effect of Low -Temperature Aging on Hydrogen-Induced Crack Growth in a Nickel-Base Superalloy." *Scripta Metallurgica.* Vol. 14. pp. 1,257–1,260. 1980.

Stern, M. and A.L. Geary. "Electrochemical Polarization 1—A Theoretical Analyses of the Shape of Polarization Curves." *Journal of the Electrochemical Society.* Vol. 104, No. 1. pp. 56–63. 1957.

Summers, T.S.E., R.B. Rebak, T.A. Palmer, and P. Crook. "Influence of Thermal Aging on the Mechanical and Corrosion Properties of GTAW Welds on Alloy N06022." Scientific Basis for Nuclear Waste Management XXV. Symposium Proceedings 713. B.P. McGrail and G.A. Cragnolino, eds. Warrendale, Pennsylvania: Materials Research Society. pp. 45–52. 2002.

Summers, T.S.E., R.B. Rebak, and R.R. Seeley. "Influence of Thermal Aging on the Mechanical and Corrosion Properties of C-22 Alloy Welds." UCRL–JC–137727. Livermore, California: Lawrence Livermore National Laboratory. 2000.

Tawancy, H.M. "Precipitation Characteristics of μ-Phase in Wrought Nickel-Base Alloys and Its Effect on Their Properties." *Journal of Materials Science.* Vol. 31. pp. 3,929–3,936. 1996.

Was, G.S. and R.M. Kruger. "A Thermodynamic and Kinetic Basis for Understanding Chromium Depletion in Ni-Cr-Fe Alloys." *Acta Materialia.* Vol. 33. pp. 841–854. 1985.

Young, L.M., G.M. Catlin, P.L. Andresen, and G.M. Gordon. "Constant Load SCC Initiation Response of Alloy 22 (UNS N06022), Titanium Grade 7, and Stainless Steel at 105 °C." Proceedings of the CORROSION 2003 Conference. Paper No. 685. Houston, Texas: NACE International. 2003.

Zhao, J.-C., M. Larsen, and V. Ravikumar. "Phase Precipitation and Time-Temperature-Transformation Diagram of Hastelloy X." *Materials Science and Engineering.* Vol. 293A. pp. 112–119. 2000.